University of Southampton

Faculty of Physical Science and Engineering

Zepler Institute for Photonics and Nanoelectronics

Optoelectronics Research Centre

Mid-Infrared Pulse Generation via Orientation Patterned Gallium Arsenide Parametric Devices

by

Qiang Fu

Thesis for the degree of Doctor of Philosophy

July 2020

University of Southampton

Abstract

Faculty of Physical Sciences and Engineering

Zepler Institute for Photonics and Nanoelectronics

Optoelectronics Research Centre

Thesis for the degree of Doctor of Philosophy

Mid-Infrared Pulse Generation via Orientation Patterned Gallium Arsenide Parametric Devices

by

Qiang Fu

Mid-infrared (mid-IR) pulsed lasers are finding increasing applications in the areas of industrial processing, spectroscopy, medicine, and chemistry due to the presence of characteristic vibrational absorptions of a large number of molecules in this spectral region. Optical parametric devices (OPDs), as one of the most promising solutions for mid-infrared generation, have attracted much attention. Nonlinear crystals are key elements for OPDs and the recently developed material system, orientation-patterned gallium arsenide (OP-GaAs), is deemed as an outstanding nonlinear gain element for the mid-IR spectral region. This thesis describes a systematic study of the development of mid-IR OPDs based on OP-GaAs, including optical parametric generators (OPGs), amplifiers (OPAs), oscillators (OPOs) and their variants. Several 2-μm, picosecond, thulium-doped-fibre master oscillator power amplifier (Tm:MOPA) systems, employing gain-switched laser diode seeding, are developed as the pump source for the OP-GaAs OPDs, greatly increasing their flexibility and potential for real-world applications.

In a simple single-pass configuration, an OP-GaAs OPG is pumped by a high-peak-power, low-repetition rate (1 MHz) Tm:MOPA, and provides a wide wavelength tuning range of 2550-2940 nm (signal) and 5800-8300 nm (idler) as well as a high peak power of 2.8 kW (signal) and 1.7 kW (idler). The OPG naturally generates an output with a broad spectral linewidth. In order to control and narrow the spectral linewidth, a wavelength-tunable Cr:ZnSe laser is employed as a seed laser to change the

OPG into an OPA. Compared to the OPG, the OPA offers a lower pump power requirement and higher conversion efficiency. The OPA signal and idler spectral linewidth is narrowed to 0.7 cm^{-1} and 1.4 cm^{-1}, respectively, and a maximum output peak power of 11.4 kW and 2.8 kW for signal and idler is obtained. However, the OPA requires an external seed laser and therefore its tuning range is mainly limited by that of the seed laser.

To overcome the tuning limitation, a novel cascaded OPG-OPA is proposed and developed that combines the good features of the OPG and OPA. In the cascaded OPG-OPA, the OPG output signal spectrum is controlled and filtered and then used as the seed source for the OPA. Without using an external seed laser, a tuning range of 2552-2960 nm (signal) and 5733-8305 nm (idler) covering the entire wavelength regime that the OP-GaAs gratings provided is demonstrated, and controlled output signal and idler linewidths of 1.4 cm^{-1} and 9 cm^{-1} are achieved, respectively.

The mid-IR output beam of OPGs and OPAs are typically not diffraction limited due to the lack of any active spatial control. In contrast, OPOs with cavity structures, can offer mid-IR output at high beam qualities. An idler-resonant OP-GaAs OPO, synchronously pumped by another Tm:MOPA system operating at a high repetition rate of 100 MHz, is demonstrated and delivers a near-diffraction-limited output beam for the mid-IR idler. Power scaling of the OP-GaAs OPO is then investigated, pumped by a high-average-power Tm:MOPA, and a total mid-IR maximum output power of 9.7 W is obtained with wide wavelength tunablity (2.9-3.3 μm for signal, 4.9-6.4 μm for idler). The output characteristic shows a thermal roll-over which is cured in the final work section via active water-cooling of the OP-GaAs crystal. The final work also demonstrates the flexibility allowed by the gain-switched-diode seeding of the pump laser, delivering a controllable pulse repetition-rate (100 MHz – 1 GHz) and duration (95 ps – 1.1 ns) OPO with a maximum total output power of 13.7 W at a signal and idler wavelength of 3.3 μm and 4.9 μm, respectively.

Table of Contents

List of Figures

List of Tables

Research Thesis: Declaration of Authorship

Print name: Qiang Fu

Title of thesis: Mid-Infrared Pulse Generation via Orientation Patterned Gallium Arsenide Parametric Devices

I declare that this thesis and the work presented in it are my own and has been generated by me as the result of my own original research.

I confirm that:

1. This work was done wholly or mainly while in candidature for a research degree at this University;
2. Where any part of this thesis has previously been submitted for a degree or any other qualification at this University or any other institution, this has been clearly stated;
3. Where I have consulted the published work of others, this is always clearly attributed;
4. Where I have quoted from the work of others, the source is always given. With the exception of such quotations, this thesis is entirely my own work;
5. I have acknowledged all main sources of help;
6. Where the thesis is based on work done by myself jointly with others, I have made clear exactly what was done by others and what I have contributed myself;
7. Parts of this work have been published as the journal and conference publications listed in Appendix A.

Signature: ..... Date: .....

Acknowledgements

First of all, I have to say that I really enjoy my PhD research journey at Optoelectronics Research Centre (ORC). To me, ORC is like one of the world's leading trains for photonics research, and my supervisors are a part of the engine of the train. At the beginning of my PhD, I was a passenger in the train, and at the nearly end of my PhD journey I finally become a component of the train.

I express my sincere gratitude to my fantastic supervisory team: Prof. David J. Richardson, Prof. David P. Shepherd, Dr. Lin Xu, and Dr. Shaif-ul Alam. I thank Prof. David J. Richardson who has demonstrated his far-reaching academic knowledge, superior memory, and distinguished working efficiency to me. Although he supervises many PhD students simultaneously, he has paid much attention and valuable time on me. His instructions and feedbacks are always constructive, supportive and timely. If I would further my academic career in the future, he is definitely an exceptional model to me. I thank Prof. David P. Shepherd who came up with my PhD project idea and welcomed me into the ORC four years ago. I still remember the moment that I received the PhD offer from him, which has turned out a life-changing opportunity for me. His kindness, responsibility, attitude, and professional work deeply impressed me. Thinking of the literatures he recommended, fruitful discussions we had, and his excellent proofreading skills, I would always fancy a pint with him! I thank Dr. Lin Xu who has helped me in countless experimental details and theoretical study. I could not finish my PhD in a smooth way without his instructions. He also taught me in person how to "keep calm and carry on" when I struggled in research problems. I thank Dr. Shaif-ul Alam who offered his expertise in fibre lasers to me. I learned real-life concerns of industrial lasers from him, and he made me believe that the usefulness of the lasers developed in the lab. Overall, I am proud of having such an outstanding supervisory team, and their efforts are extremely meaningful to me.

A special thank-you to our "two micron" colleagues: Dr. Sijing Liang, Dr. Shaoxiang Chen and Mr. Zhengqi Ren. Dr. Liang is, to some extent, a teacher to me when I first came to the ORC lab. I learned my very first fibre cleaving and splicing from her. With her help, I could independently work in the lab only within a few months. We spent much time doing experiments together, and her PhD project is a vitally important basis of my PhD project. I thank Dr. Chen, a simulation expert, who gave me many useful instructions of modelling of fibre lasers. I thank Mr. Ren who is my classmate, colleague, and housemate. We worked in

the same lab during most of my PhD time. I enjoy the favourable discussions and delighted cooperation with him.

I would like to thank Dr. Yongmin Jung, Dr. Peter C. Shardlow, Dr. Di Lin, Dr. Jonathan H. V. Price, Dr. Saurabh Jain, Dr. Hans Christian Mulvard, Dr. Juliano G. Hayashi, Dr. Neda Baktash, Dr. Yujun Feng, Dr. Li Shen, Dr. Ian Davidson, Dr. Ping Hua, Mr. Andrea Ventura, Mr. Shuichiro Rikimi, Mr. Sheng Zhu, Mr. Hao Li, Miss Dong Wu, Mr. Duanyang Xu, and Mr. Yudi Wu who have helped me in various ways through my PhD.

I thank my financial support from the ORC and China Scholarship Council for my PhD study.

Last but not least, I would like to express my wholehearted gratitude to my beloved wife, my parents, my older sister and my whole family for their endless support and understanding. I could not summarise their contributions here in a few words, but they have incorporated into myself. I believe the only way to repay them is to be a better husband, a better son, a better brother, and a better man.

List of Abbreviations

AC	autocorrelator
AR	anti-reflection
ASE	amplified spontaneous emission
BPM	birefringence-phase-matching
ChG	chalcogenide
CSP	$CdSiP_2$
CW	continuous wave
DRO	doubly-resonant oscillator
DM	dichroic mirror
FBG	fibre bragg grating
FOM	figure of merit
FWHM	full width at half maximum
GaAs	gallium arsenide
Ge	germanium
HCF	hollow core fibre
HR	high reflection
HVPE	hydride vapor phase epitaxy
HWP	half-wave plate
KTA	$KTiOAsO_4$
KTP	$KTiOPO_4$
LMA	large-mode-area
LN	lithium niobate
LPF	long-pass filter

MA	mode adapter
MBE	molecular beam epitaxy
MI	modulation instability
mid-IR	mid-infrared
OC	output coupler
OPA	optical parametric amplifier
OPD	optical parametric device
OPG	optical parametric generator
OP-GaAs	orientation-patterned gallium arsenide
OP-GaP	orientation-patterned gallium phosphide
OPO	optical parametric oscillator
OSNR	output signal to noise ratio
PBS	polarising beam splitter
PC	polarisation controller
PM	polarisation maintaining
PPKTP	periodically poled $KTiOPO_4$
PPKTA	periodically poled $KTiOAsO_4$
PPLN	periodically poled lithium niobate
QCL	quantum cascade laser
QPM	quasi-phase-matching
QWP	quarter-wave plate
SC	Supercontinuum
SHG	second harmonic generation
SPM	self-phase modulation
SRO	singly-resonant oscillators

TDF	thulium-doped fibre
TDFA	thulium-doped fibre amplifier
Tm:MOPA	thulium-doped fibre master oscillator power amplifier
WDM	wavelength-division multiplexer
ZGP	$ZnGeP_2$

Chapter 1

Introduction

1.1 Motivation

Since the first laser was realised in the visible part of the spectrum by T.H. Maiman in 1960 [1], development of optical coherent sources at different wavelengths ranging from ultraviolet to far-infrared (terahertz region) has advanced tremendously, and such laser sources have been applied in various industrial and scientific fields. In particular, mid-infrared (mid-IR, 2-20 μm) laser sources are increasingly of considerable interest for applications involving identification of specific organic molecules, as this spectral region corresponds to the location of characteristic vibrational absorptions of organic materials. Also, the mid-IR spectral region coincides with two wide atmospheric transmission windows (3-5 μm and 7-12 μm). Thus, developing bright sources at these wavelengths is attractive for efficient detection and/or utilisation of a wide variety of biological, toxic, dangerous or polluting organic materials in medical, industrial, scientific, and environmental fields [2].

Current solutions for generation of coherent mid-IR radiation are:

i) Directly from laser gain media. This includes semiconductor lasers, especially quantum cascade lasers [3-5], rare-earth-doped lasers (thulium, holmium, erbium, praseodymium, dysprosium and other dopants) [6, 7], Cr^{2+}/Fe^{2+} doped II-VI compound lasers [8], chemical lasers [2], gas lasers (He-Ne, CO, CO_2 laser, etc.) [9-13], and hollow core fibre (HCF) gas lasers [14-17].

ii) Mid-IR frequency conversion of common near-IR or short-wavelength mid-IR sources. This includes optical parametric devices (OPDs) [6], Raman lasers [6, 18], and supercontinuum (SC) generation [19].

Although the mid-IR laser sources have progressed remarkably in the recent decades, development of such sources remains less mature than their near-infrared counterparts and still represents a rapidly evolving frontier of laser development research.

This thesis is dedicated to systematically develop and investigate mid-IR OPDs, specifically, based on orientation-patterned gallium arsenide (OP-GaAs), which is a high-performance mid-IR nonlinear crystal. Different OP-GaAs OPDs (optical parametric generators (OPGs), amplifiers (OPAs), cascaded OPG-OPAs, and optical parametric oscillators (OPOs)) were studied to achieve different output characteristics. Research on tailoring the output characteristics of OP-GaAs OPDs is important because, for real devices, the idealised properties of high efficiency, high average/peak power, high pulse energy, wide mid-IR wavelength tunability, good beam quality, and controllable linewidth, repetition-rate, and pulse-duration, are challenging to achieve simultaneously. The thesis will also have a particular emphasis on mid-IR generation in a wavelength band of 5-6 μm for mid-IR power delivery potentially using our in-house-fabricated tellurite-based HCFs. Moreover, this specific wavelength band coincides with the zero-dispersion wavelengths of standard-geometry step-index chalcogenide fibres [20], and thus such laser sources can potentially work as a pump source for chalcogenide-fibre-based SC generation in mid-IR.

In terms of temporal domain, this thesis concentrated on pulsed parametric devices rather than continuous wave as pulsed lasers can provide useful output characteristics such as high peak power, and are also naturally easier operate at lower average pump powers. In particular, picosecond parametric devices are the main devices developed in this thesis. Such sources when compared with femtosecond (typical broadband spectra) and nanosecond (long temporal duration) devices, offer a compromise between spectral and temporal resolutions in spectroscopic applications. Importantly, it also operates in a temporal regime that allows the use of very simple primary pump seed sources, i.e. gain-switched diode lasers. To date, there are no reports of picosecond OP-GaAs OPDs, apart from a low-average-power OPG [21], thus this thesis reports a new area of development for these devices.

In contrast to laser gain media, the nonlinear media utilised in parametric devices do not offer energy storage (no upper energy levels with life time involved), therefore picosecond pump sources are required for picosecond output. For an OP-GaAs OPD, the pump source needs to have a wavelength longer than 1.7 μm in order to avoid two-photon-absorption [22], and such picosecond pump sources are difficult to be found in the market. Hence, this thesis also reports on the development of such novel pump sources for the OP-GaAs OPDs.

Specifically, the work described in this thesis demonstrates the development of a mid-IR OP-GaAs OPG, an OPA, a cascaded OPG-OPA, and several OPOs. The OPG and OPA are pumped by a high-peak-power, picosecond, thulium-doped fibre master oscillator power amplifier (Tm:MOPA) system, which in turn is seeded by a 2-μm gain-switched laser diode operating at a 1-MHz repetition rate. The OPG output is widely tunable, has high peak power, and a broad spectral linewidth. To further boost the high peak power and narrow the linewidth, an OP-GaAs OPA is realised initially using a Cr:ZnSe seed laser, but its tuning range limited by that of the seed laser. To overcome the limited tuning, a cascaded OPG-OPA is developed with a broadly tunable, high-peak-power and narrow-linewidth output. The mid-IR output beam of such devices are typically not diffraction limited due to lack of any active spatial control. However, an idler-resonant OP-GaAs OPO, synchronously pumped by another 2-μm, gain-switched-laser-diode seeded, picosecond, Tm:MOPA system operating at a high repetition rate of 100 MHz, is demonstrated which achieves a near-diffraction-limited idler output beam. Power scaling work of the OP-GaAs OPO is then carried out pumped by a high-average-power Tm:MOPA, and a total mid-IR maximum output power of 9.7 W is obtained with wide wavelength tunablity. Finally, in order to demonstrate the flexible and controllable nature of the OPO output, a controllable repetition-rate and pulse-duration Tm:MOPA system is then used to pump the OP-GaAs OPO, offering variable repetition-rate and pulse-duration mid-IR output characteristics.

1.2 Thesis outline and novelty

Chapter 1 briefly introduced the research motivation of this thesis and the main topics of our work.

Chapter 2 provides the background of this thesis, including three-wave-mixing theory, mid-IR OPDs and recent progresses made for OP-GaAs based OPDs, thulium-doped fibre lasers, a theory necessary for modelling of device performance, and so on.

Chapters 3-7 present all the experimental works on the development of the OP-GaAs OPDs, and each chapter i) introduces the OPDs and motivation; ii) describes the corresponding pump system; iii) discusses the OPD experimental results and analysis; and iv) provides a concluding summary.

Chapter 3 describes a mid-IR, high-peak-power, picosecond OP-GaAs OPG and OPA. An OPG tuning range of 2550-2940 nm (signal) and 5800-8300 nm (idler) is demonstrated with a maximum peak power of ~2.8 kW (signal) and ~1.7 kW (idler), and with spectral

bandwidths of 20 nm (signal, 29 cm^{-1}) and 200 nm (idler, 33 cm^{-1}). When seeded by a 0.6 cm^{-1}-linewidth tunable Cr:ZnSe laser, an OP-GaAs OPA is realised with a maximum peak power of ~11.4 kW and ~2.8 kW, and much narrower spectral bandwidths of 0.7 cm^{-1} (signal) and 1.4 cm^{-1} (idler). This is the first report of a high-power picosecond OP-GaAs OPG and OPA and was published in *Optics Letters* [23].

Chapter 4 demonstrates a mid-IR, widely tunable, narrow-linewidth, cascaded OPG-OPA. A diffraction grating, together with an adjustable aperture, is used as a spectral filter to narrow the signal linewidth of the OPG stage, which is then utilised as the seed for the OPA stage. A widely tunable output in the range of 2552-2960 nm (signal) and 5733-8305 nm (idler) is obtained, and maximum peak powers of 11.1 kW and 4.5 kW are obtained for signal and idler, respectively. The OP-GaAs cascaded OPG-OPA is designed to fully explore the OPA tuning range, and this design combined with its output characteristics is the main novelty to this work, which was published in *IEEE Journal of Selected Topics in Quantum Electronics* [24].

Chapter 5 depicts a mid-IR, high-beam-quality, watt-level, widely-tunable OP-GaAs OPO. It is also pumped by a picosecond Tm:MOPA system, but in a synchronous fashion that is different from the previous single-pass pumping for the OPG and OPA. With an idler-resonant cavity, a near-diffraction-limited performance of idler is obtained with M^2 values of 1.06 (x-direction) by 1.03 (y-direction). An OPO tuning range of 2997-3661 nm and 4394-6102 nm is achieved, with maximum average powers of 1.18 W (idler) and 0.51 W (signal). This work represents the first report of an idler-resonant synchronously fibre-laser-pumped OP-GaAs OPO, and also with near-diffraction-limited beam qualities at idler wavelengths. These results were published in *Optics Letters* [25].

Chapter 6 manifests a mid-IR, widely-tunable, high-average-power, picosecond OP-GaAs OPO, which is a power scaling work based on the OPO in Chapter 5. A maximum total average output power of 9.7 W is obtained, corresponding to signal and idler output powers of 5.7 W (0.60 kW peak power) and 4.0 W (0.42 kW peak power), respectively. A thermally induced power roll-off is observed when the pump power is higher than 25.5 W. To mitigate the thermal effects, an optical chopper is placed before the OPO to provide a burst mode operation and a reduced thermal load. We then observe a linear growth in the OPO output power over the full range of available pump powers, confirming thermal effects as the origin of the roll-off observed under continuous pumping. The maximum peak powers of signal and idler are estimated to be over 0.79 kW and 0.58 kW, respectively in this instance. A

wide mid-IR wavelength tuning range of 2895-3342 nm (signal) and 4935-6389 nm (idler) is demonstrated. This work was the highest average-power reported for an OP-GaAs OPO also with wide wavelength tunablity at the time, and it was published in *Optics Express* [26].

Chapter 7 presents a mid-IR, high-power, variable repetition-rate, adjustable pulse-duration OP-GaAs OPO. By manipulating the pump pulse characteristics, the OP-GaAs OPO can be operated at variable repetition rates from 100 MHz – 1 GHz, and at controllable pulse durations from ~95 ps – ~1.1 ns. With a water cooling plate applied on the crystal to mitigate thermal effects, a linear growth in the OPO output power at a full range of pump powers is achieved (without the chopper placed before the cavity, as stated in Chapter 6). A maximum total output average power of 13.7 W is then obtained, with 9.2 W of signal and 4.5 W of idler and with a signal and idler wavelength of 3.3 μm and 4.9 μm, respectively. This is the first high-power OP-GaAs OPO with such flexible properties in terms of repetition rates and pulse durations and it has been published in *Optics Express* [27].

Chapter 8 gives a concluding summary for the whole thesis work and provides a discussion of possible future directions.

Reference

[1] T. H. Maiman, "Stimulated optical radiation in ruby," *Nature,* vol. 187, no. 4736, pp. 493-494, 1960.

[2] F. K. Tittel *et al.*, "Mid-infrared laser applications in spectroscopy," in *Solid-State Mid-Infrared Laser Sources*, Berlin, Germany: Springer Berlin Heidelberg, 2003, pp. 458-529.

[3] M. Razeghi *et al.*, "Recent progress of quantum cascade laser research from 3 to 12 μm at the Center for Quantum Devices [Invited]," *Applied Optics,* vol. 56, no. 31, pp. H30-H44, 2017.

[4] D. Heydari *et al.*, "High brightness angled cavity quantum cascade lasers," *Applied Physics Letters,* vol. 106, no. 9, pp. 091105, 2015.

[5] Y. Bai *et al.*, "Room temperature quantum cascade lasers with 27% wall plug efficiency," *Applied Physics Letters,* vol. 98, no. 18, pp. 181102, 2011.

[6] I. T. Sorokina, and K. L. Vodopyanov, *Solid-State Mid-Infrared Laser Sources*: Springer Science & Business Media, 2003.

[7] B. M. Walsh *et al.*, "Mid infrared lasers for remote sensing applications," *Journal of Luminescence,* vol. 169, pp. 400-405, 2016.

[8] S. B. Mirov *et al.*, "Frontiers of mid-IR lasers based on transition metal doped chalcogenides," *IEEE Journal of Selected Topics in Quantum Electronics,* vol. 24, no. 5, pp. 1-29, 2018.

[9] C. Patel, "CW high power N_2–CO_2 laser," *Applied Physics Letters,* vol. 7, no. 1, pp. 15-17, 1965.

[10] C. B. Moore *et al.*, "Vibrational energy transfer in CO_2 lasers," *The Journal of Chemical Physics,* vol. 46, no. 11, pp. 4222-4231, 1967.

[11] M. Bhaumik, "High-efficiency electric-discharge CO lasers," in *Inst. Phys. Conf. Ser*, 1976, pp. 243-67.

[12] A. B. Petersen *et al.*, "Infrared molecular lasers pumped by electronic‐vibrational energy transfer from Br($4^2P_{1/2}$): CO_2, N_2O, HCN, and C_2H_2" *Applied Physics Letters,* vol. 27, no. 5, pp. 305-307, 1975.

[13] C. Liu *et al.*, "Dispersion effects in a high‐gain 3.39-μ He–Ne Laser," *Journal of Applied Physics,* vol. 40, no. 9, pp. 3556-3563, 1969.

[14] M. R. Abu Hassan *et al.*, "Cavity-based mid-IR fiber gas laser pumped by a diode laser," *Optica,* vol. 3, no. 3, pp. 218-221, 2016.

[15] Z. Wang *et al.*, "Efficient diode-pumped mid-infrared emission from acetylene-filled hollow-core fiber," *Optics Express,* vol. 22, no. 18, pp. 21872-21878, 2014.

[16] M. Xu *et al.*, "Mid-infrared 1 W hollow-core fiber gas laser source," *Optics Letters,* vol. 42, no. 20, pp. 4055-4058, 2017.

[17] A. V. V. Nampoothiri *et al.*, "Hollow-core optical fiber gas lasers (HOFGLAS): a review [Invited]," *Optical Materials Express,* vol. 2, no. 7, pp. 948-961, 2012.

[18] L. Cao *et al.*, "High peak power 2.8 μm Raman laser in a methane-filled negative-curvature fiber," *Optics Express,* vol. 26, no. 5, pp. 5609-5615, 2018.

[19] J. H. V. Price *et al.*, "Mid-IR supercontinuum generation from nonsilica microstructured optical fibers," *IEEE Journal of Selected Topics in Quantum Electronics,* vol. 13, no. 3, pp. 738-749, 2007.

[20] C. R. Petersen *et al.*, "Mid-infrared supercontinuum covering the 1.4–13.3 μm molecular fingerprint region using ultra-high NA chalcogenide step-index fibre," *Nat Photon,* vol. 8, no. 11, pp. 830-834, 2014.

[21] P. S. Kuo *et al.*, "Optical parametric generation of a mid-infrared continuum in orientation-patterned GaAs," *Optics Letters,* vol. 31, no. 1, pp. 71-73, Jan. 2006.

[22] P. G. Schunemann, "New nonlinear optical crystals for the mid-infrared," in *Advanced Solid State Lasers Conference (ASSL)*, Berlin, 2015, pp. AM2A.2.

[23] L. Xu *et al.*, "Thulium-fiber-laser-pumped, high-peak-power, picosecond, mid-infrared orientation-patterned GaAs optical parametric generator and amplifier," *Optics Letters,* vol. 42, no. 19, pp. 4036-4039, Oct. 2017.

[24] Q. Fu *et al.*, "Widely tunable, narrow-linewidth, high-peak-power, picosecond mid-infrared optical parametric amplifier," *IEEE Journal of Selected Topics in Quantum Electronics*, vol. PP, no. 99, pp. 1-1, 2018.
[25] Q. Fu *et al.*, "High-beam-quality, watt-level, widely tunable, mid-infrared OP-GaAs optical parametric oscillator," *Optics Letters*, vol. 44, no. 11, pp. 2744-2747, 2019.
[26] Q. Fu *et al.*, "High-average-power picosecond mid-infrared OP-GaAs OPO," *Optics Express*, vol. 28, no. 4, pp. 5741-5748, 2020.
[27] Q. Fu *et al.*, "Controllable duration and repetition-rate picosecond pulses from a high-average-power OP-GaAs OPO," *Optics Express*, vol. 28, no. 22, pp. 32540-32548, 2020.

Chapter 2

Background theory

2.1 Introduction

In this chapter, the background theory that underpins the experimental work of this thesis will be introduced, including introduction to three wave mixing, optical parametric devices (OPDs), orientation-patterned gallium arsenide (OP-GaAs), thulium-doped fibre (TDF) lasers, gain-switching, self-phase modulation (SPM), and modulation instability (MI) in optical fibres. Furthermore, essential calculations for tuning curves, pump acceptance bandwidths, walk-off effects and operation thresholds of OP-GaAs OPDs will be given at the end of the chapter.

2.2 Principle of three-wave mixing in $\chi^{(2)}$ nonlinear optics

Nonlinear optics is a comprehensive study on interaction behaviour between optical materials and light, and to some extent it can be considered as a "by-product" of lasers because the nonlinear phenomenon requires intense light (typically a laser beam) to be observed. In 1961 (i.e. one year after the invention of the laser), the first demonstration of second harmonic generation in crystalline quartz was reported by Franken [1]. After that, many researchers concentrated their interests on developing nonlinear-optics-based laser devices and their theoretical description.

For a transparent material in which an intense optical field $\boldsymbol{E}$ is applied, a polarization $\boldsymbol{P}$ is induced that depends nonlinearly upon $\boldsymbol{E}$ and can be given by

$$\boldsymbol{P} = \varepsilon_0\chi^{(1)}\boldsymbol{E} + \varepsilon_0\chi^{(2)}\boldsymbol{E^2} + \varepsilon_0\chi^{(3)}\boldsymbol{E^3} + \ldots \qquad (2.2.1)$$

where ε_0 is the vacuum permittivity, $\chi^{(1)}$ is the first order susceptibility that describes linear optics, $\chi^{(2)}$, $\chi^{(3)}$ are known as the second and third order optical susceptibilities, which

correspond to nonlinear optics. If only considering $\chi^{(2)}$ nonlinear interactions, and substituting the electric displacement field **D** expressed by

$$\mathbf{D} = \varepsilon_0 \boldsymbol{E} + \boldsymbol{P} \tag{2.2.2}$$

into Maxwell's equations for non-conducting and non-magnetic media, the mixing of three monochromatic, continuous, plane waves (ω_p, ω_s, ω_i), assuming a slowly varying envelope approximation and ignoring losses, can be given by [2]

$$\frac{dE(\omega_p)}{dz} = i\frac{2\omega_p d_{eff}}{n_p c}E(\omega_s)E(\omega_i)e^{-i\Delta kz} \tag{2.2.3}$$

$$\frac{dE(\omega_s)}{dz} = i\frac{2\omega_s d_{eff}}{n_s c}E(\omega_p)E^*(\omega_i)e^{i\Delta kz} \tag{2.2.4}$$

$$\frac{dE(\omega_i)}{dz} = i\frac{2\omega_i d_{eff}}{n_i c}E(\omega_p)E^*(\omega_s)e^{i\Delta kz} \tag{2.2.5}$$

where $E(\omega_m)$ are electric field amplitudes of the three waves (m=p,s,i indicates pump, signal and idler respectively), n_m are the refractive indices at the three frequencies ω_m, z is the propagation direction of three waves with collinear assumption, d_{eff} is the effective nonlinear coefficient of the nonlinear material, c is the speed of light in a vacuum and Δk is the wave vector mismatch. The expression for Δk is

$$\Delta k = k_p - k_s - k_i = 2\pi\left(\frac{n_p}{\lambda_p} - \frac{n_s}{\lambda_s} - \frac{n_i}{\lambda_i}\right) \tag{2.2.6}$$

where λ_m are the wavelengths of three waves.

Assuming no pump depletion, equation 2.2.3-2.2.5 can be solved with the well-known Manley-Rowe relations that indicate energy conservation:

$$\frac{1}{\omega_s}\frac{dI(\omega_s)}{dz} = \frac{1}{\omega_i}\frac{dI(\omega_i)}{dz} = -\frac{1}{\omega_p}\frac{dI(\omega_p)}{dz} \tag{2.2.7}$$

where $I(\omega_m)$ are the intensities of the three waves. The expression for the power conversion efficiencies η from pump to signal/idler in three-wave nonlinear processes can be obtained [2],

$$\eta \propto \frac{d_{eff}^2}{n^3}\mathrm{sinc}^2\left(\frac{\Delta k\, L}{2}\right) \tag{2.2.8}$$

where n is refractive index and L is the nonlinear material length. The value of d^2_{eff}/n^3 contains the material parameters that contribute to nonlinear processes, giving a useful figure of merit (FOM) for each nonlinear media. Fig. 2.2.1 shows the dependence of η on $\Delta kL/2$. Obviously, Δk being zero is a significant condition for high conversion efficiency in nonlinear conversion. This is called phase matching and is in accordance with momentum conservation.

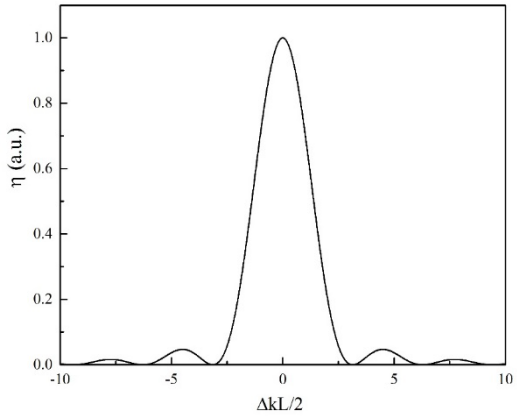

Fig. 2.2.1. Dependence of conversion efficiency η on $\Delta kL/2$.

2.3 Quasi-phase-matching

Birefringence-phase-matching (BPM) and quasi-phase-matching (QPM) are the two common phase-matching techniques. BPM is fulfilled by utilising the different dispersion relations between beams with different polarisations in non-centrosymmetric systems, which can be realised in a critical (angle tuning) or noncritical (temperature tuning) manner. However, optically isotropic materials such as gallium arsenide (GaAs) cannot reach this condition due to lack of birefringence. QPM was invented to conquer this constraint, and its basic idea is that inverting the orientation of nonlinear media over every coherence length ($\pi/\Delta k$) can bring the generated optical field back into phase allowing growth, as depicted in Fig. 2.3.1. If the phase-matching condition cannot be fulfilled (red line, Fig. 2.3.1), the field amplitude will periodically oscillate without any growth. In BPM a linear growth of field amplitude can be realised (black line, Fig. 2.3.1), which performs better than that of QPM (blue line). However, in reality, QPM enables accessibility to larger nonlinear coefficients in nonlinear media despite suffering a reduction in d_{eff} that depends on the QPM order and duty cycle [3]. Thus QPM still can provide a higher conversion efficiency (Eq. 2.8) compared with BPM. Furthermore, QPM allows nonlinear generation at all wavelengths of

the material transparency window by design of the grating period, whereas BPM can only work at a limited range of wavelengths where phase-matching is physically possible. This thesis will focus on the QPM phase-matching technique in OP-GaAs, a material with high nonlinear coefficients and wide mid-IR transparency, but which cannot support BPM.

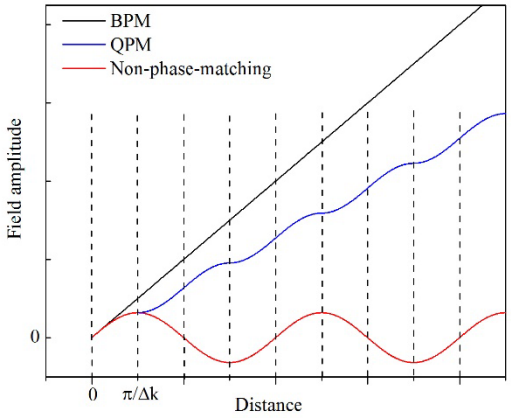

Fig. 2.3.1. Generated field amplitude over distance in nonlinear media under BPM, QPM and non-phase-matching conditions.

Under QPM condition, Equations 2.2.3-2.2.5 can be modified accordingly - modulating d_{eff} with a period Λ generates Fourier components for compensating Δk. Δk and the phase-matching condition is then given by the following equation:

$$\Delta k = k_p - k_s - k_i - \frac{2\pi}{\Lambda} = 2\pi\left(\frac{n_p}{\lambda_p} - \frac{n_s}{\lambda_s} - \frac{n_i}{\lambda_i} - \frac{1}{\Lambda}\right) = 0 \qquad (2.3.1)$$

Note that, Equation 2.3.1 indicates first-order QPM with a duty cycle of 50%, which is the case discussed throughout this thesis. Furthermore, noncritical phase-matching is utilised in this thesis for QPM, which is a common practice albeit a critical QPM was experimentally demonstrated recently [4]. Complex QPM crystal structures, such as high-order QPM, chirped and waveguide structures, are also interesting for many applications [3], but this is not of concern for this thesis.

2.4 Optical parametric devices

Most OPDs are based on the nonlinear optical susceptibility tensor $\chi^{(2)}$ and are down-conversion devices related to three-wave mixing. Because of historical reasons, these waves are named pump, signal and idler (with angular frequencies ω_p, ω_s, ω_i, respectively), which have the relationship $\omega_p > \omega_s \geq \omega_i$ (the case of $\omega_s = \omega_i$ is named as degenerate). In three-wave optical parametric processes, the energy conservation and momentum conservation must be obeyed:

$$\omega_p = \omega_s + \omega_i \tag{2.4.1}$$

$$\mathbf{k}_p = \mathbf{k}_s + \mathbf{k}_i \tag{2.4.2}$$

where $\mathbf{k}_p$, $\mathbf{k}_s$, $\mathbf{k}_i$ are wave vectors of pump, signal and idler, respectively. Equation 2.4.1, in accordance with Equation 2.2.7, represents the energy law, whereas Equation 2.4.2 stands for the momentum conservation, which has the other name of phase matching (Equation 2.3.1).

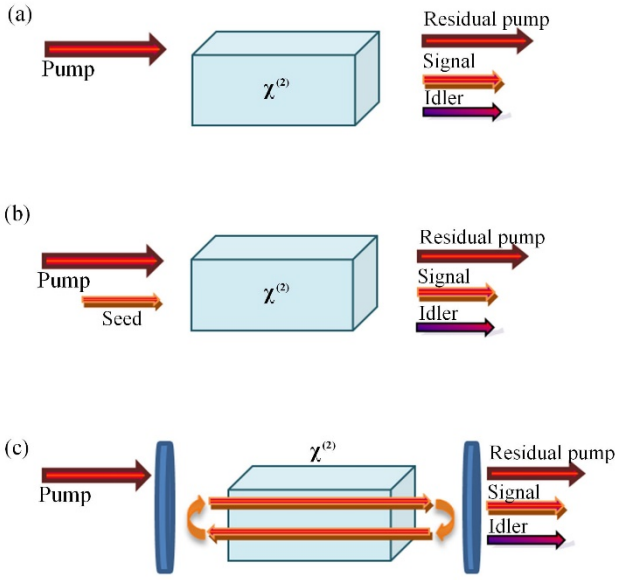

Fig. 2.4.1. Setup of optical parametric devices: (a) OPGs (b) OPAs (c) OPOs

There are three classic forms of OPDs: optical parametric generators (OPGs), amplifiers (OPAs), and oscillators (OPOs), as shown in Fig. 2.4.1. OPGs (Fig.2.4.1 (a)) can generate signal and idler without any initial input signal. The physical origin of the optical parametric generation is spontaneous parametric fluorescence attributed to quantum fluctuations of the vacuum that are then amplified to macroscopic power levels. An OPG has attractive features such as setup simplicity, high tolerance for alignment, and broad spectral output for applications (demonstrated in Chapter 3), but it has limitations such as high threshold (sometimes pump intensities close to the damage threshold of nonlinear materials) and giving little control over the properties of the output pulses.

OPAs, (Fig.2.4.1 (b)) compared with OPGs, have another input (signal or idler) as a seed, and thus can provide control of the output characteristics (e.g. bandwidth, tunability) via control of the seed. These characteristics make OPAs valuable for many applications, including optical parametric chirped-pulse amplification of femtosecond pulses [5]. On the

other hand, the tunability of OPAs can only be accessed if one of the inputs is tunable, as reported in Chapter 3 and Chapter 4.

OPOs have optical cavities (Fig. 2.4.1 (c)), which provide feedback for the signal, idler or even pump. Singly-resonant oscillators (SROs) and doubly-resonant oscillators (DROs) are two common forms of OPO. In SROs, either signal or idler resonates in the OPO cavity whereas, in DROs, both signal and idler resonate. Compared with DROs, SROs have higher thresholds but are more stable, which makes SROs more practical and common in use. It should be noted that the cavity may not necessarily be a simple two-mirror cavity as shown in Fig. 2.4.1 (c). For example, synchronously pumped OPOs typically need more than two mirrors to create a cavity length that is matched to the pump pulse repetition rate, which is the case for the OPOs demonstrated in Chapter 5 and 6. Compared to OPAs, there is no need for an input seed, as the seed of OPOs initially comes from the OPG process. An OPO, acting similarly to a laser, has a laser resonator cavity with threshold and gain properties. However, OPOs are based on parametric amplification that is determined by phase matching rather than stimulated emission. In other words, there is no energy exchange between the nonlinear material and the light in OPOs. Hence, at least in theory, there is no thermal input into the nonlinear crystal, which is attractive for high average power operation. While the optical cavity adds complexity it allows further control of output characteristics, such as tunabilty and spectral bandwidth, delivers higher beam qualities, and generally requires less pump power to approach an oscillation threshold.

Overall, different OPDs have their own unique output characteristics, so that development of various high-performance OPDs is of interest for a variety of applications.

2.5 OP-GaAs in mid-IR

Frequency conversion devices require good nonlinear crystals as a key component. Oxide nonlinear crystals, for example $LiNbO_3$ (LN), $KTiOPO_4$ (KTP), $KTiOAsO_4$ (KTA), and their QPM versions - periodically poled LN (PPLN), PPKTP, PPKTA, have revealed their superiorities for nonlinear frequency conversion in the near-infrared and visible spectral regions, but in the mid-IR they have limited transparency (not beyond than 4-5 μm) due to multi-phonon absorption at longer wavelengths. In contrast, many non-oxide nonlinear materials have broad transparency in the mid-IR, and were first demonstrated for developing up-conversion devices based on CO_2 and CO gas lasers [6, 7]. In more recent times, many applications look towards the use of compact solid-state mid-IR laser sources. Down-conversion of near-infrared solid-state lasers into mid-IR is therefore becoming more

attractive and is also benefiting from the development of a group of non-oxide nonlinear materials for down-conversion process, such as OP-GaAs, $ZnGeP_2$ (ZGP), $CdSiP_2$ (CSP), and orientation-patterned gallium phosphide (OP-GaP). In this thesis, I shall concentrate on the OP-GaAs nonlinear gain media but many of the device demonstrations described would be easily transferable to other mid-IR nonlinear media.

As already mentioned in section 2.3, GaAs is an isotropic material that has no routes to realise BPM, and hence it has to be fabricated in an orientation patterned manner for QPM in order to access its very large nonlinear coefficient d_{14} (94 pm/V). To date, there are two growth methods for fabricating OP-GaAs: plate stacking and epitaxial growth. In the plate-stacking method several GaAs plates, with alternating orientation, are directly bonded together [8], which is good for the production of large crystal apertures. Although a 0.1-0.3% optical loss per interface was successfully achieved [9], it remains a challenge to use this specialist, time-consuming, method to fabricate OP-GaAs with small periods. In contrast, epitaxial growth of OP-GaAs [10] has become commercially available after optimisation of the processes of wafer bonding, molecular beam epitaxy (MBE) and hydride vapor phase epitaxy (HVPE). Its basic process is: i) MBE produces an inverted GaAs layer on the top of a prepared non-inverted GaAs layer with a non-polar germanium (Ge) buffer layer in between, ii) photolithography patterned etching is used to periodically remove the inverted GaAs layer and Ge layer to leave a grating structure with patterned orientation for further growth, iii) regrowth of the entire wafer by MBE and HVPE, maintaining the orientation pattern in up to a thickness (~1 mm) that is accessible for OPDs. This method provides an engineerable QPM, low loss (<0.01 cm^{-1}), high damage threshold OP-GaAs wafer that can be cut and polished for several mid-IR OPDs. In spite of a relatively high-cost, the benefits of a well-developed, repeatable, low-loss, growth technique has made this the method of choice. The OP-GaAs used in this thesis is grown by the epitaxial technique (by Dr. Peter G. Schunemann's team in BAE systems Inc. MER15-1813, P.O. Box 868, Nashua, U.S.). Fig. 2.5.1(a) shows the photo of an OP-GaAs wafer with multiple gratings with periods from 57 μm to 65 μm with a step of 2 μm. The red rectangles with a dimension of 25 mm × 21 mm, identify where cutting, grinding, and polishing took place to give two pieces of final OP-GaAs crystals with a reduced length of 20 mm. The area outside of the red dashed circle (Fig. 2.5.1 (a)) is where the wafer was covered by a holder during MBE process. Fig. 2.5.1 (b) shows a photo of a real OP-GaAs sample used in our OPD experiments, and it was mounted on a mechanical holder that attached to an oven to enable temperature tuning. The design of the used QPM periods will be explained in section 2.9.1.

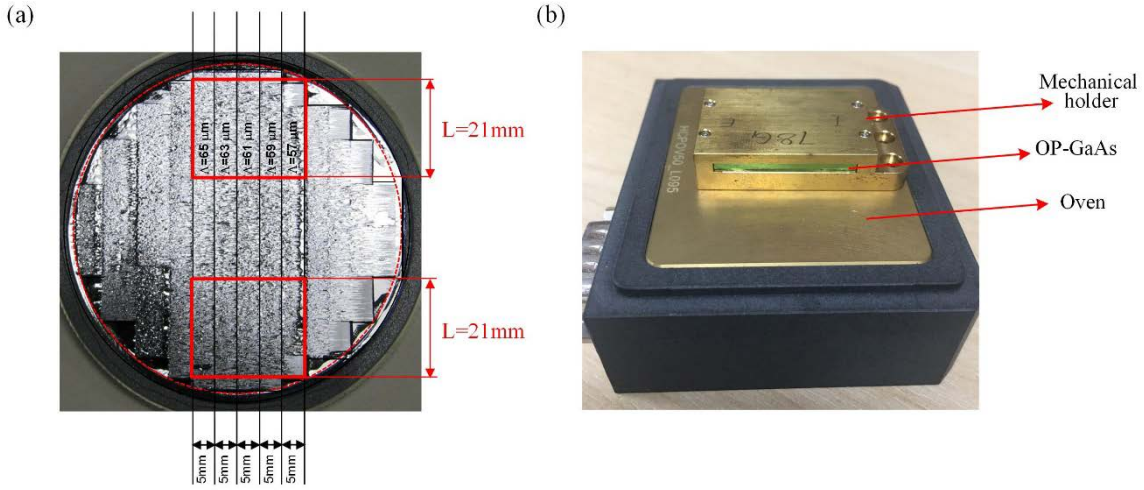

Fig. 2.5.1. (a) OP-GaAs wafer with multi-gratings (provided by BAE systems); (b) OP-GaAs mounted on a mechanical holder that attached to an oven.

A number of intrinsic properties (transparency, FOM, thermal conductivity, and phase matching type) of OP-GaAs, which are useful for OPD developments, are listed in Table 2.5.1. They are compared with other mid-IR nonlinear crystals, including ZGP, CSP, OP-GaP, and three oxide QPM crystals - PPLN, PPKTP and PPKTA. Albeit OP-GaAs is transparent at ~1 μm, pumping laser wavelengths for OP-GaAs have to be >1.7 μm owing to two-photon-absorption induced by high-intensity pump beams [11]. TDF lasers, working at around 2-μm wavelength, have been considered as a good candidate for directly pumping OP-GaAs to obtain longer mid-IR wavelengths in OPDs, offering the possibility of compact sources with high efficiency [12-14], which will be introduced in section 2.7. Oxide crystals, as stated before, have difficulty to operate beyond 5 μm, although their fabrication process is relative mature and cheaper compared with fabricating OP-GaAs or OP-GaP. ZGP and CSP are birefringent crystals with tuning ranges limited by the requirements of birefringent phase-matching (BPM), even though they have high FOM of ~189, and ~264 pm^2/V^2, respectively. OP-GaAs is the highest FOM QPM crystal (~246 pm^2/V^2) with a good thermal conductivity (55 W/m/K), which allows a high-power operation. OP-GaP has an even higher thermal conductivity of 110 W/m/K, but a slightly lower FOM of ~166 pm^2/V^2. Note that there are many other nonlinear crystals (such as $PbGa_2GeSe_6$, $AgGaGeS_4$) that can be used for mid-IR OPDs, but they are not included in Table 2.5.1 because of their modest properties [15-17]. Nevertheless, fabricating and searching for new high-performance nonlinear crystals is an ongoing research topics.

Table. 2.5.1. Common mid-IR nonlinear crystal comparison.

	OP-GaAs	OP-GaP	ZGP	CSP	PPLN	PPKTP	PPKTA
Transparency (μm)	0.9- 17	0.6 – 12	0.7 -12	0.5 -9	0.4-5.5	0.35-4.3	0.35-5.3
d^2_{eff}/n^3 (pm^2/V^2)	~246	~166	~189	~264	~68	~49	~45
Thermal conductivity (W/m/K)	52	110	35	14	5	~3	~2
Linear thermal expansion (10^{-6} K^{-1}) (along optical z axis)	5.7	5.3	15.9	-17	1.7	-0.2	NA
dn/dT (10^{-6} K^{-1}) (at 1 μm)	322	136	148	173	7.4	6.5	8.6
Phase-matching type	QPM	QPM	BPM	BPM	QPM	QPM	QPM
Ref.	[18, 19]	[19]	[18, 19]	[20-22]	[23-25]	[19, 25]	[25]

OP-GaAs, again as an isotropic crystal (similar to OP-GaP), theoretically allows pumping with any polarisation, but accessing different nonlinear coefficients. For the OP-GaAs samples used in this thesis (Fig. 2.5.1), the key crystallographic axes are sketched in Fig. 2.5.2 (a). [$\bar{1}$10] is orientated along its length (the pump beam propagation direction), [110] along its width, and [001] along its height. Kuo et al. modelled the theoretical values of d^2_{eff} of such OP-GaAs samples as a function of the orientation of a linearly polarised pump beam [26], which is replotted here in Fig. 2.5.2 (b). The results are calculated for the case that the OP-GaAs is ideal and there are no polarisation control components (if for example it is used within an OPO cavity). It should be noted that in practice, the polarisation can be affected by thermally induced birefringence and other polarisation dependant losses [26, 27]. The theoretical value of d^2_{eff} is equal to d^2_{14} (94 pm/V) with a pump linearly polarised along [110] and [001], and maximises at a pump polarisation direction along [111] (35° relative to [110]) with a value of ~1.33 d^2_{14}. With this pump polarisation the generated signal and idler is also polarised along [111] [26].

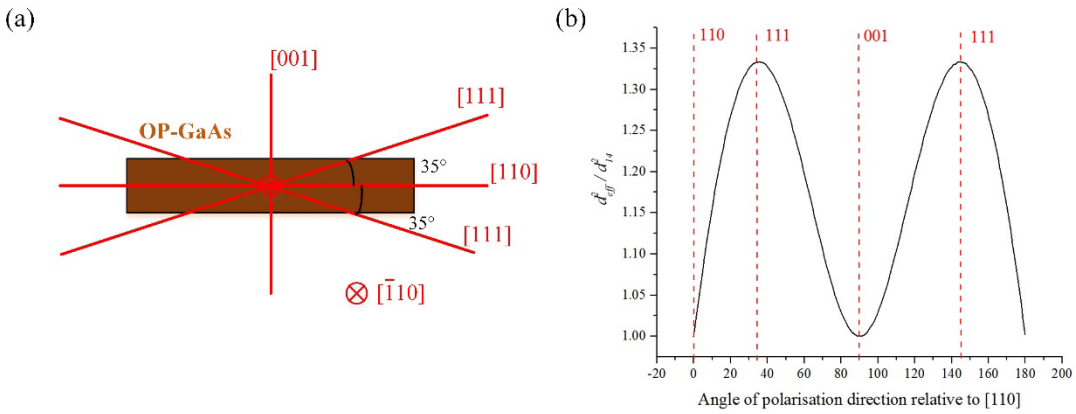

Fig. 2.5.2. (a) OP-GaAs crystallographic axes; (b) d^2_{eff}/d^2_{14} versus pump polarisation angle relative to [110].

Laser-induced damage of OP-GaAs devices is another crucial factor that needs to be considered. It has previously been reported that the anti-reflection coatings applied to the OP-GaAs crystal are the first thing to damage which occurred at a fluence of 1.35 J/cm^2 and a pulse duration of 28 ns, as reported in [28], and it was found that the damage fluence becomes lower as the pump pulse duration (τ_p) reduces, following a $\tau_p^{1/2}$ law [18].

2.6 State-of-the-art of OP-GaAs optical parametric devices

To date, various OP-GaAs OPDs have been reported covering the wavelength region from 2.3 μm up to ~14 μm, as tabulated in Table 2.6.1. Almost all OP-GaAs OPDs have been carried out in either the nanosecond or femtosecond regime, apart from Ref. [29] working in a picosecond regime. In this picosecond work, although a remarkable ~80 kW of peak power was achieved, its corresponding average power was not provided in the letter but can be inferred to be <1 mW (with a maximum 5 kHz repetition rate determined by its pump source (Spectra-Physics OPA-800)). Therefore, development of picosecond mid-IR laser sources still remains an area in need of exploration.

Table 2.6.1. A survey of reported OP-GaAs OPDs.

	OPD type	OPD wavelength (μm)	OP-GaAs period (μm)	OP-GaAs length (mm)	Temporal regime	Maximum Output	Peak power (kW)	Pump source
Ref.[29]	OPG	4.5-10.7	166.6	17.5	1 ps/NA	80 nJ/ NA	80	OPA
Ref.[30]	OPG	2.8/6.9	NA	34	NA/41 kHz	2 μJ/ 0.082 W	NA	Tm,Ho: fibre laser
Ref.[31]	OPA	3.9/4.5	63.8	41	30 ns/20 kHz	35 μJ/ ~0.7 W	1.2	Ho:YAG laser
Ref.[32]	OPA	3.9/4.4	60.5	25	71 ns/1 kHz	101 μJ/ 0.101 W	1.4	Ho:YLF laser
Ref.[33]	OPO	3-6	60.5	0.5	70 fs/98.56 MHz	NA	NA	TDF laser
Ref.[13]	OPO	2.6-7.5	51.5	0.5	90 fs/115 MHz	0.63 nJ/ 0.073 W	7	TDF laser
Ref.[14]	OPO	2.6-6.1	60.5	0.5	93 fs/75 MHz	0.49 nJ/ 0.037 W	5.3	TDF laser
Ref.[34]	OPO	4.4-5.4	92	0.5	100 fs/182 MHz	0.055 nJ/ 0.01 W	0.55	Cr:ZnSe laser
Ref.[35]	OPO	3.3-5	53	0.5	100 fs/418 MHz	0.19 nJ/ ~0.08 W	0.96	TDF laser

Ref.[36]	OPO	3.6-5.6	92	0.5	130 fs/175 MHz	0.62 nJ/ 0.11 W	4.8	Cr:ZnS laser
Ref.[37]	OPO	3.8	53	0.5	157 fs/110 MHz	1.25 nJ/ 0.137 W	8	TDF laser
Ref.[38]	OPO	2.3-9.1	61.2	11	6 ns/10 Hz	3 μJ/ 3×10^{-5} W	0.5	PPLN OPO
Ref.[39]	OPO	4-14.2	150	20	20 ns/2 kHz	7 μJ/ 0.014 W	0.35	PPLN OPO
Ref.[26]	OPO	4.8 / 6.7	130	11	26 ns/100 Hz	3 μJ/ 3×10^{-4} W	0.1	PPLN OPO
Ref.[28]	OPO	3.4/5.2	62	16	28 ns/10 kHz	44.3 μJ/ 0.443 W	1.58	Tm:Ho:YLF laser
Ref.[40]	OPO	10.3-10.9	72.6	10	36 ns/100 Hz	2 μJ 0.0002 W	0.55	Tm:YAP microlaser
Ref.[41]	OPO	8.5-11.5	76-84	15.4	~50 ns/500 Hz	~100 μJ 0.05 W	~2	Tm,Ho:YLF laser
Ref.[30]	OPO	2.8/6.9	NA	19	57 ns/41 kHz	31.7 μJ/ 1.3 W	0.56	Tm,Ho: fibre laser
Ref.[42]	OPO	~3-5	63	20	65 ns/20 kHz	143 μJ/ 2.85 W	2.2	Ho:YAG laser
Ref.[43]	OPO	3-5	63	20	70 ns/100 kHz	77 μJ/ 7.7 W	1.1	Ho:YAG laser
Ref.[12]	OPO	2.4/10.6	74.5	40	100 ns/50 kHz	16 μJ/ 0.8 W (idler)	0.16	TDF laser
Ref.[44]	OPO	3.8/4.7	63.5	39.7	CW	5.3 W	0.0053	Ho:YAG laser

According to the information of Table 2.6.1, we can see that if targeting longer wavelengths (>7 μm) in the mid-IR, a larger OP-GaAs period is required, and the generated average output power is typically low (<0.1 W). For nanosecond OPDs, centimetre scale lengths of OP-GaAs are frequently used, while <1 mm length of OP-GaAs is employed for femtosecond OPDs in order to enlarge the pump acceptance bandwidth. For the picosecond OPDs developed in this thesis, a compromise between commercial availability and pump acceptance bandwidth determines the lengths used, as will be discussed in section 2.9.2.

The pump sources for previously developed OP-GaAs OPDs include bulk lasers (Tm, Ho, Cr doped), other OPDs (PPLN based), and fibre lasers (Tm, Ho doped). In this thesis we chose to use picosecond TDF laser pump sources as they enable us to reach relatively high average powers and pulse energies (compared to femtosecond pulses), while still accessing the ultrashort pulse application regime and benefitting from the efficiency, beam quality, and robustness of a diode-pumped nearly all-fibre pump system.

2.7 Thulium-doped fibre lasers and gain-switching

TDF lasers, which operate at 1.9-2.1 μm, attract great attention owing to properties that include broad tunability, high efficiency, and potential for short-pulse operation. TDF lasers have important applications in bio-medical treatment, spectroscopy and nonlinear frequency conversion [45-48]. Specifically, TDF lasers can be used as efficient pump sources for mid-IR OPOs, as already presented in Table 2.6.1. The two main pump bands for TDF lasers are 780-800 nm and 1550-1750 nm. 780-800 nm pumping can achieve a quantum efficiency of more than 100% for the $^3F_4 \rightarrow {}^3H_6$ laser transition owing to the well-known "2 for 1" cross-relaxation process [49]. This pump band also takes advantages of the maturation of 0.8-μm diode technology, due to the large market for pumping Tm- and neodymium-doped crystals [50]. In contrast, 1550-1750 nm pumping normally relies on erbium/ytterbium-doped fibre sources operating at ~1.55 μm. These sources can offer high-power, high-brightness, pump light for TDF lasers.

Scaling the peak power of short-pulse TDF lasers is desirable for pumping OPDs and many works have been carried out in this area in recent years, as depicted in Table 2.7.1. The TDFs with the highest peak powers have generally been demonstrated in master oscillator power amplifier (MOPA) configurations. However, their seed lasers are normally rather complicated Q-switched or mode-locked sources, and the amplifiers often involve advanced fibre rod structures to access the highest powers. In this work we rely on a much simpler configuration, namely amplification of a gain-switched laser diode. In previous work, the workers at the Optoelectronics Research Centre (ORC) have demonstrated a 100-kW peak power from a TDF MOPA (Tm:MOPA) using a standard large-mode-area step-index TDF (25 μm), directly seeded by a gain-switched laser diode, meanwhile utilising it as a pump system for nonlinear SC generation in fluoride fibres [51].

Table 2.7.1. Comparison of power scaling of TDF lasers in different temporal regimes.

	Peak power	Fibre core diameter	Fibre type	Seed source	Ref.
Nanosecond	1 MW	80 μm	Photonic crystal fibre rod	Q-switched fibre laser	[52]
Picosecond	231 kW	80 μm	Photonic crystal fibre rod	Mode-locked fibre laser	[53]
Femtosecond	2 GW	81 μm	Fibre rod	Mode-locked fibre laser	[54]
Picosecond	100 kW	25 μm	Standard TDFs	Gain-switched diode	[51]

Gain-switching is a versatile technique for pulse generation (from picoseconds to microseconds) by which the gain in a laser diode is modulated by the injection current. The laser diode is typically biased by a constant current that is below lasing threshold current and then, as an electric pulse is imposed upon it, the carrier density increases. Once the diode reaches its threshold, an optical pulse will be generated from the laser diode. The pulse shape and duration depends strongly on the electric pulses, as depicted in Fig. 2.7.1 (based on the theory in [55, 56]). It shows three gain-switched optical pulses and corresponding carrier densities, with increasing duration of ideal, rectangular, electric pulses. If employing a long electric pulse (red, blue line in Fig. 2.7.1), a relaxation oscillation occurs with several peaks sitting on the leading edge of the optical pulse [57]. In contrast, a single-peak pulse can be generated if an appropriate duration of the electrical pulse imposed (black line in Fig. 2.7.1).

In this thesis, we use gain-switched diodes as simple and versatile sources for Tm:MOPA seeding, and eventually as pump sources for OP-GaAs OPDs. A single-peak picosecond gain-switched pulse operation was used in most of the work reported here, Chapters 3 to 6, as it enables a high peak power from the Tm:MOPA system. A longer gain-switched pulse is also used and for the variable pulse-duration OPDs, as described in Chapter 7.

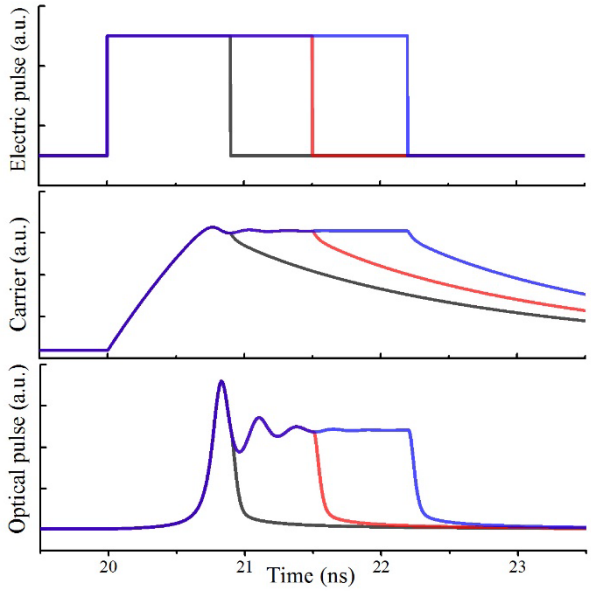

Fig. 2.7.1. Typical gain-switched optical pulses and their corresponding electric pulses and carrier density in laser diode.

2.8 Nonlinearity in fibre amplifiers - self-phase modulation and modulation instability

In an ideal standard solid-core optical fibre, the centrosymmetric structure determines the disappearance of the second-order nonlinearity (Equation 2.2.1), and thus the third-order nonlinearity becomes the dominant effect. For an optical pulse propagating through an optical fibre, a nonlinear length L_{NL} is defined to describe the length over which the third-order nonlinearity becomes significant, as expressed by [58]

$$L_{NL} = \frac{1}{P_0 \gamma} \tag{2.8.1}$$

where P_0 is the peak power of the optical signal pulse propagating in the fibre, and γ is nonlinear parameter. The nonlinear parameter is related to nonlinear-index coefficient n_2, the signal carrier frequency ω_0, the speed of light in vacuum c, and the signal mode field area in the fibre A_{eff}, and it is given by

$$\gamma = \frac{n_2 \omega_0}{c A_{eff}} \tag{2.8.2}$$

A similar counterpart dispersion length, which describes the length over which the dispersion starts to play a role, is defined by

$$L_D = \frac{T_0^2}{|\beta_2|} \tag{2.8.3}$$

where T_0 is the input pulse duration, and β_2 represents group velocity dispersion.

If the fibre length L is much less than L_{NL} or L_D, the nonlinear or dispersive effects can be neglected during signal light propagation, and inversely the nonlinear or dispersive effects become significant as the fibre length is comparable or larger than L_{NL} or L_D, respectively. As stated before, high-power picosecond fibre amplifier systems are a main feature of this thesis. Applying estimated values of T_0=10 ps and $\beta_2 \sim$ -20 ps^2/km (for standard TDFs [59]) into Eq. 2.8.3, an L_D of ~5 km is obtained, which is much greater than a typical length of fibre in an amplifier chain. Hence, dispersive effects are considered to be ignorable in this thesis. In contrast, nonlinear effects need to be investigated due to the high peak powers (at kilowatts level) in the picosecond system leading to values of L_{NL} of the order of a few meters.

SPM is one of the most important nonlinear effects occurring in optical fibres. It can be interpreted by a general solution of the nonlinear Schrödinger equation, neglecting dispersion effects and fibre losses:

$$U(L,T) = U(0,T)e^{i\phi_{NL}(L,T)} \tag{2.8.4}$$

where $U(L,T)$ is the field amplitude at a position $z=L$ and a time $t=T$, $U(0,T)$ is the field amplitude at the initial position $z=0$, and ϕ_{NL} is nonlinear phase term that can expressed by

$$\phi_{NL}(L,T) = |U(0,T)|^2 \frac{L}{L_{NL}} \tag{2.8.5}$$

Eq. 2.8.4 and 2.8.5 describe that the propagating signal pulse shape is determined by the initial pulse shape and remains unchanged, whilst its phase changes with the fibre length L, the nonlinear length L_{NL}, and specifically the pulse amplitude $U(0,T)$ itself. Consequently, this is a self-phase-modulation phenomenon, and it leads to a change in the spectral domain and a constant shape in temporal domain. Fig. 2.8.1 shows a typical spectral evolution over distance computed using the nonlinear Schrödinger equations and assuming an initially non-chirped Gaussian pulse. Spectral bandwidth broadening and spectral peak modulation is theoretically predicted as the optical pulse propagating along an optical fibre.

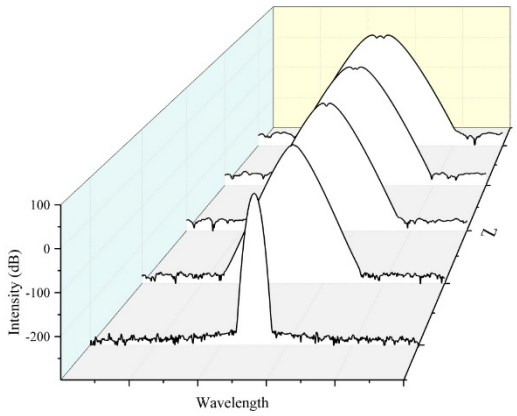

Fig. 2.8.1. Spectral evolution induced by self-phase modulation.

MI is another nonlinear phenomenon that needs to be considered. It originates from perturbation in background noise, but it can only have a power gain in the anomalous dispersion regime of optical fibres [58]. Since 2-μm-wavelength TDF amplifiers naturally work in the anomalous dispersion regime for standard silica-based fibres, MI can affect the performance of TDF lasers or amplifiers. The gain spectra of MI is given by

$$g(\Omega) = |\beta_2 \Omega|(\frac{4}{|\beta_2| L_{NL}} - \Omega^2)^{1/2} \quad (2.8.6)$$

where Ω is the frequency shift from the central frequency. Figure 2.8.2 shows a typical gain spectra of MI in optical fibres calculated using the above equation. It appears on the both side of central frequency with a symmetric nature. Because it comes from background noise, specifically in TDF lasers or amplifiers, a broader SPM spectra can be deemed as an initial seed for MI.

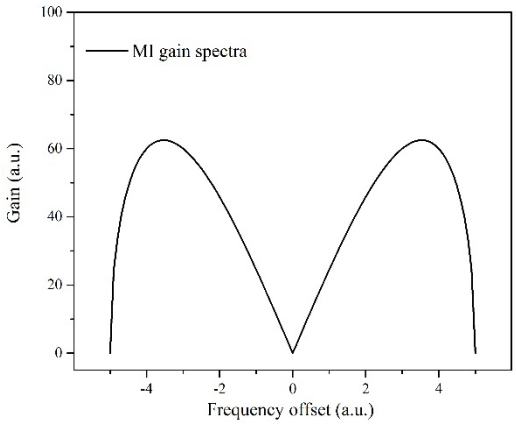

Fig. 2.8.2. Typical gain spectra of modulation instability.

2.9 Design considerations for Mid-IR OP-GaAs optical parametric devices

2.9.1 OP-GaAs tuning characteristics

Commercially available 1952, 1992, and 2007-nm laser diodes (Eblana Photonics) were selected as the seed lasers for the OPD pump system. Using the dispersion relations of GaAs [60] and equations 2.3.1, 2.4.1, 2.4.2, we can design a multi-grating OP-GaAs crystal for picosecond mid-IR generation, targeting a wavelength range of 5-6 μm. Tuning can be achieved either by varying the temperature of the OP-GaAs or by selecting a different grating period of the OP-GaAs. With five grating periods: 57, 59, 61, 63, 65 μm, the theoretical tuning ranges of signal and idler are 2.7-3.7 μm and 4.4-7.4 μm, respectively, for a 2007-nm pump (Fig. 2.9.1 (a)), 2.7-3.4 μm and 4.8-7.6 μm, respectively, for a 1992-nm pump (Fig. 2.9.1 (b)), and 2.5-2.9 μm and 5.6-8.3 μm, respectively, for 1952-nm pump (Fig. 2.9.1 (c)).

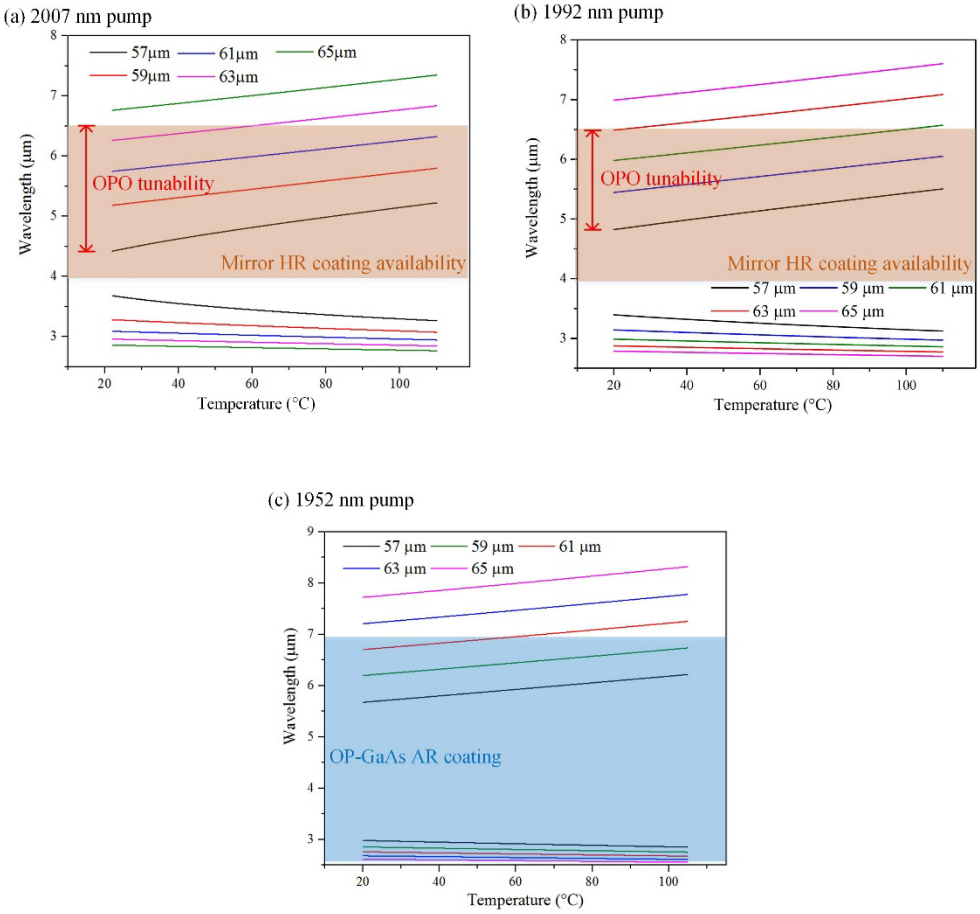

Fig. 2.9.1. Theoretical signal and idler tuning curves at a pump wavelength of 2008 nm (a), 1992 nm (b), and 1952 nm (c).

As mentioned in Chapter 1, the targeted wavelength band (5-6 μm) is not only for general spectroscopic applications but also potentially aimed for power delivery using our in-house fabricated mid-IR HCFs and for pumping a chalcogenide fibre to generate broadband SC further into the mid-IR (Chapter 8). Because these applications often require coupling to optical fibres, a high-beam-quality mid-IR source is strongly desired, and a mid-IR OPO is deemed to be the main target OPD, rather than an OPG or OPA. This is due to the extra spatial-mode control it can deliver for a 5-6 μm idler (in this case) in an idler-resonant OPO cavity. The 2008 or 1992 nm seed laser diodes were selected as the OPO pumping wavelengths because their corresponding tuning curves (Fig. 2.9.1 (a), (b)) can fully cover the target wavelength band of 5-6 μm. However, cavity mirror coating also limits the OPO tunability. The brown shaded areas in Fig. 2.9.1 (a), (b) indicate the commercially available high reflectivity (HR) coating ranges, and the red arrows shows the idler tuning wavelengths that OP-GaAs OPOs can provide.

In terms of the OPGs or OPAs described in this thesis, the main target is to demonstrate the capability of producing high-power at long mid-IR wavelengths, in comparison to previously

reported OP-GaAs devices seen in Table 2.6.1. Therefore, we chose the 1952 nm seed laser diode for the OPG and OPA pump source development, leading theoretically to long-wavelength generation (>8 μm) in the mid-IR, as shown in Fig. 2.9.1 (c). However, the blue shaded area indicates the OP-GaAs anti-reflection (AR) coating range. The output characteristics from the OPG or OPA with wavelengths that are not overlapped with the AR coating range will, to some extent, be affected.

2.9.2 Pump spectral acceptance bandwidth

The pump spectral acceptance bandwidth is the range of pump frequencies that can pump a single signal/idler frequency. For developing a suitable 2-μm pumping source for OP-GaAs OPDs, this pump acceptance bandwidth should be considered. The expression for the pump acceptance bandwidth is [2]

$$\delta\omega_p = \left| \frac{C}{\left(v_p^{-1} - v_{s/i}^{-1}\right)L} \right| \tag{2.9.1}$$

where C is a constant value of 5.56 determined by the FWHM width of the sinc^2 efficiency curve [61] (Fig. 2.2.1), v_p and $v_{s/i}$ are the group velocities ($\partial\omega/\partial k$, calculated by using material dispersion relation) of pump and signal/idler, and L is the crystal length [62]. Equation 2.9.1 can also be interpreted as a measure of the temporal walk-off of the signal and idler pulses from the pump pulse (i.e. it incorporates the difference in group velocities). The crystal length L can be designed to be very short (< 1 mm) when a broad spectral band pumping is required (typically for a femtosecond pumping regime). Fig. 2.9.2 shows that the 2-μm pump acceptance bandwidth of OP-GaAs is inversely proportional to the crystal length. In this thesis, a commercially available OP-GaAs length of 2 cm for the development of mid-IR OPDs was chosen, resulting in a requirement that the spectral linewidth of the pump (the Tm:MOPA system) should be less than ~1.5 nm.

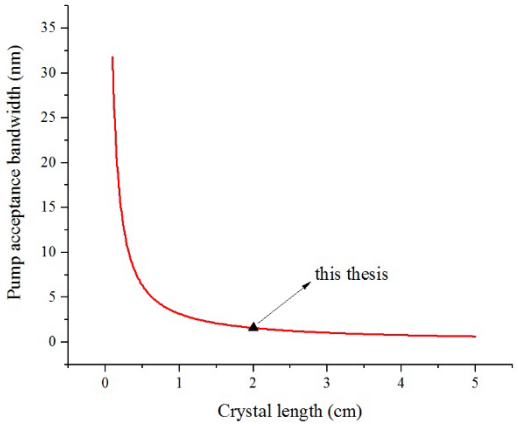

Fig. 2.9.2. Pump acceptance bandwidths versus nonlinear crystal lengths. Triangle: the case for this thesis with a crystal length of 2 cm.

2.9.3 Temporal and spatial walk-off

Temporal walk-off describes the fact that, in general, the pump, signal and idler pulses travel at different group velocities as they propagate inside the crystal. After a certain length of propagation, the signal and/or idler pulse will separate from the pump pulse in the time domain, such that they stop interacting with each other. If the crystal length is longer than the three wave interaction length, the excess length is unproductive. Ref [63] defines an effective crystal length (or interaction length, L_{eff}) that reflects the temporal walk-off effects on OPDs. L_{eff} is related to the group velocity mismatch in a form of v^{-1}_p - v^{-1}_i, (as already given in the last section) and the pump pulse duration. In this thesis, for a 20-mm length of OP-GaAs crystal, assuming the pump, signal and idler wavelengths of 2, 3, and 6 μm, and expecting the signal and idler pulse durations are similar to that of pump, L_{eff} can be calculated and plotted against pump pulse durations in Fig. 2.9.3. The pump pulses involved in this thesis are no shorter than 46 ps with a corresponding L_{eff} >19.9 mm.

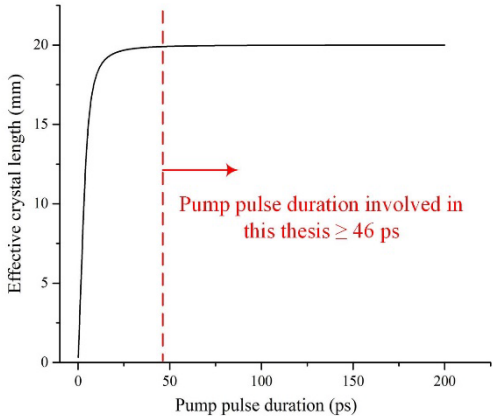

Fig. 2.9.3. Effective crystal lengths with different pump pulse durations.

Spatial walk-off has a similar definition with temporal walk-off but describes the three-wave mismatch in the spatial domain. It originates from birefringence in nonlinear crystals that can lead to a mismatch of Poynting vector for the three waves, hindering the performance of OPDs. However, for OPDs using isotropic crystals, such as OP-GaAs, the spatial walk-off is zero.

2.9.4 Parametric gain and threshold

For a practical OPD, the operating threshold power requirement is obviously an essential factor to be considered. A theoretical threshold value provides a guidance for designing the OPD and developing its pump source.

Solving Equations 2.2.3-2.2.5, and assuming no pump depletion and no losses, the incremental gain G^{inc} in the three-wave mixing processes is given by [2]

$$G^{inc} = \left|\frac{E_s(L)}{E_s(0)}\right|^2 - 1 = \Gamma^2 L^2 \frac{sinh^2(gL)}{(gL)^2} \tag{2.9.2}$$

where

$$\mathrm{g} = \sqrt{\Gamma^2 - (\Delta k/2)^2} \tag{2.9.3}$$

$$\Gamma^2 = \frac{2\omega_s \omega_i d_{eff}^2 I_p}{n_s n_i n_p \varepsilon_0 c^3} \tag{2.9.4}$$

where L is the length of nonlinear material (OP-GaAs, in this thesis), I_p is pump intensity, and ε_0 is permittivity of free space.

In OPGs, parametric signals are initialised and generated from spontaneous quantum noise (at ~nW power level), so that no threshold is exhibited in principle. However, Ref. [25, 29] offers a practical method to estimate the "observable OPG threshold" with a semi-empirical gain factor of ~10^{10} (ie. G^{inc}=10^{10}) when parametric outputs are easy to be observed by general measurement tools. P. S. Kuo et al. used this method for an OP-GaAs OPG threshold calculation and found good consistency between experimental and theoretical results [29]. For this thesis, with a pump at 1952 nm, and assuming no phase mismatch, the theoretical OP-GaAs gain at different pump power intensity thresholds and different signal wavelengths (2940, 2740, and 2550 nm) can be obtained, as shown in Fig.2.9.4. A lower intensity threshold of 164 MW/cm^2 is estimated at 2940 nm than that of 178 MW/cm^2 at 2550 nm. Assuming a repetition rate of 1 MHz, a pulse duration of 50 ps and a beam waist of 80 μm, an estimated threshold peak power of ~33 kW and average power of ~1.6 W are obtained at

a signal wavelength of 2940 nm. Reaching an OPG threshold means that the generated signal and idler can achieve a macroscopic level after amplification from quantum noise. If applying an external seed for signal or idler (OPA cases), a tangible signal and idler output can be obtained at a pump power intensity considerably lower than the OPG threshold pump power intensity.

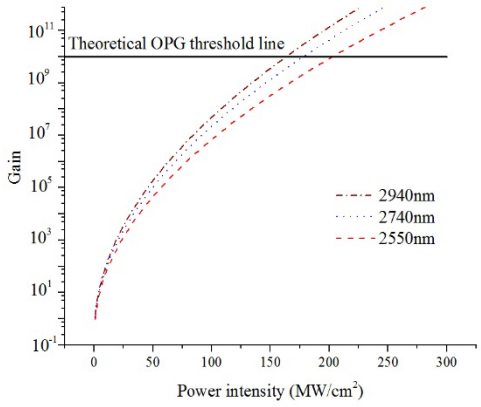

Fig 2.9.4. Parametric gain at different pump power intensities and at signal wavelengths of 2940, 2740, and 2550 nm.

For calculating thresholds in OP-GaAs OPOs, a plane-wave, CW OPO case is first considered. In the low-gain limit of such OPOs, the threshold can be reached when the gain per pass can compensate round-trip losses, and is given by [2]

$$G^{inc} \approx \Gamma^2 L^2 sinc^2\left(\frac{\Delta kL}{2}\right) = \varepsilon \tag{2.9.5}$$

where ε is the round-trip loss for either resonant signal or idler.

However, in practice, the three interacting waves are normally focused for pumping nonlinear materials rather than being plane waves. Guha has derived a gain expression for the low-gain-limit with focused CW wave beams [64]. Before discussing his expression, two parameters should be introduced [2]:

$$\xi = L/\mathrm{b} \tag{2.9.6}$$

$$\mathrm{b} = 2\pi\, n\, w_0^2/\lambda \tag{2.9.7}$$

where w_0 is the radius of the focusing beam waist. ξ is called the focusing factor. ξ=1 is the well-known condition called confocal focusing, whereas ξ>1 and ξ<1 represent tight and loose focusing, respectively. For a signal-resonant OPO, the incremental signal power gain per pass given by Guha is then [64]

$$G^{inc} = \frac{128\pi^2 d_{eff}^2 L}{n_p n_s \lambda_i^2 \lambda_s c \varepsilon_0} P_p \xi_s \, \mathrm{Re}(h_2) \tag{2.9.8}$$

where P_p represents the pump power, ξ_s is the signal focusing factor, and h_2 is a complex parameter introduced by Guha, whose real part depends on focusing factors and working wavelengths.

Hanna et al. [65] considered synchronous pumping rather than CW pumping, and modified Guha's expression (equation 6.8) by introducing two factors; One factor is the effective length of nonlinear material, L_{eff}, related to temporal walk-off (demonstrated in last section) which becomes a significant factor for pump pulses durations typically less than < 1 ps [63]. The other parameter, g_t, corresponds to averaging of the gain due to the temporal pulse shape. For Gaussian-shaped pulses, g_t is given by $\tau_p^2/(\tau_p^2 + \tau_s^2)$, where τ_p, τ_s are pulse durations of pump and signal, respectively. Applying this to the idler-resonant OPO case, the modified incremental gain expression becomes,

$$G^{inc} = \frac{128\pi^2 d_{eff}^2 L_{eff} g_t}{n_p n_i \lambda_s^2 \lambda_i c \varepsilon_0} P_p \xi_i \, \mathrm{Re}(h_2) \tag{2.9.9}$$

By using the gain-equal-loss relation, this modified gain expression has been used to calculate the threshold of SPOPOs with good agreement with experimental results [65]. Taking an example of our OP-GaAs case, λ_p=2008 nm, λ_i=6000 nm, n_p=3.351, n_i=3.304, L=2 cm, τ_p=100 ps, τ_s=100 ps, the theoretical average-power threshold under different focusing conditions against fractional idler power losses per round trip is plotted in Fig. 2.9.5, assuming a repetition rate of 100 MHz. The requirement for partial output coupling of the idler beam from the OPO cavity is a loss factor that increases the oscillation threshold. According to Fig. 2.9.5, when low pump powers are available (<5 W), confocal focusing or somewhat tighter is preferred due to the need for a relatively low threshold, whereas a looser focusing is useful when having sufficient pump powers and there is a need to avoid thermal effects and/or potential crystal damage.

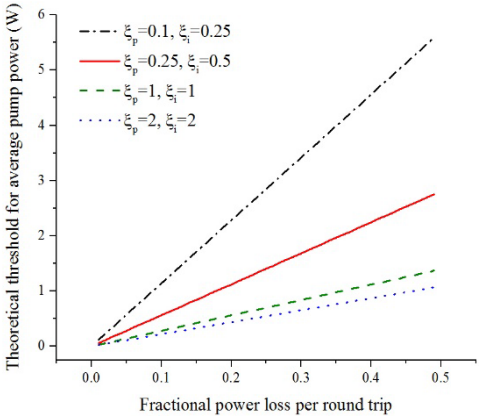

Fig. 2.9.5. Theoretical thresholds for average pump power of idler-resonant OP-GaAs OPOs under different focusing conditions.

2.10 Summary

This chapter has provided an overview of the background and theory related to the work described in this thesis, with an emphasis on the recent advances in OP-GaAs OPDs. The design considerations for such OPDs are given, and will be used in the following chapters where OPDs are experimentally investigated. The experimental performance of the OPDs will also be compared to the theoretical expectations developed here, such as the tuning characteristics and operating thresholds.

Reference

[1] P. A. Franken *et al.*, "Generation of optical harmonics," *Physical Review Letters*, vol. 7, no. 4, pp. 118-119, 1961.

[2] R. W. Boyd, *Nonlinear Optics*: Academic press, 2019.

[3] D. S. Hum, and M. M. Fejer, "Quasi-phasematching," *Comptes Rendus Physique*, vol. 8, no. 2, pp. 180-198, 2007.

[4] V. Kemlin *et al.*, "Widely tunable optical parametric oscillator in a 5 mm thick 5% MgO:PPLN partial cylinder," *Optics Letters*, vol. 38, no. 6, pp. 860-862, 2013.

[5] G. Cerullo, and S. D. Silvestri, "Ultrafast optical parametric amplifiers," *Review of Scientific Instruments*, vol. 74, no. 1, pp. 1-18, 2003.

[6] G. C. Bhar *et al.*, "Nonlinear optical laser devices using GaSe," *Applied Physics B*, vol. 61, no. 2, pp. 187-190, 1995.

[7] H. D. Riccius, and K. J. Siemsen, "Up-conversion of CO laser lines by difference-frequency mixing in proustite (Ag_3AsS_3)," *Physics Letters A*, vol. 45, no. 5, pp. 377-378, 1973.

[8] L. Gordon *et al.*, "Diffusion-bonded stacked GaAs for quasiphase-matched second-harmonic generation of a carbon dioxide laser," *Electronics Letters*, vol. 29, no. 22, pp. 1942-1944, 1993.

[9] Y. S. Wu, "Improved GaAs bonding process for quasi-phase-matched second harmonic generation," *Journal of The Electrochemical Society*, vol. 145, no. 1, pp. 366, 1998.

[10] M. J. Angell *et al.*, "Growth of alternating <100>/<111> - oriented II - VI regions for quasi - phase - matched nonlinear optical devices on GaAs substrates," *Applied Physics Letters*, vol. 64, no. 23, pp. 3107-3109, 1994.

[11] P. G. Schunemann, "New nonlinear optical crystals for the mid-infrared," in *Advanced Solid State Lasers Conference (ASSL)*, Berlin, 2015, pp. AM2A.2.

[12] J. Wueppen *et al.*, "1.95 μm-pumped OP-GaAs optical parametric oscillator with 10.6 μm idler wavelength," *Optics Letters*, vol. 41, no. 18, pp. 4225-4228, Sep. 2016.

[13] V. O. Smolski *et al.*, "Coherence properties of a 2.6–7.5 μm frequency comb produced as a subharmonic of a Tm-fiber laser," *Optics Letters*, vol. 41, no. 7, pp. 1388-1391, Apr. 2016.

[14] N. Leindecker *et al.*, "Octave-spanning ultrafast OPO with 2.6-6.1μm instantaneous bandwidth pumped by femtosecond Tm-fiber laser," *Optics Express*, vol. 20, no. 7, pp. 7046-7053, Mar. 2012.

[15] V. V. Badikov *et al.*, "Crystal growth and characterization of a new quaternary chalcogenide nonlinear crystal for the mid-infrared: $PbGa_2GeSe_6$," *Crystal Growth & Design*, vol. 19, no. 8, pp. 4224-4228, 2019.

[16] W. Huang *et al.*, "Polycrystal synthesis, crystal growth, structure, and optical properties of $AgGaGe_nS_{2(n+1)}$ (n = 2, 3, 4, and 5) single crystals for mid-IR laser applications," *Inorganic Chemistry*, vol. 58, no. 9, pp. 5865-5874, 2019.

[17] S. Das, "Optical parametric oscillator: status of tunable radiation in mid-IR to IR spectral range based on $ZnGeP_2$ crystal pumped by solid state lasers," *Optical and Quantum Electronics*, vol. 51, no. 3, pp. 70, 2019.

[18] A. Grisard *et al.*, "Quasi-phase-matched gallium arsenide for versatile mid-infrared frequency conversion," *Optical Materials Express*, vol. 2, no. 8, pp. 1020-1025, 2012.

[19] D. N. Nikogosyan, *Nonlinear optical crystals: a complete survey*: Springer Science & Business Media, 2006.

[20] L. Gonzalez *et al.*, "Second Harmonic Generation in $CdSiP_2$," *Proceedings of SPIE - The International Society for Optical Engineering*, 2009.

[21] P. G. Schunemann *et al.*, "$CdSiP_2$: a new nonlinear optical crystal for 1- and 1.5-micron-pumped mid-IR generation," in *Advanced Solid-State Photonics*, Denver, Colorado, 2009, pp. TuC6.
[22] J. Wei *et al.*, "Measurement of refractive indices of $CdSiP_2$ at temperatures from 90 to 450 K," *Optical Materials Express*, vol. 8, no. 2, pp. 235-244, 2018.
[23] L. E. Myers *et al.*, "Multigrating quasi-phase-matched optical parametric oscillator in periodically poled $LiNbO_3$," *Optics Letters*, vol. 21, no. 8, pp. 591-593, 1996.
[24] J. R. Schwesyg *et al.*, "Optical loss mechanisms in magnesium-doped lithium niobate crystals in the 300 to 2950 nm wavelength range," in *Advances in Optical Materials*, Istanbul, 2011, pp. AIThE3.
[25] I. T. Sorokina, and K. L. Vodopyanov, *Solid-State Mid-Infrared Laser Sources*: Springer Science & Business Media, 2003.
[26] P. S. Kuo *et al.*, "GaAs optical parametric oscillator with circularly polarized and depolarized pump," *Optics Letters*, vol. 32, no. 18, pp. 2735-2737, 2007.
[27] W. A. Clarkson *et al.*, "Simple method for compensation of thermally-induced birefringence in high-power solid-state lasers," in *CLEO/Europe Conference on Lasers and Electro-Optics*, 1998, pp. 151-151.
[28] P. G. Schunemann *et al.*, "2.05-μm-laser-pumped orientation-patterned gallium arsenide (OPGaAs) OPO," in *Conference on Lasers and Electro-Optics/Quantum Electronics and Laser Science and Photonic Applications Systems Technologies*, Baltimore, Maryland, 2005, pp. CThQ4.
[29] P. S. Kuo *et al.*, "Optical parametric generation of a mid-infrared continuum in orientation-patterned GaAs," *Optics Letters*, vol. 31, no. 1, pp. 71-73, Jan. 2006.
[30] B. Donelan *et al.*, "OPG and OPO Nonlinear Conversion in OP-GaAs using 2 μm Single Oscillator Pump Sources," in *Nonlinear Optics*, Waikoloa, Hawaii, 2017, pp. NTu2A.2.
[31] G. Bloom *et al.*, "Optical parametric amplification of a distributed-feedback quantum-cascade laser in orientation-patterned GaAs," *Optics Letters*, vol. 35, no. 4, pp. 505-507, Feb. 2010.
[32] D. French *et al.*, "Energy-scalable pulsed mid-IR source using orientation-patterned GaAs," *Optics Letters*, vol. 36, no. 4, pp. 496-498, Feb. 2011.
[33] K. F. Lee *et al.*, "Carrier envelope offset frequency of a doubly resonant, nondegenerate, mid-infrared GaAs optical parametric oscillator," *Optics Letters*, vol. 38, no. 8, pp. 1191-1193, 2013.
[34] K. L. Vodopyanov *et al.*, "Mid-IR frequency comb source spanning 4.4–5.4 μm based on subharmonic GaAs optical parametric oscillator," *Optics Letters*, vol. 36, no. 12, pp. 2275-2277, 2011.
[35] K. F. Lee *et al.*, "Midinfrared frequency comb from self-stable degenerate GaAs optical parametric oscillator," *Optics Express*, vol. 23, no. 20, pp. 26596-26603, Oct. 2015.
[36] V. O. Smolski *et al.*, "Cr:ZnS laser-pumped subharmonic GaAs optical parametric oscillator with the spectrum spanning 3.6-5.6 μm," *Optics Letters*, vol. 40, no. 12, pp. 2906-2908, Jun. 2015.
[37] O. H. Heckl *et al.*, "Three-photon absorption in optical parametric oscillators based on OP-GaAs," *Optics Letters*, vol. 41, no. 22, pp. 5405-5408, Nov. 2016.
[38] K. L. Vodopyanov *et al.*, "Optical parametric oscillation in quasi-phase-matched GaAs," *Optics Letters*, vol. 29, no. 16, pp. 1912-1914, 2004.
[39] K. L. Vodopyanov *et al.*, "Grating tunable 4 - 14 μm GaAs optical parametric oscillator pumped at 3 μm," *Optics Express*, vol. 22, no. 4, pp. 4131-4136, Feb. 2014.
[40] Q. Clément *et al.*, "Longwave infrared, single-frequency, tunable, pulsed optical parametric oscillator based on orientation-patterned GaAs for gas sensing," *Optics Letters*, vol. 40, no. 12, pp. 2676-2679, Jun. 2015.

[41] R. K. Feaver *et al.*, "Longwave-IR optical parametric oscillator in orientation-patterned GaAs pumped by a 2 μm Tm,Ho:YLF laser," *Optics Express,* vol. 21, no. 13, pp. 16104-16110, 2013.
[42] C. Kieleck *et al.*, "High-efficiency 20–50 kHz mid-infrared orientation-patterned GaAs optical parametric oscillator pumped by a 2 μm holmium laser," *Optics Letters,* vol. 34, no. 3, pp. 262-264, 2009.
[43] A. Hildenbrand *et al.*, "Compact efficient mid-infrared laser source: OP-GaAs OPO pumped by Ho^{3+}: YAG laser," in *Proc. SPIE 8187*, 2011, pp. 81870H.
[44] P. G. Schunemann *et al.*, "CW mid-IR OPO based on OP-GaAs," in *2013 Conference on Lasers and Electro-Optics - International Quantum Electronics Conference*, Munich, 2013, pp. JSII_2_3.
[45] N. M. Fried, and K. E. Murray, "High-power thulium fiber laser ablation of urinary tissues at 1.94 μm," *Journal of Endourology,* vol. 19, no. 1, pp. 25-31, 2005.
[46] S. Ishii *et al.*, "Coherent 2 μm differential absorption and wind lidar with conductively cooled laser and two-axis scanning device," *Applied Optics,* vol. 49, no. 10, pp. 1809-1817, 2010.
[47] I. Mingareev *et al.*, "Welding of polymers using a 2μm thulium fiber laser," *Optics & Laser Technology,* vol. 44, no. 7, pp. 2095-2099, 2012.
[48] A. M. Heidt *et al.*, "High power diode-seeded fiber amplifiers at 2 μm—from architectures to applications," *IEEE Journal of Selected Topics in Quantum Electronics,* vol. 20, no. 5, pp. 525-536, 2014.
[49] D. J. Richardson *et al.*, "High power fiber lasers: current status and future perspectives [Invited]," *Journal of the Optical Society of America B,* vol. 27, no. 11, pp. B63-B92, 2010.
[50] S. Christensen *et al.*, "Developments in thulium-doped fiber lasers offer high powers," in *21st annual meeting of the LEOS, IEEE Lasers and Electro-Optics Society,* 2008, pp. 121569145.
[51] A. M. Heidt *et al.*, "100 kW peak power picosecond thulium-doped fiber amplifier system seeded by a gain-switched diode laser at 2 μm," *Optics Letters,* vol. 38, no. 10, pp. 1615-1617, 2013.
[52] C. Gaida *et al.*, "Amplification of nanosecond pulses to megawatt peak power levels in Tm^{3+}-doped photonic crystal fiber rod," *Optics Letters,* vol. 38, no. 5, pp. 691-693, 2013.
[53] S. Guillemet *et al.*, "High energy sub-nanosecond thulium-doped all-fibre laser based on a rod-type photonic-crystal fibre amplifier," in *Advanced Solid State Lasers*, Berlin, 2015, pp. ATh2A.27.
[54] C. Gaida *et al.*, "Thulium-doped fiber chirped-pulse amplification system with 2 GW of peak power," *Optics Letters,* vol. 41, no. 17, pp. 4130-4133, 2016.
[55] P. Paulus *et al.*, "Generation and optimum control of picosecond optical pulses from gain-switched semiconductor lasers," *IEEE Journal of Quantum Electronics,* vol. 24, no. 8, pp. 1519-1523, 1988.
[56] D. Pataca *et al.*, "Gain-switched DFB lasers," *Journal of Microwaves and Optoelectronics,* vol. 1, pp. 46-63, 1997.
[57] K. Y. Lau, "Gain switching of semiconductor injection lasers," *Applied Physics Letters,* vol. 52, no. 4, pp. 257-259, 1988.
[58] G. P. Agrawal, *Nonlinear Fiber Optics*: Academic press, 2012.
[59] S. Kharitonov *et al.*, "Kerr nonlinearity and dispersion characterization of core-pumped thulium-doped fiber at 2 μm," *Optics Letters,* vol. 41, no. 14, pp. 3173-3176, 2016.
[60] T. Skauli *et al.*, "Improved dispersion relations for GaAs and applications to nonlinear optics," *Journal of Applied Physics,* vol. 94, no. 10, pp. 6447-6455, 2003.

[61] H. Hung, “An adaptive mid-infrared ultrashort pulse source for applications in coherent control,” *PhD thesis, University of Southampton*, 2008.
[62] F. Kienle, “Advanced high-power optical parametric oscillators synchronously pumped by ultrafast fibre-based sources,” *PhD thesis, University of Southampton*, 2012.
[63] M. J. McCarthy, and D. C. Hanna, “All-solid-state synchronously pumped optical parametric oscillator,” *Journal of the Optical Society of America B*, vol. 10, no. 11, pp. 2180-2190, 1993.
[64] S. Guha, “Focusing dependence of the efficiency of a singly resonant optical parametric oscillator,” *Applied Physics B*, vol. 66, no. 6, pp. 663-675, 1998.
[65] D. C. Hanna *et al.*, “Synchronously pumped optical parametric oscillator with diffraction-grating tuning,” *Journal of Physics D: Applied Physics*, vol. 24, no. 16, pp. 2440, 2001.

Chapter 3

High-peak-power, picosecond, mid-infrared optical parametric generator and amplifier based on OP-GaAs

3.1 Introduction

Optical parametric generators (OPGs), with their simple single-pass nature, are very attractive as compact devices that are less costly and less sensitive to external perturbations than other optical parametric devices (OPDs). OPGs based on orientation-patterned gallium arsenide (OP-GaAs) have previously been studied to realise mid-IR continuum from 4.5 to 10.7 μm working in the picosecond regime (1 ps) but with relatively low output pulses energies of ~80 nJ [1]. Another nanosecond OP-GaAs OPG was reported with a higher total output pulse energy of 2 μJ at signal and idler wavelengths of 2.80 and 6.88 μm, but with a low average power of 82 mW [2].

OPGs injected by external seed lasers can work as optical parametric amplifiers (OPAs), thereby combining the spectral and spatial (beam-quality) characteristics of the seed while taking advantage of the high gain that nonlinear frequency-conversion techniques can offer. The first OPA based on OP-GaAs was realised by seeding with a 4.5-μm quantum-cascade laser (QCL) and pumping with a Ho:YAG Q-switched laser [3]. The OPA provided a gain of 53-dB and generated 30-ns pulses with a peak power of 580 W. In later work, [4], a QCL-seeded thulium-doped fibre (TDF) -laser-pumped OP-GaAs OPA was demonstrated with a tuning range from 8 to 10 μm and output pulses with ~30 ns duration. The output peak power, however, was reported to be less than 200 W. To date OP-GaAs OPAs working in the ultrafast regime, i.e. picosecond and shorter, have not been demonstrated.

In this chapter, I first describe the development of the pump source for our OP-GaAs OPG and OPA work: a TDF master oscillator power amplifier (Tm:MOPA) system operating at a

wavelength of 1952 nm, generating 94-ps-duration pulses at 1-MHz repetition rate and employing simple, direct diode-seeded amplification. Secondly, I demonstrate a widely tunable OPG based on OP-GaAs with a tuning range of 2550-2940 nm (signal) and 5800-8300 nm (idler). The maximum average output powers from the OP-GaAs OPG were 260 and 160 mW for the generated signal (2930 nm) and idler (5960 nm), respectively. The corresponding peak powers (and pulse energies) for the signal and idler were 2.7 and 1.7 kW (0.26 and 0.16 μJ), respectively. By injection-seeding with a narrow linewidth continuous-wave (CW) laser for OPA operation, both the output signal and idler spectral linewidth were significantly decreased, and output powers as high as 1.07 W and 0.26 W, for signal (2605 nm) and idler (7785 nm) respectively, were obtained. A maximum peak power of 13.3 kW (signal) and 3.2 kW (idler) was achieved at an overall conversion efficiency of 36%. The corresponding maximum pulse energies for signal and idler were 1.07 μJ and 0.26 μJ, respectively.

The experimental work described in this chapter was carried out in collaboration with Dr. Sijing Liang. Section 3.2 describes building the pump system for the OP-GaAs OPG and OPA, for which the experimental work was mainly conducted by Dr. Liang (more experimental details can be found in Dr. Liang's PhD thesis [5]). Section 3.3 and 3.4 demonstrate the experimental setup and results for the OP-GaAs OPG and OPA, for which the experiment was mainly conducted by the author. Section 3.5 summarises this chapter and gives a concluding remark. The work described in this chapter has previously been published, in part, here [6-9].

3.2 High-peak-power, thulium-doped fibre amplifier system – OPG/OPA pump

3.2.1 Experimental setup

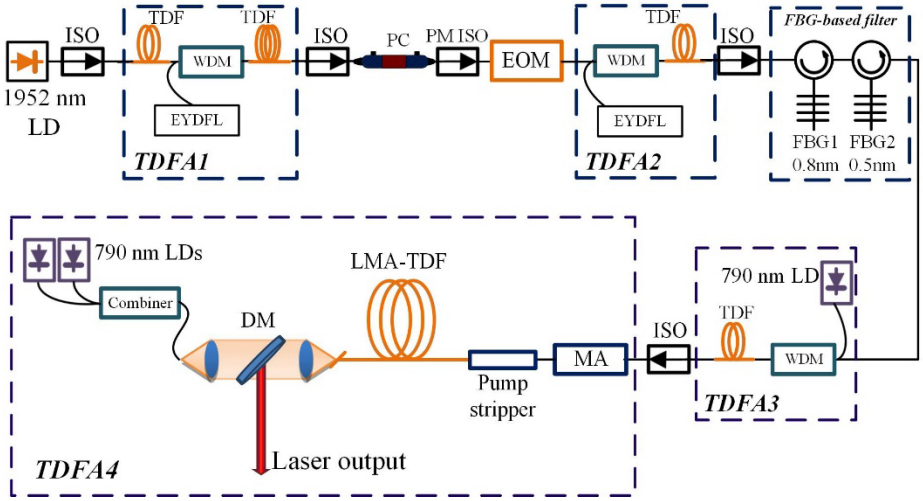

Fig. 3.2.1. Schematic diagram of gain-switched laser diode seeding, Tm:MOPA system. LD: laser diode; ISO: isolator; TDF: thulium doped fibre; TDFA: thulium doped fibre amplifier; WDM: wavelength-division multiplexer; EYDFL: erbium/ytterbium co-doped fibre laser; PC: polarisation controller; PM ISO: polarisation maintaining isolator; EOM: electro-optic modulator; FBG: fibre bragg grating; MA: mode adapter; LMA-TDF: large-mode-area thulium-doped fibre; DM: dichroic mirror.

Figure 3.2.1 shows the schematic of the Tm:MOPA system consisting of a seed laser and four fibre amplifier stages. This system was a non-polarisation maintaining (non-PM) system apart from the seed laser, a PM isolator (PM ISO), and an electro-optic modulator (EOM). The seed laser was a 1952-nm discrete-mode laser diode (Eblana Photonics, EP1948-DM-PM) biased by a 16-mA current (under CW lasing threshold 20 mA) and gain-switched by 5-V electrical pulses (provided by a pulse generator HP 8131A) with a 420-ps duration at a 1-MHz repetition rate, giving a ~1 μW output power and linear-polarised output. After a polarisation insensitive optical isolator, the 1952-nm pulses were first amplified by a core-pumped TDF amplifier (TDFA1, Fig.3.2.1), which consisted of a 8-m-long TDF (OFS TmDF200) forward pumped by a home-made Er/Yb co-doped fibre laser at 1565 nm through a 1565/2000nm wavelength-division multiplexer (WDM). Another piece of 4-m-long TDF was placed between the WDM and the isolator to absorb the backward amplified spontaneous emission (ASE) and to provide more gain at longer wavelengths, similar to the setup described in [10]. TDFA1 provided ~40 dB of gain for the seed pulses, and the excess ASE of TDFA1 was greatly mitigated by the EOM (Photline, MX2000-LN-01), which acted as a time gate to pass only the optical pulses. A polarisation controller (PC, Fig. 3.2.1) and

a PM ISO were placed before the EOM to adjust the input polarisation state (i.e. to ensure a maximum output from the EOM), and a low signal power after the EOM of 1.2 mW was obtained due to the 9.7-dB insertion loss of the EOM and associated polarisation-sensitive components. TDFA2 was a conventional core-pumped fibre amplifier using a 2-m-long in-house-fabricated TDF (8.5-μm core, 100-μm cladding, NA=0.2, core pump absorption ~95 dB/m at 1560 nm) pumped by another 1565-nm Er/Yb co-doped fibre laser, and increased the signal power to 48 mW. A grating-based filter, comprising a pair of circulators and two fibre bragg gratings (FBGs, bandwidth 0.8 nm, 0.5 nm), was used to remove ASE and improve the output signal noise ratio (OSNR). The grating-based filters introduced a loss of ~12 dB, resulting in an average power of ~3 mW. To compensate the high loss induced by the grating-based filter and to further suppress the potential nonlinearities, a cladding-pumped third amplifier stage was built with a 2.5-m-long TDF with a core diameter of 11 μm and a cladding absorption of ~6 dB/m at 790 nm. TDFA3 boosted the signal power to 60 mW at a slope efficiency of 22% and the resulting signal was coupled into TDFA4. An in-house-fabricated mode-field adaptor was used before the final-stage amplifier to match the fundamental mode of the two dissimilar fibres and hence reduce the coupling loss and improve the signal beam quality. TDFA4 comprised of a large-mode-area (LMA) TDF having a core / cladding diameter of 25 μm / 250 μm and NA of 0.09 / 0.46, with a length of 1.3 m and a cladding pump absorption of ~9.5 dB/m. A backward pumping scheme was chosen rather than forward pumping in order to minimise nonlinear effects [11]. This stage was pumped by two spatially combined 790-nm laser diodes with a maximum output power of 60 W. The LMA-TDF was cooled by a water-cooling system with a fixed temperature of 15°C. The residual pump was eliminated by an in-house-made pump stripper in order to avoid backward light coupled into former components. The free end of the LMA-TDF was terminated with an angle-polished core-less endcap (4°) to avoid signal feedback and to allow for signal beam expansion and reduction of peak intensity at the glass/air interface. The endcap was purged by nitrogen to lower its temperature and hence to resist potential thermal damage.

3.2.2 Experimental results and discussion

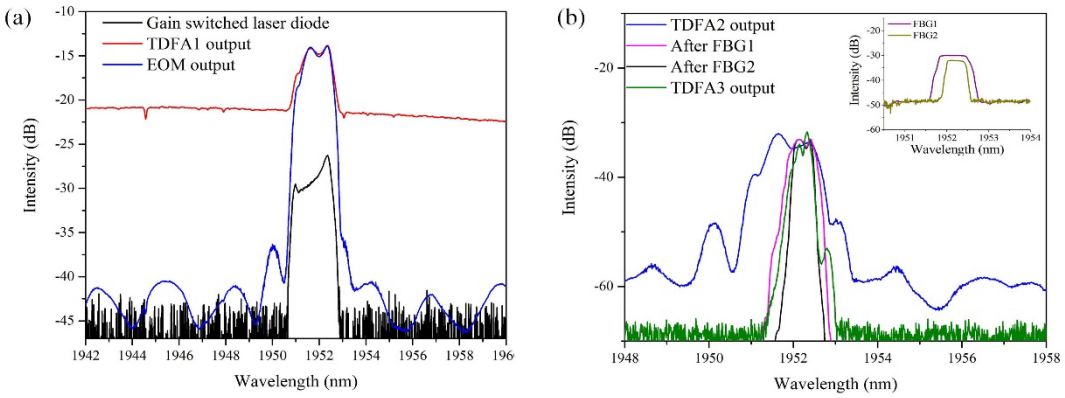

Fig. 3.2.2. (a) Spectra of gain-switched seed diode, spectra at the outputs of the TDFA1 and EOM. (b) Spectra at TDFA2 output, after FBG1, and FBG2 based filter, and spectra after TDFA3; inset: reflection spectra of two FBGs.

Fig. 3.2.2 (a) shows the spectral characteristics of the gain-switched seed diode, TDFA1 output, and EOM output. The gain-switched seed diode spectra had a 3-dB bandwidth of 0.9 nm, and was slightly distorted at the output of TDFA1 due to self-phase modulation (SPM). The initial OSNR for the immediate output of the gain-switched laser diode was >15 dB, which degraded to ~6 dB after the TDFA1, but was then improved by the EOM to ~22 dB. After TDFA2, depicted in Fig. 3.2.2 (b), the signal OSNR was slightly degraded to ~16 dB but was remarkably improved to > 40 dB by the two FBG-based filters, meanwhile the spectra bandwidth was gradually narrowed to a full width at half maximum (FWHM) of 0.5 nm. The inset of Fig. 3.2.2 (b) shows the reflection spectra of two FBGs with FWHMs of 0.8 nm and 0.5 nm for FBG1 and FBG2, respectively, tested by an in-house-fabricated 2-μm ASE source combined with optical circulators. Note that the FBG-based filter significantly determined the final spectral bandwidth of the Tm:MOPA system, which is a key factor for pumping OPDs based on OP-GaAs, as stated in section 2.9.2. After signal getting amplified in TDFA3, the spectra was again slightly distorted (due to the SPM) without OSNR degradation.

The temporal profiles from the gain-switched seed diode was measured to be 91 ps by an extended InGaAs photodetector (EOT, ET-5000F, bandwidth >12.5 GHz) and an oscilloscope (Tektronix, CSA 803A, with 50 GHz bandwidth), as depicted in Fig. 3.2.3 (a). The pulse duration of the optical pulses were unchanged (91 ps) as they propagated through TDFA1 and TDFA2. The temporal resolution of the detection system was tested by measuring the pulse duration of a 2-μm ~500-fs mode-locked laser and was found to be ~60 ps. The signal pulse was characterised after FBG1 and FBG2, using the photodetector, giving

a shortened duration of 60 ps (Fig. 3.2.3 (b) inset). However, this should be considered an upper limit of the pulse duration due to the limitation of the photodiode bandwidth. Instead, a second harmonic generation (SHG) based autocorrelator (AC, APE PulseLink, maximum measurable pulse duration ~50 ps) offered more accurate pulse characterisation with a measured FWHM of the AC trace of 49 ps, corresponding to a pulse duration of 35 ps assuming a Gaussian temporal pulse shape (Fig. 3.2.3 (b)). This shortening is likely due to the interplay between the chirp present on the original pulse and the spectral properties of the FBGs. The optical pulses then propagated with a constant pulse duration through TDFA3 and were input to TDFA4 (the final amplifier).

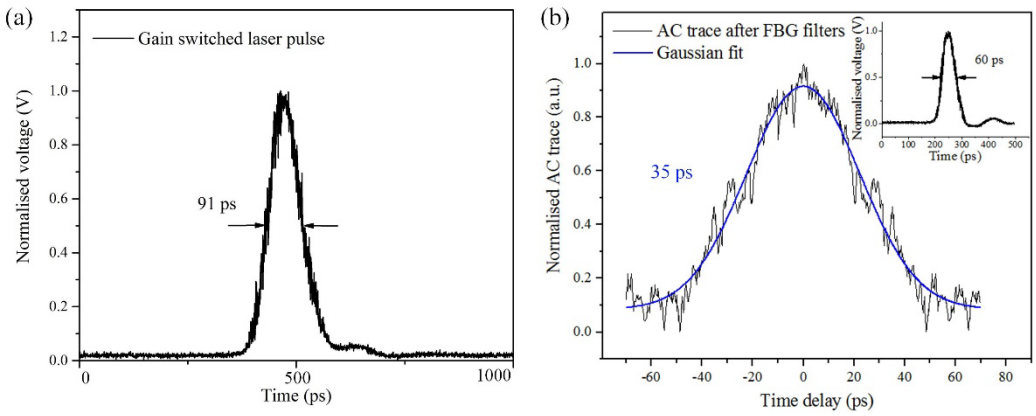

Fig. 3.2.3. (a) Gain-switched seed laser pulse. (b) Auto-correlator trace of optical pulses after the FBG filters; inset: short pulse profile measured by the photodiode.

Fig. 3.2.4 (a) shows the average power and the AC trace (inset) of the output pulses from TDFA4 (i.e. from the Tm:MOPA system). The maximum output power of 10.3 W was obtained at a slope efficiency of 29.5% and at an overall MOPA gain of ~70 dB. The inset AC trace of the output pulse at the maximum output power has a FWHM of 49 ps corresponding to a Gaussian FWHM pulse width of 35 ps, demonstrating that the optical pulse duration did not change when passing through any of the TDFAs and was only affected by the optical filters. The maximum peak power for the TDFA4 was calculated to be 294 kW. The output spectra of TDFA4 at different output powers are shown in Fig. 3.2.4 (b). The central spectra transformed into a multi-peak feature with the increase of output power and an onset of MI was observed (inset of Fig. 3.2.4 (b)) starting at an output power of 9 W and becoming more obvious at 10.3 W, which limited the power scaling.

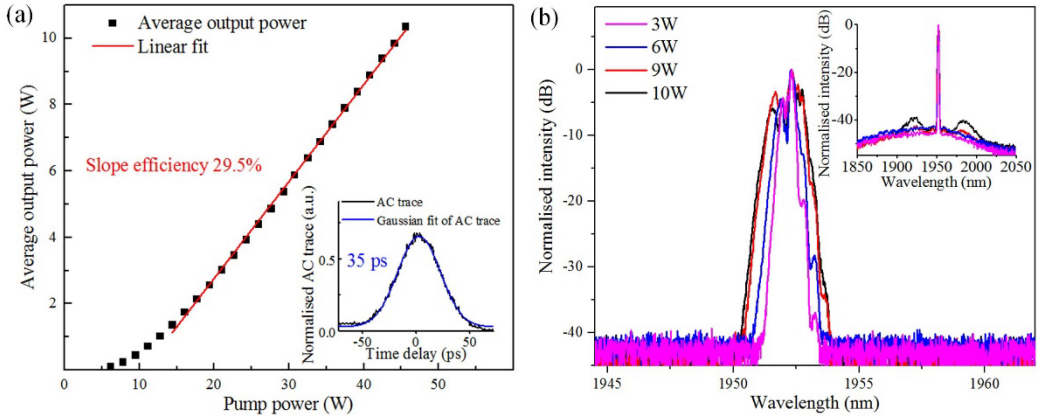

Fig. 3.2.4. (a) Output powers of Tm:MOPA system (TDFA4); inset: autocorrelator trace from TDFA4 at maximum output power. (b) Spectra at different output powers in TDFA4.

The relatively low repetition rate (1 MHz) of the Tm:MOPA system combined with the relatively low extinction ratio of EOM of (25 dB), allowed for the possibility that CW ASE light was also amplified through the MOPA system, which would result in a lower peak power from the final output than the value calculated above. Therefore, in order to further confirm the authenticity of the peak power of the Tm:MOPA system, we switched the pulse repetition frequency between 1 MHz and 8 MHz to check the fact that the peak power should be increased proportionally to the decrease in the pulse repetition frequency with the same average output power. The extended InGaAs detector (EOT, ET-5000F) and an oscilloscope were employed to record the voltage amplitudes on a reflection of the peak power of the Tm-MOPA system operating at 1 MHz and 8 MHz, as shown in Fig. 3.2.5. With a linear fit, the experimental slope at 1 MHz (41.0) is ~7.7 times higher than that of 8 MHz (5.3), as expected if all the energy remains in the pulse. These results verified the high peak power in the picosecond pulses. It should be noted that the ease of changing the repetition rate also demonstrates the versatility of gain-switching systems, and was later used to demonstrate a controllable repetition-rate OP-GaAs optical parametric oscillator (OPO), which will be described in Chapter 7.

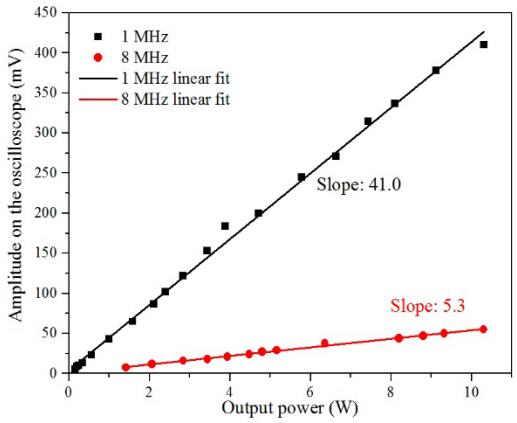

Fig. 3.2.5. Peak power test at repetition rates of 1 MHz and 8 MHz.

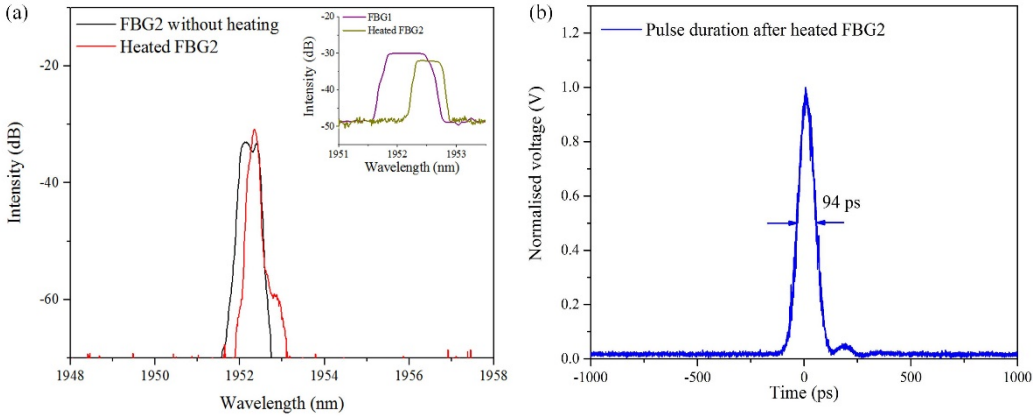

Fig. 3.2.6. (a) Spectra after FBG2 with heating and without heating; inset: reflection spectra of FBG1 and heated FBG2. (b) The pulse duration of optical pulses after heated FBG2.

This source has been used for pumping indium fluoride fibres for supercontinuum (SC) generation spanning 750 nm to 5 μm, as reported in [12]. However, its central multi-peak spectra (Fig. 3.2.4 (b)) is not beneficial to OP-GaAs OPDs. For example, at the maximum output of 10.3 W, although FWHM bandwidth was 0.18 nm, only ~46% optical power was contained within this bandwidth. A more effective 10-dB bandwidth was defined to be ~1.7 nm, which contains ~95% of optical power, and this effective bandwidth was broader than the acceptance bandwidth of the OP-GaAs OPDs calculated in section 2.9.2 (~1.5 nm). In order to narrow the linewidth and avoid the multi-peak spectra in TDFA4 (i.e. before SPM effects become significant), an additional temperature-control oven was employed on FBG2, heating it from room temperature to 60°C. The reflection spectra of FBG2 (inset of Fig. 3.2.6 (a)) was consequently shifted to a longer wavelength compared with the unheated spectra (inset of Fig. 3.2.2 (b)), and the overlapped reflection spectra between two FBGs became narrower, resulting in a signal spectra of 0.16 nm FWHM bandwidth, as shown in Fig. 3.2.6 (a). The corresponding pulse duration was measured by the photodiode to be 94 ps (Fig.

3.2.6 (b)) possibly due to interaction between the frequency chirp of the gain-switched pulses and filter spectral responses. This pulse duration (94 ps) remains unchanged in the following TDFA3 and TDFA4 at a full range of output powers. The output power after heated FBG2 was reduced to ~1.5 mW but TDFA3 offered a flexible gain to maintain a same input power (60 mW) for seeding TDFA4. However, the output performance of the TDFA4 was found less efficient with the maximum output power decreased to 7 W at the same pump level, which is probably because of the degradation over time of the pump stripper during the long run SC generation experiment work. Fig. 3.2.7 (a) shows that the signal spectra was gradually broadened in TDFA4 with increasing pump power, again caused by SPM but the broadening was less severe (because of longer pulse durations leading to lower peak powers), resulting in a single peak spectra with a 0.26-nm FWHM bandwidth at 7 W output (containing 71% of the optical power).

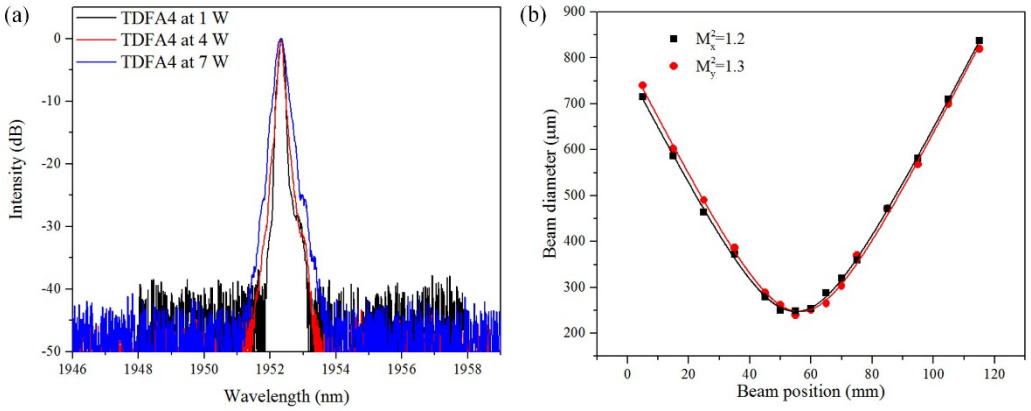

Fig. 3.2.7. (a) Spectra of Tm:MOPA system (TDFA4) after heating FBG2. (b) Beam quality of the Tm:MOPA output.

The beam quality of the Tm:MOPA system, while using the heated FBG2, at the maximum output power was measured to be M_x^2=1.2, M_y^2=1.3 using a Nanoscan beam profiler (OPHIR), as depicted in Fig. 3.2.7 (b). The Tm:MOPA system was then employed as a pump for an SHG experiment, carried out using a periodically poled lithium niobate (PPLN) nonlinear crystal. The PPLN crystal was poled at a period of 29 μm and mounted in an oven with a set temperature of 105°C to realise quasi-phase-matching. 1.6 W of 976-nm frequency-doubled light was realised at a pump power of 3.2 W, as reported in [13]. This experiment further confirmed that the Tm:MOPA system, with the heated FBG2, was ready to serve as a pump for nonlinear frequency conversion in OP-GaAs OPDs.

Overall, the maximum available pump power from the 1952-nm Tm:MOPA system was 7 W at a repetition rate of 1 MHz. With a pulse duration of 94 ps, the corresponding maximum

pulse energy and peak power are calculated to be 7 μJ and 74 kW, respectively. The final output had a 0.24 nm FWHM bandwidth and a beam quality of M^2=1.3.

3.3 OP-GaAs OPG and OPA setup

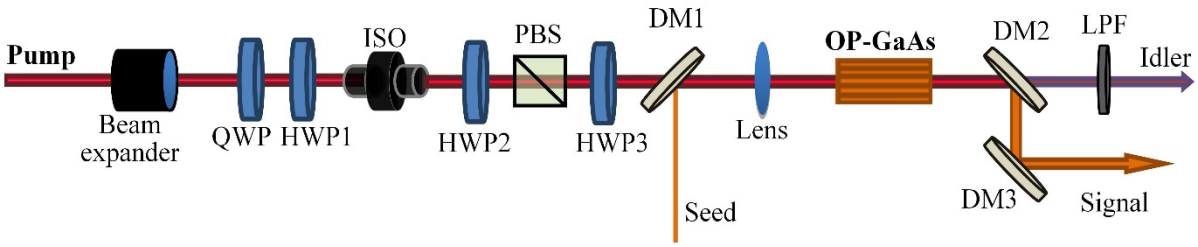

Fig. 3.3.1. Experimental setup of the OPG (unseeded) and OPA (seeded). QWP, quarter-wave plate; HWP, half-wave plate; ISO, isolator; PBS, polarising beam splitter; DM, dichroic mirror; LPF, long-pass filter.

The configuration of the OPG and OPA is shown in Fig. 3.3.1. The pump beam was first expanded by a beam expander (2X) to avoid potential damage of the following optical components. To prevent any feedback into the amplifier system and to define a distinct linear state of polarisation for subsequent frequency conversion, the output beam from the beam expander was passed through a free-space polarisation-sensitive isolator. The Tm:MOPA itself did not use polarisation-maintaining fibres, so a quarter-wave plate (QWP) and a half-wave plate (HWP1) was put before the isolator to maximise the output power but there was still a relatively high measured loss of ~1.5 dB. As a result, the available average power from the MOPA system, after passing through the various optical elements before the OP-GaAs crystal was 3.7 W. The power input to the OPG/OPA was varied using HWP2 placed before a polarising beam splitter (PBS), as shown in Fig. 3.3.1. HWP3 was then used to rotate the beam linear-polarisation orientation to realise optimised nonlinear generation in an OP-GaAs crystal. The beam after the dichroic mirror (DM1, Fig. 3.3.1) was focused into the OP-GaAs by an uncoated CaF_2 lens with a beam waist of 80 μm ($1/e^2$ radius of intensity). The 20-mm-long OP-GaAs crystal (BAE Systems) had five gratings with periods ranging from 57 μm to 65 μm in steps of 2 μm. Each grating had a dimension of 1-mm thickness (aligned to the [001] crystallographic axis), 5-mm width (aligned to [110]) and 20-mm length (aligned to $[1\bar{1}0]$), and the pump beam propagated along the length of the crystal. The crystal was mounted in an oven to allow temperature tuning. Both end facets of the OP-GaAs were anti-reflection (AR) coated at the pump (R<1%) and signal (R<6%) wavelengths, but had a reflection of up to 17% at the longest idler wavelength (~8 μm). The relatively high loss at the idler wavelength was because the coating was designed for an OPO with a different pumping wavelength of 2007 nm (as discussed in section 2.9.1) and could easily be reduced

in future if required. The signal output was extracted using two dichroic mirrors (DM2, DM3, Fig. 3.3.1), with high transmission at the pump and idler wavelengths and high reflection at the signal wavelength. The idler power was measured after a long-pass filter (LPF, Fig. 3.3.1), which had a short wavelength cut-off at 4.5 μm. The signal and idler output powers discussed in the following text correspond to that immediately after the OP-GaAs crystal, taking into account the losses of the DMs and LPF but not the AR coatings on the crystal.

3.4 OP-GaAs OPG and OPA results and discussion

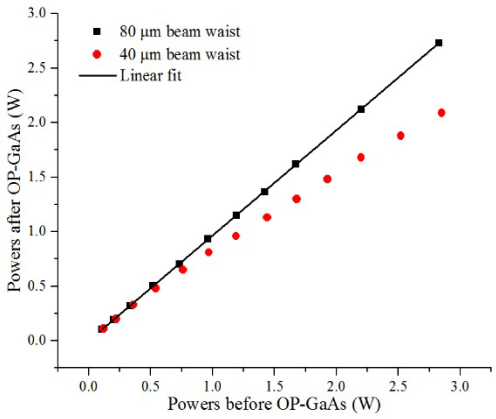

Fig. 3.4.1. Intrinsic loss measurements of the OP-GaAs crystal.

The intrinsic loss of the OP-GaAs crystal was first investigated by measuring powers before and after the OP-GaAs. The pump beam was focused by two different lenses (f=100, 50 mm) resulting in two different beam waists (80, 40 μm) and therefore different intensities at the focal point inside the crystal, with the experimental results shown in Fig. 3.4.1. With a beam waist of 80 μm (f=100 mm), the intrinsic loss of the OP-GaAs remained at ~4% as the input power increased, whereas the loss of OP-GaAs increased to ~27% at a pump power of 2.8 W for a beam waist of 40 μm (close to the confocal focusing condition). Since there was no evidence for optical damage, this can be attributed to a three-photon absorption effect induced by the high intensity inside the crystal starting to become significant from ~1 W (~423 MW/cm^2 of peak intensity for Gaussian beam) with the beam waist of 40 μm [14, 15]. With the maximum pump power of 3.7 W, we can therefore calculate that a minimal beam waist of ~77 μm can be used before three-photon absorption becomes significant, and thus a beam waist of 80 μm was chosen for the OPG and OPA experiments. With this focusing, the maximum intensity at the focal point in the OP-GaAs crystal was thus around 392 MW/cm^2.

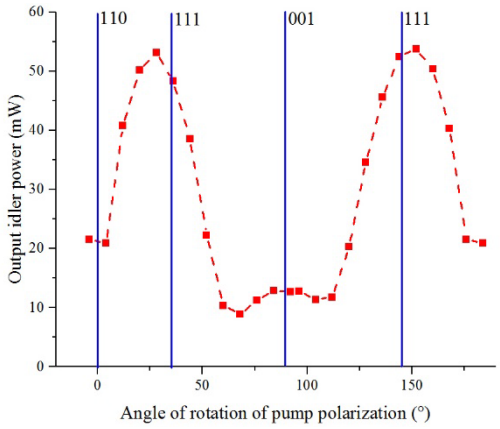

Fig. 3.4.2. Idler average output power versus the pump polarisation angle and the corresponding crystal axis.

Without seed laser injection, the generation of signal (2930 nm) and idler (5860 nm) pulses was observed at a minimum pump threshold of around 1.6 W with the pump polarisation set at an angle close to coincidence with [111] (experimentally it is at ~6° with respect to [111]) in the single-pass OPG process. To investigate the behaviour and influence of the pump polarisation on the three-wave mixing in the OP-GaAs, we measured the generated idler output power against the angle of the input pump polarisation, and plot them in Fig.3.4.2. As stated in section 2.5, theoretical models predict that the effective nonlinear coefficient has a maximum when the pump polarisation is aligned to the [111] direction (35° to the [110]) direction [16]. The small observed discrepancy (~6°) could possibly be explained by the presence of stress induced birefringence in the OP-GaAs [17, 18]. The experimental threshold average power of 1.6 W corresponds to a power peak intensity of ~169 MW/cm^2. According to the theory demonstrated in section 2.9.4, a theoretical threshold intensity value of 164 MW/cm^2 is estimated at the pump and signal wavelengths of 1952 nm and 2930 nm, which is in good agreement with experimental results.

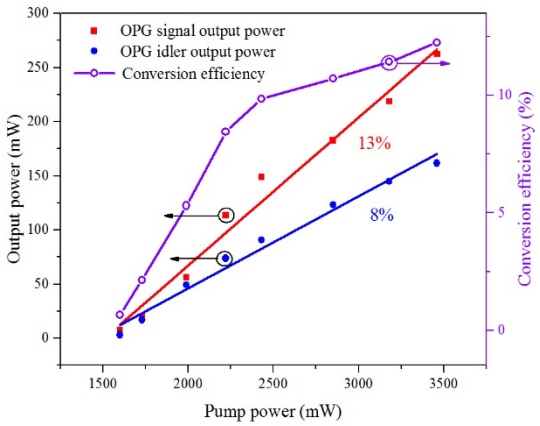

Fig. 3.4.3. (Left) Signal and idler output power as a function of pump power in OPG operation with linear fits. (Right) Total power conversion efficiency versus pump power. The solid line is to guide the eye.

Using a grating period of 57 μm and an oven temperature of 50 ℃, signal at a wavelength of 2930 nm and idler at a wavelength of 5860 nm were generated from the OP-GaAs crystal with a maximum average power of 260 mW and 160 mW, respectively, when pumped at 3.5 W. The measured signal and idler output powers from the OP-GaAs OPG are shown in Fig. 3.4.3. The slope efficiency of generated signal and idler were 13% and 8%, respectively. Considering the total output power, the overall power conversion efficiency of the OPG was 12%. Unfortunately, the pulse duration of the signal and idler pulses could not be measured due to the lack of suitable equipment, but they can be expected to be equal to or slightly shorter than that of the pump in the OPG process [19]. In this case, the peak power of the generated signal and idler pulses are at least 2.8 kW and 1.7 kW, respectively. By using different OP-GaAs grating periods and oven temperatures, the signal (idler) wavelength could be tuned from 2550 nm to 2940 nm (5800 nm to 8300 nm), as shown in Fig. 3.4.4. The signal and idler spectra were measured by a spectrum analyser (Bristol 721, ~0.1 nm resolution) and a monochromator (Bentham TMc300V, ~4 nm resolution), respectively. The multiple spectral modulated lines indicates the absorption of light by H_2O in the air, as shown in Fig. 3.4.5 (a). The spectral linewidths were relatively broad at 20 nm (29 cm^{-1}) and 200 nm (33 cm^{-1}) for the signal and idler respectively, but with a discrepancy compared to theoretical OPG bandwidth of ~20 cm^{-1} [20]. One possible reason for the discrepancy is that the high pump intensity induced nonlinear effects. Using the nonlinear refractive index of ~1.5×10^{-13} cm^2/W for GaAs at 2 μm [15] and the maximum pump intensity of 392 MW/cm^2, the nonlinear phase shift was calculated to be ~2.3 radians, which indicates the nonlinear effects (such as SPM) have indeed become important [1]. The OPG bandwidth could also be broadened due to effects such as grating errors, temperature variation along the crystal, and focusing effects. Note that the pump acceptance bandwidth requirement was not critical for

the spontaneous OPG process which had rather high parametric gain, but is important for OPAs and OPOs. Fig. 3.4.5 (b) shows the measured OPG signal and idler wavelengths (red dots) compared with the theoretical curves, as provided in section 2.9.1. Theoretical and measured wavelength values are overall in good consistency despite of slight wavelength mismatch possibly caused by the period errors of OP-GaAs crystal generated during the manufacturing process. The beam qualities of generated OPG signal (2930 nm) and idler (5860 nm), when using the OP-GaAs with a grating period of 57 μm, were measured as shown in Fig. 3.4.6. The signal beam quality was $M^2_x = 1.7$ and $M^2_y = 1.8$, and the idler beam quality was $M^2_x = 2.3$ and $M^2_y = 2.4$ in the horizontal (x) and vertical (y) planes.

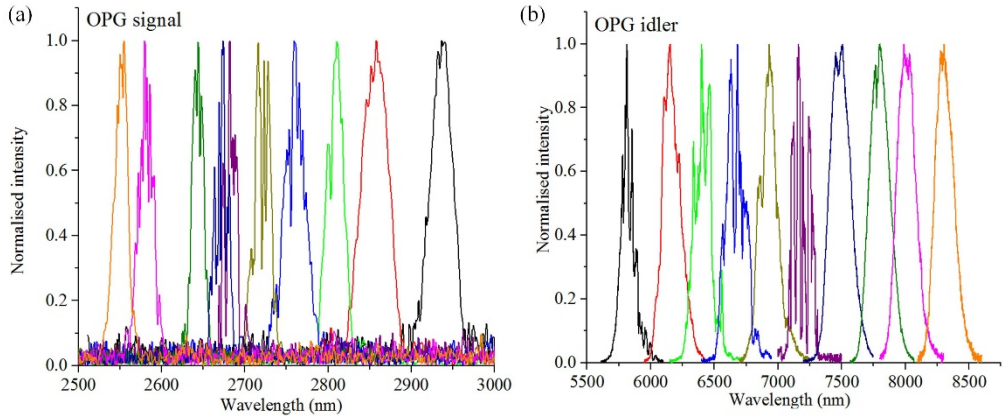

Fig. 3.4.4. Measured spectra for signal (a) and idler (b) from the tunable OPG.

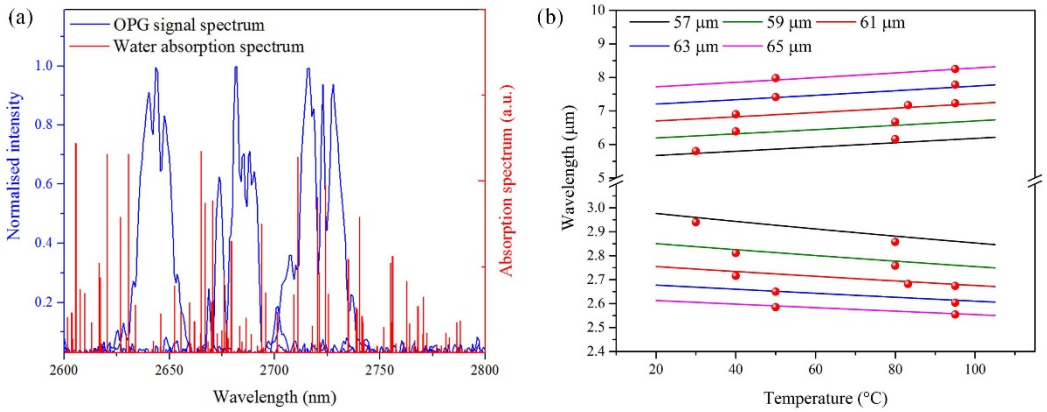

Fig. 3.4.5. (a) Measured OPG signal spectra compared with water absorption spectra (Hitran Database). (b) Calculated tuning cure in comparison with measured wavelengths for different OP-GaAs periods.

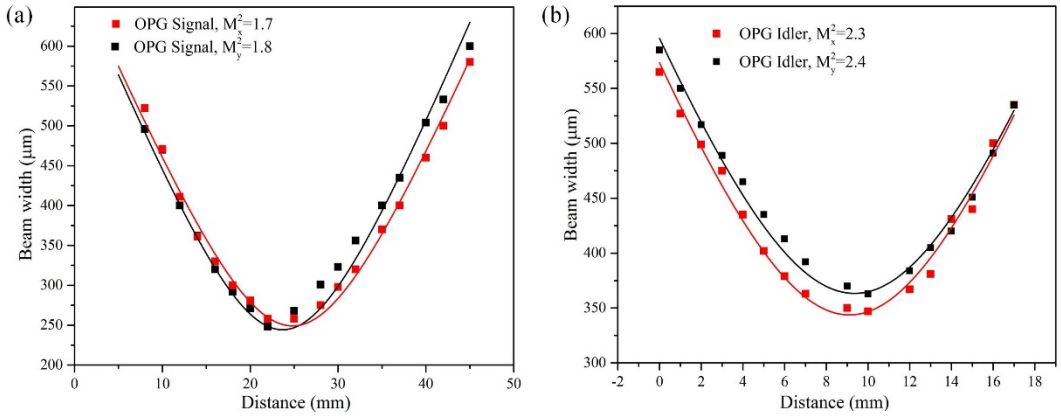

Fig. 3.4.6. M^2 measurement for OPG signal at 2930 nm (a) and idler at 5860 nm (b) in the x and y direction for OP-GaAs with grating period of 57 μm.

Some applications, such as chemical sensing, require mid-IR laser sources with large spectral tunability but with narrow linewidth to achieve high spectral resolution [4]. In order to narrow the spectral linewidth, a commercial CW tunable Cr:ZnSe laser (IPG Ltd) was employed as an injection signal to seed the OPG for OPA operation. The seed laser had a linewidth of 0.6 cm^{-1} and wavelength tunability from 1.9 μm to 2.7 μm. The seed and pump beams were combined by a dichroic mirror (DM1, Fig. 3.3.1). Due to the elliptical output beam-shape of the seed laser, the beam waist after the focusing lens was 140 μm by 80 μm in the horizontal and vertical planes, respectively. Thus, there was only one direction where the pump (waist size 80 μm) and signal beams had good overlap. As the seed beam was horizontally linearly polarised (aligned to [110]), the pump polarisation was also chosen to be parallel to the seed to maximise the conversion efficiency [18]. With 280 mW of seed laser power at a wavelength of 2650 nm, the pump threshold decreased, as expected, to approximately 1 W. Figure 3.4.7 shows that the output powers of the generated signal (CW seed subtracted) and idler increased linearly with slope efficiencies of 42% and 11%, respectively. The maximum signal power of 1.07 W at 2650 nm and idler power of 0.26 W at 7440 nm, were obtained at a pump power of 3.7 W. The corresponding maximum overall power conversion efficiency was 35% and the effective total slope efficiency was 53%. Taking into account the duty cycle of the 94-ps pulses and the 1-MHz repetition rate, the effective seed pulse energy was 26.3 pJ (peak power of 280 mW) within the pulse duration. Thus the maximum output pulse energy of 1.07 μJ (average power of 1.07 W) represents a parametric gain of 46 dB. Assuming the signal and idler had the same pulse durations as the pump, the attainable peak power was 11.3 kW and 2.7 kW for the signal and idler, respectively.

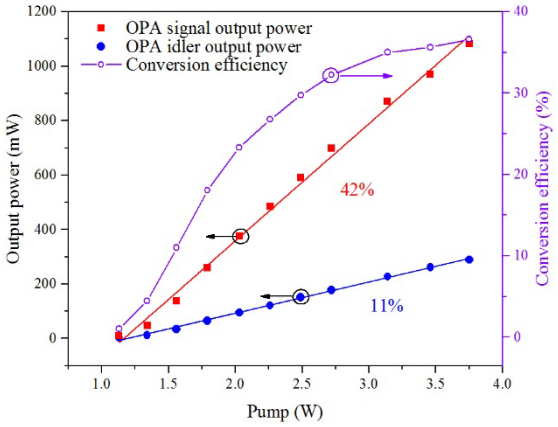

Fig. 3.4.7. (Left) Signal and idler output power as a function of pump power in OPA operation. Circles are measured data points and the solid lines are linear fits. (Right) Total power conversion efficiency versus pump power. The solid line is purely to guide the eye.

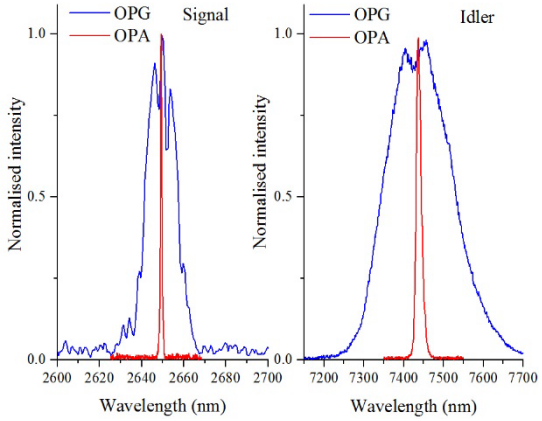

Fig. 3.4.8. Measured spectra for signal (left) and idler (right) in both OPG and OPA operation regimes.

Fig. 3.4.8 shows the measured OPA spectra in a comparison with OPG spectra. The OPA signal linewidth at a wavelength of 2650 nm was reduced to 0.5 nm, while the idler linewidth (7436 nm) was narrowed to 8.5 nm. As a result, the OPA leads to more than 20 times increase in spectral density compared to the OPG. As expected, the frequency bandwidth was essentially transferred from the pump (1.3 cm^{-1}) to the idler (1.4 cm^{-1}), with the narrower seed bandwidth (0.56 cm^{-1}) being transferred to the amplified signal (0.71 cm^{-1}) [21]. By tuning the seed wavelength, a tunable output signal from 2557 nm to 2684 nm (limited by the tunability of the seed laser) and a tunable idler from 7168 nm to 8267 nm were achieved from the OP-GaAs OPA by using different grating periods and temperatures, as shown in Fig. 3.4.9. Therefore, the OPA has generated tunable signal and idler picosecond pulses with narrow linewidth and high peak power, which could also be potentially suitable for techniques such as mid-IR differential absorption LIDAR [22].

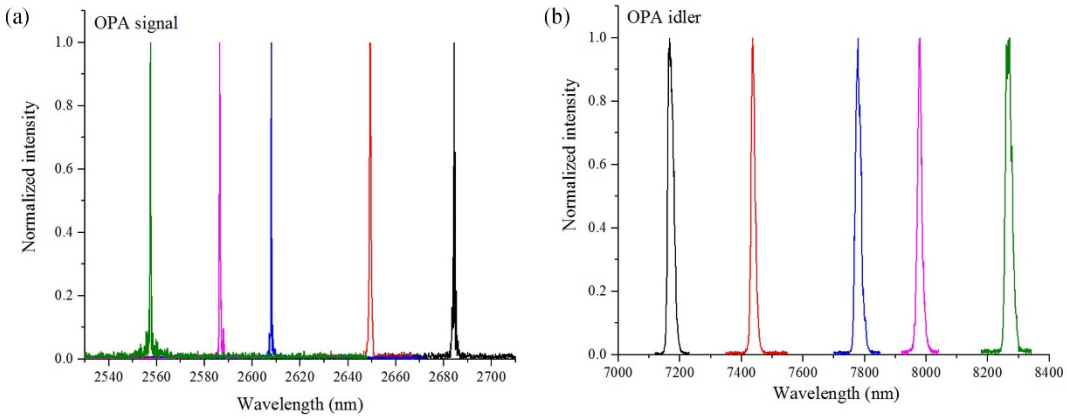

Fig. 3.4.9. Measured OPA signal and idler spectra.

The beam quality of the OPA seed laser was characterised (Fig. 3.3.10) and found to be good (M_x^2 =1.1 and M_y^2 =1.2) but with an elliptical beam shape. This feature led to a poor spatial overlap with pump beam as stated previously, and thus the signal beam quality was measured to be M_x^2 = 2.8 and M_y^2 = 2.7, which was degraded compared to the OPG, as shown in Fig. 3.3.10. However, the idler beam quality was measured to be M_x^2 = 1.9 and M_y^2 = 1.8, which was improved in comparison to that beam quality in OPG mode.

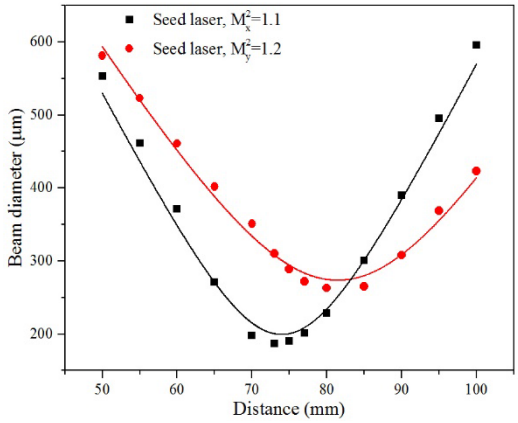

Fig. 3.4.10. Cr:ZnSe laser (OPA seed) beam quality measurement.

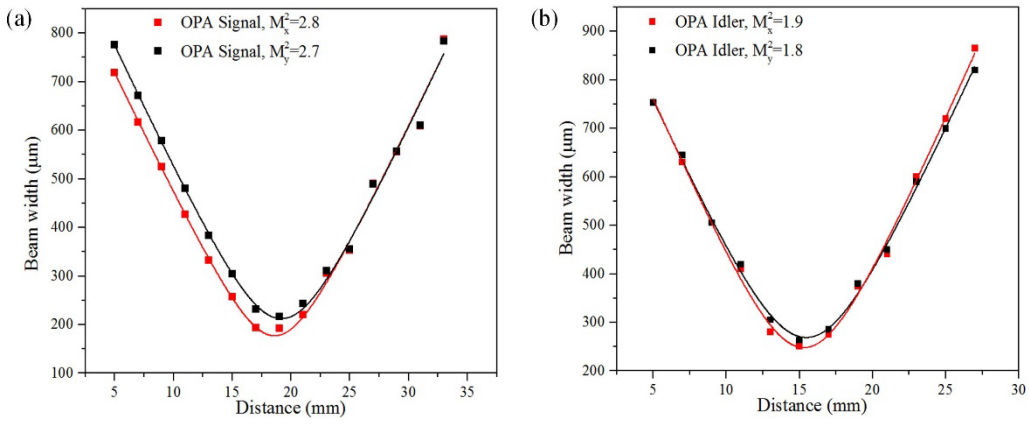

Fig. 3.4.11. OPA signal and idler beam qualities measurement.

An exploration of the requirement and influence of the seed laser power on the parametric gain in the single-pass OPA process was performed. With the pump power fixed at 3 W, the signal output powers when seeding the OPA at different power levels were measured. As illustrated in Fig. 3.4.12, the extractable power from the OPA becomes saturated as the seeding peak power exceeds 100 mW. For smaller seed powers gains as high as ~60 dB were observed.

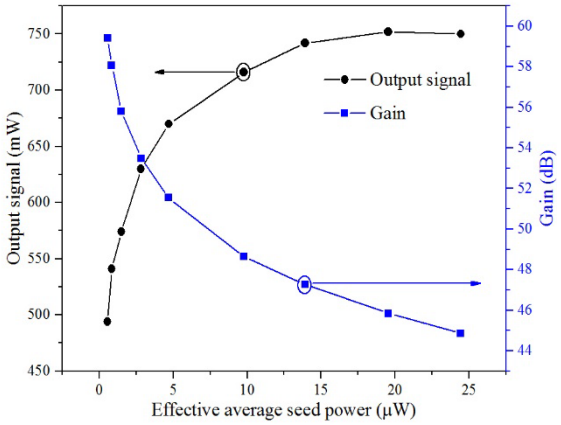

Fig. 3.4.12. Signal output power and gain as a function of different seeding power in OPA.

3.5 Summary

In conclusion, I have demonstrated a high-peak-power, widely tunable, picosecond OPG and OPA based on OP-GaAs pumped by a gain-switched-diode-seeded Tm:MOPA system employing direct amplification. The pump Tm:MOPA system was compact and flexible capable of generating 1952-nm high-peak-power picosecond pulses with a narrow linewidth spectrum (0.24 nm) controlled by two FBGs. For pumping OP-GaAs, an available maximum average power of 3.7 W was obtained corresponding to a pulse peak power of ~39 kW at a repetition rate of 1 MHz and a pulse duration of ~94 ps.

The OPG has generated signal and idler with broad wavelength tuning ranges of 2550 - 2940 nm and 5800 - 8300 nm, with maximum output average (peak) powers of 260 mW (3 kW) for signal and 160 mW (2 kW) for idler at a wavelength of 2930 and 5860 nm, respectively. The spectral linewidth were 20 nm (29 cm^{-1}) and 200 nm (33 cm^{-1}) for the signal and idler.

In OPA operation, seeded with a 0.6 cm^{-1} linewidth continuous-wave tunable Cr:ZnSe laser, the signal and idler linewidth was narrowed from to 0.5 nm (0.71 cm^{-1}) and 8.5 nm(1.4 cm^{-1}), respectively, and a small signal parametric gain up to 60 dB was achieved. At an overall conversion efficiency of 35%, the maximum signal power of 1.07 W at 2650 nm and idler power of 0.26 W at 7440 nm were obtained at an overall conversion efficiency of 35%, with

corresponding peak powers of 11.3 kW (signal) and 2.7 kW (idler). The OPA tuning range of 2557 nm to 2684 nm (signal) and 7168 nm to 8267 nm (idler) was only limited by the tunability of the seed laser. This OPA tuning limitation will be addressed in next chapter.

Reference

[1] P. S. Kuo *et al.*, "Optical parametric generation of a mid-infrared continuum in orientation-patterned GaAs," *Optics Letters*, vol. 31, no. 1, pp. 71-73, Jan. 2006.

[2] B. Donelan *et al.*, "OPG and OPO Nonlinear Conversion in OP-GaAs using 2 μm Single Oscillator Pump Sources," in *Nonlinear Optics*, Waikoloa, Hawaii, 2017, pp. NTu2A.2.

[3] G. Bloom *et al.*, "Optical parametric amplification of a distributed-feedback quantum-cascade laser in orientation-patterned GaAs," *Optics Letters*, vol. 35, no. 4, pp. 505-507, Feb. 2010.

[4] F. Gutty *et al.*, "High peak-power laser system tuneable from 8 to 10 μm," *Advanced Optical Technologies*, vol. 6, no. 2, pp. 95, Apr. 2017.

[5] S. Liang, "High power pulsed thulium doped fibre lasers and their applications," *PhD thesis, University of Southampton*, vol. PhD, 2018.

[6] S. Liang *et al.*, "High peak power picosecond pulses from an all-fiber master oscillator power amplifier seeded by a 1.95 μm gain-switched diode," in *Advanced Solid State Lasers Conference (ASSL)*, Nagoya, Aichi, 2017, pp. ATh3A.4.

[7] L. Xu *et al.*, "High-peak-power, picosecond, mid-infrared optical parametric generator and amplifier pumped by Tm:fiber laser," in *High-Brightness Sources and Light-driven Interactions*, Strasbourg, 2018, pp. MW1C.3.

[8] L. Xu *et al.*, "Thulium-fiber-laser-pumped, high-peak-power, picosecond, mid-infrared orientation-patterned GaAs optical parametric generator and amplifier," *Optics Letters*, vol. 42, no. 19, pp. 4036-4039, Oct. 2017.

[9] S. Liang *et al.*, "295-kW peak power picosecond pulses from a thulium-doped-fiber MOPA and the generation of watt-level >2.5-octave supercontinuum extending up to 5 μm," *Optics Express*, vol. 26, no. 6, pp. 6490-6498, 2018.

[10] A. M. Heidt *et al.*, "100 kW peak power picosecond thulium-doped fiber amplifier system seeded by a gain-switched diode laser at 2 μm," *Optics Letters*, vol. 38, no. 10, pp. 1615-1617, 2013.

[11] E. Desurvire, "Analysis of gain difference between forward- and backward-pumped erbium-doped fiber amplifiers in the saturation regime," *IEEE Photonics Technology Letters*, vol. 4, no. 7, pp. 711-714, 1992.

[12] S. Liang *et al.*, "A watt-level supercontinuum source from a fiber-laser-pumped fluoroindate fiber spanning 750 nm to 5 μm," in *Conference on Lasers and Electro-Optics (CLEO)*, 2018, pp. 1-2.

[13] L. Xu *et al.*, "Highly efficient frequency doubling and quadrupling of a short-pulsed thulium fiber laser," *Applied Physics B*, vol. 124, no. 4, pp. 59, 2018.

[14] O. H. Heckl *et al.*, "Three-photon absorption in optical parametric oscillators based on OP-GaAs," *Optics Letters*, vol. 41, no. 22, pp. 5405-5408, Nov. 2016.

[15] W. C. Hurlbut *et al.*, "Multiphoton absorption and nonlinear refraction of GaAs in the mid-infrared," *Optics Letters*, vol. 32, no. 6, pp. 668-670, 2007.

[16] P. S. Kuo *et al.*, "GaAs optical parametric oscillator with circularly polarized and depolarized pump," *Optics Letters*, vol. 32, no. 18, pp. 2735-2737, 2007.

[17] J. Wueppen *et al.*, "1.95 μm-pumped OP-GaAs optical parametric oscillator with 10.6 μm idler wavelength," *Optics Letters*, vol. 41, no. 18, pp. 4225-4228, Sep. 2016.

[18] C. Kieleck *et al.*, "High-efficiency 20–50 kHz mid-infrared orientation-patterned GaAs optical parametric oscillator pumped by a 2 μm holmium laser," *Optics Letters*, vol. 34, no. 3, pp. 262-264, 2009.

[19] L. Xu *et al.*, "High-energy, near- and mid-IR picosecond pulses generated by a fiber-MOPA-pumped optical parametric generator and amplifier," *Optics Express*, vol. 23, no. 10, pp. 12613-12618, 2015.

[20] G. D. Boyd, and D. A. Kleinman, “Parametric interaction of focused Gaussian light beams,” *Journal of Applied Physics,* vol. 39, no. 8, pp. 3597-3639, 1968.
[21] J. Prawiharjo *et al.*, “Theoretical and numerical investigations of parametric transfer via difference-frequency generation for indirect mid-infrared pulse shaping,” *Journal of the Optical Society of America B,* vol. 24, no. 4, pp. 895-905, 2007.
[22] P. Geiser *et al.*, “A subnanosecond pulsed laser-source for mid-infrared LIDAR,” *Applied Physics B,* vol. 83, no. 2, pp. 175, 2006.

Chapter 4

Cascaded OP-GaAs optical parametric generator and optical parametric amplifier

4.1 Introduction

Optical parametric amplifiers (OPAs) with both a simple single-pass nature and the possibility of high-power operation have attracted great interest. Generally, OPAs require an external laser source to serve as the seed for the parametric amplification, and a narrow-linewidth tunable seed is typically preferred to generate narrow-linewidth tunable OPA outputs for high-resolution spectroscopic applications [1-3]. In the mid-infrared (mid-IR) wavelength range, only a few laser sources, such as quantum cascaded lasers (QCLs) [4-7], are considered to be a good narrow-linewidth seed laser for such OPAs. Based on orientation-patterned gallium arsenide (OP-GaAs), G. Bloom et al. reported a 4.5-μm-wavelength QCL seeding a narrow-linewidth OPA pumped by a 2-μm Ho:YAG *Q*-switched laser. However, the generated OPA wavelength was not tunable due to the both wavelength-fixed seed and pump laser [4]. In a later report, F. Gutty et al. demonstrated an OP-GaAs OPA with a wavelength-tunable QCL seed generating 8-10 μm output with narrow-linewidth (<3.5 cm^{-1}), however, the peak power was only 140 W [6]. In Chapter 3, I reported a high-peak-power (14 kW, total mid-IR output) Cr:ZnSe-laser seeded OP-GaAs OPA with a tuning range of 2557-2684 nm (signal) and 7168 to 8267 nm (idler) and a linewidth of 0.7 cm^{-1} (signal) and 1.4 cm^{-1} (idler) [8]. While this source demonstrated high-peak-power, the tunability of the OPA was again restricted by the limited tunability of the external seed laser, and thus the OPA could not fully exploit the spectral range that the OP-GaAs crystal provides.

In this chapter, to overcome this problem, I demonstrate the development of a widely tunable, narrow-linewidth, mid-IR source based on a cascaded OP-GaAs optical parametric generator and amplifier (OPG-OPA). A diffraction grating together with an adjustable

aperture was used as a spectral filter to narrow the signal linewidth of the OPG stage, which was then employed as the seed for the OPA stage. Tuning ranges of 2552-2960 nm (signal) and 5733-8305 nm (idler) covering the entire wavelength regime that the OP-GaAs gratings provided (with the 1952-nm pump source) were demonstrated, and the output signal linewidths were narrowed from 46 cm^{-1} (OPG signal) and 51 cm^{-1} (OPG idler) to 1.4 cm^{-1} (OPA signal) and 9 cm^{-1} (OPA idler), respectively. The maximum signal and idler output powers were 400 mW (signal, 2942 nm) and 162 mW (idler, 5800 nm) with an overall conversion efficiency of 22.5% for the OPA. With a measured signal pulse duration of 36 ps using an autocorrelator (AC) (APE, PulseLink), the maximum peak power was calculated to be as high as 11.1 kW. The idler had a peak power up to 4.5 kW, assuming a similar pulse width. The output parameters of this source, together with its simple fibre-laser-pumped single-pass frequency conversion configuration, makes the cascaded OP-GaAs OPG-OPA an attractive option for mid-IR spectroscopic applications.

Section 4.2 introduces the characteristics of the pump system for the cascaded OP-GaAs OPG-OPA and Section 4.3 presents the setup of the cascaded OPG-OPA. Section 4.4 then describes the cascaded OPG-OPA experimental results and discussion and finally Section 4.5 gives a summary of this chapter. The experimental work presented in this chapter has previously been published, in part, in [9, 10].

4.2 Pump system optimisation

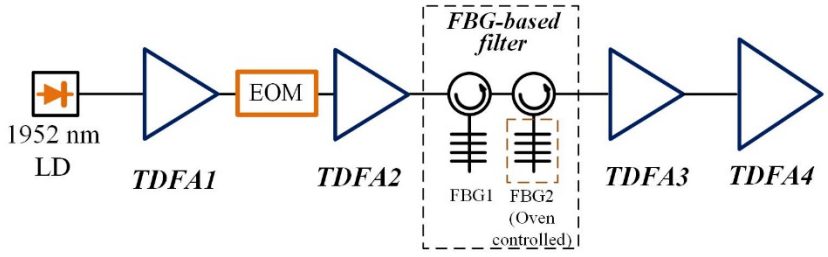

Fig. 4.2.1. Schematic diagram of Tm:MOPA system. LD: laser diode; TDFA: thulium-doped-fibre amplifier; EOM: electro-optic modulator; FBG: fibre bragg grating.

The pump source for the cascaded OPG-OPA is shown as a block diagram in Fig. 4.2.1, and is the same as the pump setup demonstrated in section 3.2.1 (detailed setup depicted in Fig. 3.2.1), which was a four-stage thulium-doped-fibre (TDF) master oscillator power amplifier (Tm:MOPA) system seeded by a 1952-nm gain-switched laser diode at a repetition rate of 1 MHz. In order to pump a cascaded OPG-OPA, a higher peak power of the Tm:MOPA was desired while maintaining a suitable pump bandwidth for OP-GaAs OPDs. Instead of

changing the MOPA system configuration or varying the average output power, we studied the influence of the transmission bandwidth of the FBG-based spectral filter on the output pulse shape/duration. As described in the last chapter, the transmission bandwidth of the filter can be varied by tuning the central wavelength of FBG2 by using temperature control. At a same maximum average output power of 7 W, we characterised the MOPA output pulses in terms of the pulse duration, the peak power and the effective 10-dB spectral bandwidth, as tabulated in Table 4.2.1.

Table 4.2.1. Final output characteristics of the Tm:MOPA with different FBG2 temperature settings.

FBG2 / Final output	22°C	40°C	60°C
pulse duration	35 ps	46 ps	94 ps
peak power	200 kW	152 kW	74 kW
10-dB spectral bandwidth	1.6 nm	0.8 nm	0.5 nm

The pulse measurement results for the temperatures of 22°C (room temperature) and 60°C have already been demonstrated in section 3.2.2. While the output pulse of 40°C was measured by the AC showing a Gaussian-like AC trace, as depicted in Fig. 4.2.2, with a full width half maximum (FWHM) of 65 ps which corresponds to a Gaussian pulse duration of 46 ps.

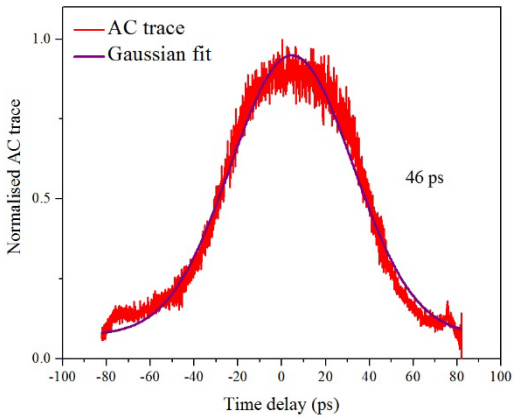

Fig. 4.2.2. Autocorrelator trace of output pulse from the Tm:MOPA system with FBG2 at 40°C.

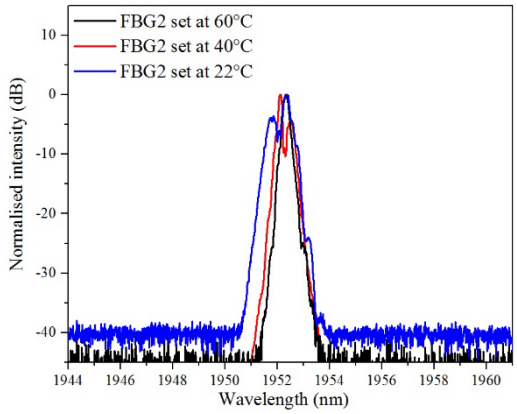

Fig. 4.2.3. Tm:MOPA final spectra at maximum output power with different FBG2 temperatures.

Fig. 4.2.3 shows a comparison of the Tm:MOPA output spectra at the maximum output power (7 W) with the FBG2 temperature set at 22°C, 40°C, and 60°C. The effective 10-dB bandwidth was 1.6, 0.8, and 0.5 nm for the FBG2 set at 22°C, 40°C, and 60°C, respectively. Severe self-phase modulation (SPM) was noticed for the room-temperature FBG2 setting, which occurred due to the relatively short pulse duration (35 ps, Fig. 3.2.4 (a)) and thus high peak power (200 kW) for the same average output power. Much reduced SPM was observed for the 60°C (94 ps, 74 kW, Fig.3.2.6 (b)) and 40°C FBG2 settings (46 ps, 152 kW, Fig. 4.2.2). In section 3.2.2, in order to have a suitable acceptance pumping bandwidth for OP-GaAs optical parametric devices (~1.5 nm), the Tm:MOPA system with the 60°C FBG2 setting was employed for the OPG and OPA work rather than that with FBG2 set at 22°C.

The pump system at the 40°C FBG2 setting can be considered as a compromise between accessing higher peak power (shorter pulses) and staying within the acceptance pump spectra bandwidth of OP-GaAs OPDs, as shown in Table 4.2.1, and was therefore used as a pump source for the cascaded OPG-OPA in this chapter. It should be noted that, other properties of the Tm:MOPA system, such as beam qualities and output powers, remained unchanged for different FBG2 temperature settings.

To further check and prove the dynamic behaviour of the MOPA output pulses with respect to the temperature control of the FBG2, we implemented the second-harmonic generation (SHG) experiment (details can be found in section 3.2.2) by using a periodically poled lithium niobate crystal. The generated second-harmonic wavelength of 976 nm would allow us to use a much faster detection system (a 32-GHz-bandwidth InGaAs photodetector (Agilent HP 83440D, 15-ps-response-time) combined with a 50-GHz-bandwidth digital communication analyser (Agilent 86100A)). Fig. 4.2.4 shows the SHG pulse profiles at the constant maximum pump power and using different FBG2 temperature settings (40°C, 50°C,

and 60°C). Pulse widths of 40, 48, 80 ps was found for FBG2 temperatures of 40°C, 50°C, and 60°C, respectively. These measurements verified the authenticity of pulse duration characterisation for the fundamental pulses (1952 nm).

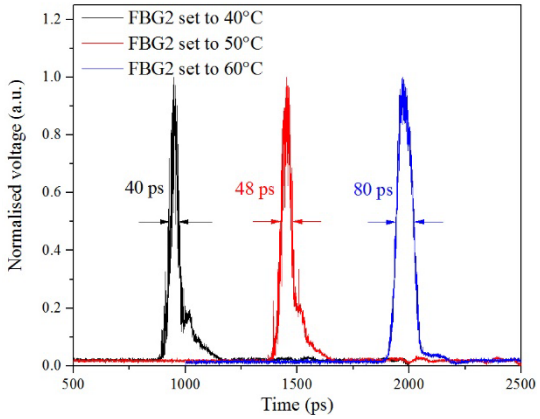

Fig. 4.2.4. SHG pulse profiles at different FBG2 temperature settings.

After this optimisation process, the final 1952-nm Tm:MOPA system was employed as a pump system for a cascaded OP-GaAs OPG-OPA with a maximum output power of 7 W. At a pulse duration of 46 ps and a repetition rate of 1 MHz, the corresponding maximum pulse energy and peak power were calculated to be 7 μJ and 152 kW, respectively. The final output had an effective 10-dB bandwidth of 0.8 nm and a beam quality of M^2=1.3.

4.3 Experimental setup of OP-GaAs cascaded OPG - OPA

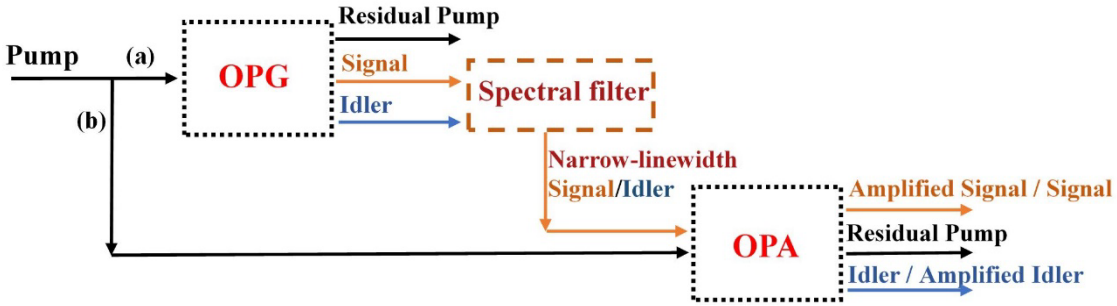

Fig. 4.3.1. Block diagram of the OP-GaAs cascaded OPG-OPA.

Fig. 4.3.1 sketches the block diagram of the OP-GaAs cascaded OPG-OPA. The basic scheme involves the seeding of an OPA with the broadband output of a commonly pumped OPG. The output from the OPG can be spectrally controlled by a spectral filter to provide a narrow-linewidth, tunable, seed for the OPA. Extra tunability is conferred by the use of different gratings within the OP-GaAs crystals. Consequently, the final OPA output has both wide tunability and narrow linewidth features operating at a fixed pump wavelength and without external seed lasers. The pump beam (black arrow, Fig. 4.3.1) is first split into two

beams, denoted here as beam (a) and (b). Beam (a) is used for pumping the OPG stage to generate broad-band signal and idler, either of which can be spectrally narrowed by a spectral filter. Filtered narrow-linewidth signal or idler can then be utilised as a seed for the OPA stage. The OPA stage combines this seed with pump beam (b) to generate amplified signal or idler. Note that in the experiments demonstrated in this chapter, only a filtered narrow-linewidth signal was used for seeding the OPA stage due to lack of suitable optics for handling the generated idler from the OPG stage. The OPG and OPA stages should fulfil the same phase-matching condition for an efficient nonlinear frequency conversion. The OP-GaAs crystals for the OPG and OPA were operated with the same grating periods and the same working temperatures in the following experiments.

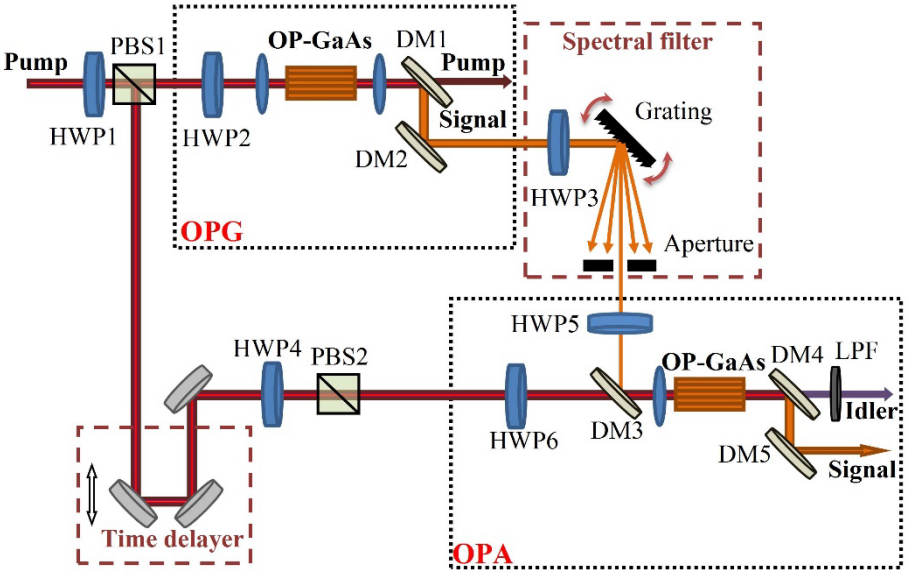

Fig. 4.3.2. Experimental setup of the cascaded OPG-OPA. HWP, half-wave plate; PBS, polarising beam splitter; DM, dichroic mirror; LPF, long-pass filter.

Fig. 4.3.2 shows the experimental setup for the cascaded OP-GaAs OPG-OPA. The available average pump power for the OPG-OPA was 5.2 W (before half wave plate 1 (HWP1)) due to losses introduced by various optical components (beam directing mirrors and a beam expander) used to bring the pump beam to HWP1. Note that the polarisation-sensitive isolator used for the previous OPG and OPA experiments in Chapter 3 (Fig. 3.3.1), was removed in order to provide the maximum available pump power for the OPG-OPA. In order to avoid possible optical feedback from the following optics, any optical components in the cascaded OPG-OPA that had surfaces that were normal to the pump beam were slightly tilted, including the HWPs and the OP-GaAs crystals. The two OP-GaAs crystals used for the cascaded OPG-OPA had the same fabrication parameters as that used in the last chapter (see section 3.3).

The pump beam first passed through HWP1 and then was split by PBS1 (Fig. 4.3.2) into two separate pump beams for the OPG and OPA stages. The pump power ratio between the two stages was controlled by the orientation of HWP1 (Fig. 4.3.2) in combination with PBS1. In the OPG stage, the pump was focused into the first OP-GaAs crystal with a beam waist of 70 μm ($1/e^2$ radius of intensity) by an uncoated calcium fluoride lens with a 75-mm focal-length. To maximise frequency conversion efficiency in the OP-GaAs, HWP2 (Fig. 4.3.2) was placed before the crystal to control the linear polarisation angle. After the crystal, another uncoated calcium fluoride lens (focal length 100 mm) was used to collimate the generated signal. A pair of dichroic mirrors (DM1 and DM2 in Fig. 4.3.2), with high reflectivity at the signal wavelengths (> 95%) and high transmission at the pump wavelength (> 90%), were used to extract the signal.

In order to convert the broad spectral output of the OPG signal generated by a particular quasi-phase-matching (QPM) grating into a tunable narrow bandwidth seed for the OPA stage, a spectral filter consisting of a diffraction grating and a narrow aperture was used. The reflective grating (GR1325-45031, Thorlabs) with 450 grooves/mm had good diffractive efficiency (>85%), across the entire signal wavelength range generated by the OP-GaAs OPG. HWP3 (Fig. 4.3.2) was used to rotate the polarisation angle of the output signal beam in order to optimise the grating diffraction efficiency. The adjustable-width slit aperture was placed after the grating to spatially filter the diffracted spectrum in one axis. Thus only a small but tunable fraction of the signal generated in the OPG passed through the aperture to seed the OPA.

In the OPA stage, the temporal delay of the pump pulses was controlled by a pair of reflective mirrors mounted on a translation stage to allow synchronism with the OPG output. HWP4 (Fig. 4.3.2) and PBS2 (Fig. 4.3.2) allowed independent control of the pump power launched into the second OP-GaAs crystal. A dichroic mirror (DM3 in Fig. 4.3.2), with coatings of high transmission (> 90%) at the pump wavelengths and high reflectivity (> 95%) at the signal wavelengths, spatially combined the pump and seed signal. The spatially and temporally overlapped beams were focused into the OP-GaAs OPA crystal, by an uncoated calcium fluoride lens (focal length 100 mm), resulting in an 80-μm beam waist for the pump beam. This focusing was chosen as a compromise between achieving the highest nonlinear gain and avoiding three-photon absorption effects, as discussed in section 3.3. The signal seed beam size was measured to be 85 μm when not filtered. Once the grating and slit aperture were in place the power was too low to accurately measure the beam size in the aperture axis but was estimated to be ~150 μm from the geometry of the experimental setup.

The slit aperture size (~2 mm) was experimentally chosen as a compromise between reducing the spectral bandwidth and maintaining a high enough output power.

4.4 Experimental results and discussion for the cascaded OPG-OPA

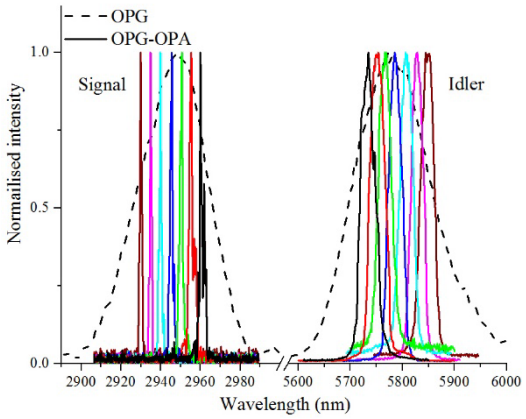

Fig. 4.4.1. Measured spectra for signal (left) and idler (right) in both OPG and OPG-OPA operation regimes based on a 57-μm QPM period grating.

For a fixed Tm:MOPA wavelength of 1952 nm and a fixed crystal temperature of 50°C, the different QPM grating periods allowed tuning of the central signal and idler wavelengths of the OPG from 2588 nm to 2919 nm (signal) and from 5892 nm to 7943 nm (idler). The generated spectrum from the OP-GaAs OPG using a particular QPM grating was also relatively broad, as expected. For example, with a QPM grating period of 57 μm and temperature of 30℃, signal at a wavelength of 2950 nm and idler at a wavelength of 5770 nm were generated from the OP-GaAs with a FWHM spectral bandwidth of 40 nm (46 cm^{-1}) and 170 nm (51 cm^{-1}), respectively, as shown in Fig. 4.4.1 (dash line).

For the OPA spectrum, taking advantage of the spectral filtering of the signal seed, the spectrum was substantially reduced to bandwidths of 1.2 nm (1.4 cm^{-1}) and 29 nm (9 cm^{-1}) for the signal and idler, respectively. For a fixed QPM grating period and temperature for both OP-GaAs crystals, the narrow linewidth spectrum of the OPA could be rapidly tuned across the broad OPG spectrum by rotating the diffraction grating angle, as can be found in Fig. 4.4.1 (solid lines). By changing grating periods and temperatures of the two OP-GaAs simultaneously, a widely and continuously tunable OP-GaAs OPG-OPA was realised. Fig. 4.4.2 shows example output spectra, in the whole tuning range from 2552 nm to 2960 nm (signal) and from 5733 nm to 8305 nm (idler), with narrow linewidths. The bandwidth of the generated signal from the OPA stage was narrower than that of the idler, because it was well defined by the seed bandwidth, which was in turn set by the spectral filter (Fig. 4.3.2). The signal and idler bandwidths show a small variation over the tuning range. This may be

due to non-optimum spatial overlap between the pump and signal beams. This could cause different spectral components and bandwidths of the diffracted signal beams to interact with the pump beam in the crystal. In addition, the pump spectra broadening could play a role in affecting idler and/or signal bandwidths (as already mentioned in section 3.4). It should be noted that if idler-handling optics was available then similar direct control of its bandwidth would also be possible in future.

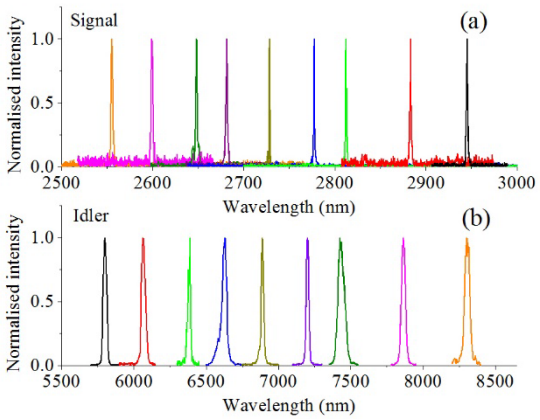

Fig. 4.4.2. Measured spectra for signal (a) and idler (b) from the tunable OPG-OPA.

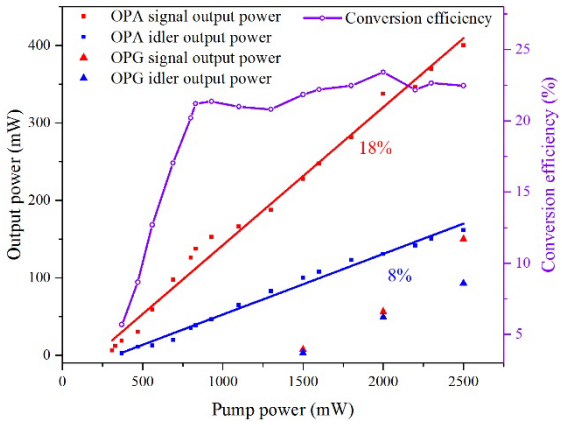

Fig. 4.4.3. (Left) Signal and idler output power as a function of pump power in OPG-OPA operation. Squares are measured OPG-OPA data points and the solid lines are linear fits. (Right) Total power conversion efficiency of the OPG-OPA versus pump power. The solid line is purely to guide the eye.

A pump-power threshold of approximately 1.5 W was measured for the OPG operating with signal and idler wavelengths of 2930 nm and 5860 nm, respectively (OP-GaAs period of 57 μm, oven temperature of 50°C). The corresponding power intensity at the threshold in the OP-GaAs crystal was 162 MW/cm^2. The measured signal and idler output powers from the OPG are shown in Fig. 4.4.3.

After a pair of dichroic mirrors (DM4, DM5 in Fig. 4.3.2) and a long-pass filter (LPF) with a short wavelength cutoff at 4.5 μm, the OPA signal and idler output powers were measured. With the OPA-stage power attenuator (HWP4 + PBS2) set at a maximal transmission, the power split ratio from the PBS1 was optimised by adjusting the HWP1 to obtain the maximum signal output power from the OPA. After this optimisation, it was observed that 2 W of pump power was incident on the OPG crystal and 2.5 W of pump power was incident on the OPA crystal. With an OPG seed signal power of ~2 mW, a maximum signal power of 400 mW, at 2942 nm, and idler power of 162 mW, at 5800 nm, were obtained for the OPA stage. The signal output power corresponded to that measured after the DMs, whereas the idler power was measured with the DMs removed but with the LPF in place and accounts for the losses of the LPF. With a 1 MHz repetition rate, the maximum pulse energies were 0.4 μJ and 0.16 μJ for the signal and idler, respectively, and the corresponding power conversion efficiency was 22.5% in the OPA stage. To investigate the influence of the pump power on the conversion efficiency in the OPA, the signal and idler output power was measured against the pump power by adjusting the OPA power attenuator (HWP4 + PBS2), as shown in Fig. 4.4.3. The increment of the signal and idler power had a linear slope efficiency of 18% and 8%, respectively. Figure 4.4.3 (right) also shows the power conversion efficiency against the input pump power for the OPA. The conversion efficiency saturated when the pump was higher than ~800 mW. The saturation at this level may be due to the non-optimised spatial overlap between the pump and the signal seed.

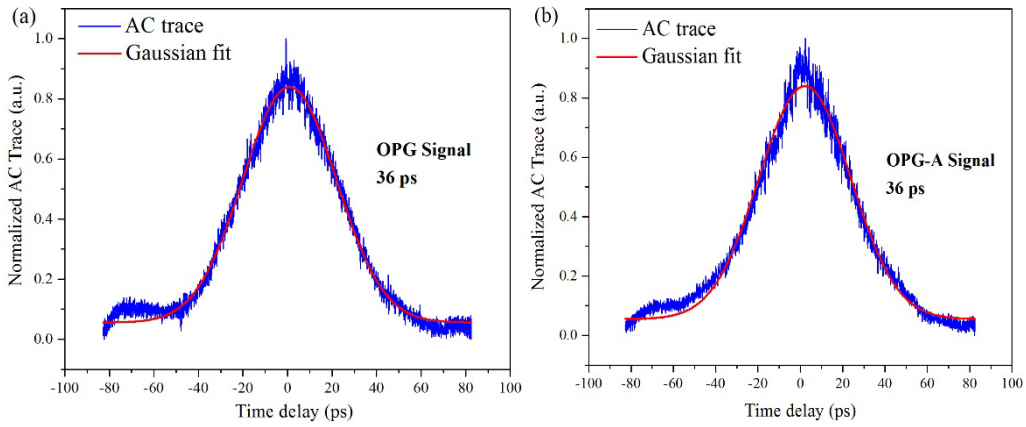

Fig. 4.4.4. Autocorrelator traces (blue) of the signal pulse of the OPG (a), signal pulse of the OPG-OPA (b), and the corresponding Gaussian fits (red).

The AC traces of the signal pulses, both for the OPG stage and the OPA stage, were measured with a commercial AC (APE, pulseLink), as shown in Fig. 4.4.4. All AC traces have Gaussian-like pulse shapes with full width at FWHM values of 51 ps for both the OPG and the OPG-OPA signal pulses. The corresponding FWHM Gaussian-pulse durations were

calculated to be 36 ps. In the OPG, the pulse duration of the generated signal seed was narrower than that of the pump pulse (46 ps, Fig. 4.2.2), whilst in the OPG-OPA, the pulse duration of the output signal followed that of the input signal seed, as expected. The pulse duration of the idler pulses could not be measured due to the lack of suitable equipment, but the generated idler pulse durations are assumed to be similar to the generated signal pulse durations both for the OPG and OPG-OPA. Therefore, the highest peak powers can be calculated to be 11.1 kW and 4.5 kW for the cascaded OPG-OPA signal (2942 nm) and idler (5800 nm), respectively. The M^2 parameters of the generated signal (2942 nm) and idler (5800 nm) beams from the OPG-OPA were characterised using a Pyrocam-based profiler (NanoScan, Photon). The output signal beam quality was measured to be $M^2_x = 2.4$ and $M^2_y = 2.2$, and the output idler beam quality was measured to be $M^2_x = 3.4$ and $M^2_y = 3.4$, as shown in Fig. 4.4.5. The beam qualities were relatively poor due to no active spatial control for either OPG or OPA, similar to that presented in section 3.4.

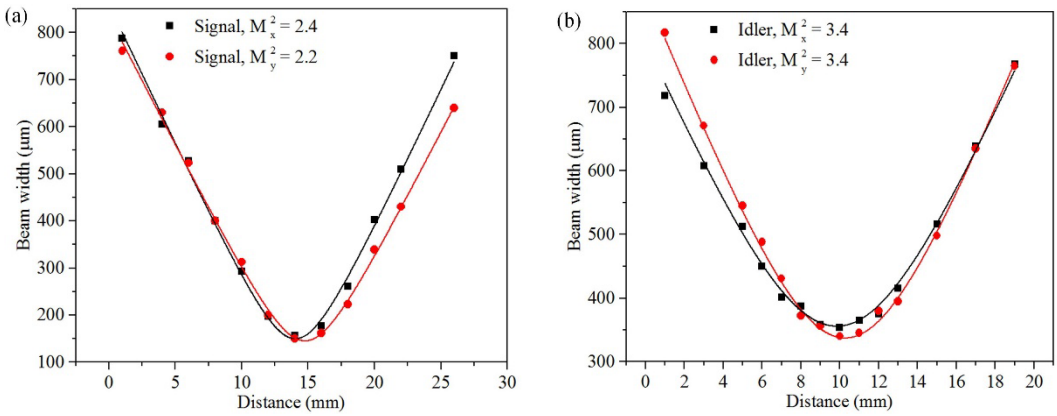

Fig. 4.4.5. M^2 measurement for OPG-OPA signal at 2942 nm (a) and idler at 5800 nm (b) in the x and y direction for OP-GaAs with grating period of 57 μm.

4.5 Summary

In conclusion, I have demonstrated a widely tunable, narrow-linewidth, high-peak-power, cascaded picosecond OPG-OPA based on OP-GaAs nonlinear crystals and a diode-seeded Tm:MOPA pump laser. The OPG-OPA has generated narrow-linewidth signal and idler beams, with wavelength tuning ranges of 2552 - 2960 nm and 5733 - 8305 nm, respectively. The maximum peak powers of 11.1 kW and 4.5 kW were obtained at a signal wavelength of 2942 nm and an idler wavelength of 5800 nm with a linewidth of 1.4 cm^{-1} and 9 cm^{-1}, respectively. The output beam qualities for generated signal and idler were $M^2 \sim 2.3$ and $M^2_x \sim 3.4$, respectively.

Table 4.5.1. Performance comparison between Cr:ZnSe laser seeded OPA and cascaded OPG-OPA.

		Wavelength (μm)	Maximum average power (W)	Maximum peak power (kW)	Linewidth (cm^{-1})	Beam quality (M^2x/y)	Pulse duration (ps)	Pump power (W)	Need for external laser
OPA	signal	2.6-2.7	1.07	11.3	0.71	2.8/2.7	94	3.7	Yes
	idler	7.2-8.3	0.26	2.7	1.4	1.9/1.8			
OPG-OPA	signal	2.6-3.0	0.40	11.1	1.4	2.4/2.2	36	5.2	No
	idler	5.7-8.3	0.16	4.5	9	3.4/3.4			

Table 4.5.1 gives a performance comparison between the OPA demonstrated in Chapter 3 (traditional OPA) and the cascaded OP-GaAs OPG-OPA. Taking advantages of the narrow-linewidth seed laser, the output linewidths of the traditional OPA was narrower than those of the OPG-OPA. The OPG-OPA still needs to be improved in terms of the output power, beam quality, and long term stability. However, without a need for external seed lasers, the OPG-OPA offers access to the full tuning range that OP-GaAs crystals can provide. Furthermore, the combination of narrow-linewidth, wide tunablity and high peak power, in a simple fibre-laser-pumped single-pass configuration, makes the cascaded OP-GaAs OPG-OPA an attractive option for mid-IR spectroscopic applications. For those spectroscopic applications that require even narrower linewidths at the longer idler wavelengths, an idler-seeded cascaded OPG-OPA would need to be realised, which should be readily possible if idler handling optics is available. In next chapter, the focus will move on to improving the beam qualities of the mid-IR output by employing an optical cavity and thus working as an optical parametric oscillator.

Reference

[1] G. Cerullo, and S. D. Silvestri, "Ultrafast optical parametric amplifiers," *Review of Scientific Instruments,* vol. 74, no. 1, pp. 1-18, 2003.

[2] F. K. Tittel *et al.*, "Mid-infrared laser applications in spectroscopy," in *Solid-State Mid-Infrared Laser Sources*, Berlin, Germany: Springer Berlin Heidelberg, 2003, pp. 458-529.

[3] S. Lambert-Girard *et al.*, "Differential optical absorption spectroscopy lidar for mid-infrared gaseous measurements," *Applied Optics,* vol. 54, no. 7, pp. 1647-1656, Mar. 2015.

[4] G. Bloom *et al.*, "Optical parametric amplification of a distributed-feedback quantum-cascade laser in orientation-patterned GaAs," *Optics Letters,* vol. 35, no. 4, pp. 505-507, Feb. 2010.

[5] Q. Clément *et al.*, "Tunable optical parametric amplification of a single-frequency quantum cascade laser around 8 μm in ZnGeP2," *Optics Letters,* vol. 38, no. 20, pp. 4046-4049, Oct. 2013.

[6] F. Gutty *et al.*, "140 W peak power laser system tunable in the LWIR," *Optics Express*, vol. 25, no. 16, pp. 18897-18906, Aug. 2017.

[7] Y. Yao *et al.*, "Mid-infrared quantum cascade lasers," *Nature Photonics,* vol. 6, no. 7, pp. 432-439, Jun. 2012.

[8] L. Xu *et al.*, "Thulium-fiber-laser-pumped, high-peak-power, picosecond, mid-infrared orientation-patterned GaAs optical parametric generator and amplifier," *Optics Letters,* vol. 42, no. 19, pp. 4036-4039, Oct. 2017.

[9] Q. Fu *et al.*, "Widely tunable, narrow-linewidth, high-peak-power, picosecond mid-infrared optical parametric amplifier," *IEEE Journal of Selected Topics in Quantum Electronics,* vol. PP, no. 99, pp. 1-1, 2018.

[10] Q. Fu *et al.*, "Picosecond fiber-laser-pumped widely tunable, narrow-linewidth, high-peak-power, mid-infrared OP-GaAs OPA," in *Conference on Lasers and Electro-Optics (CLEO)*, San Jose, California, 2018, pp. STh3F.2.

Chapter 5

High-beam-quality, idler-resonant, picosecond mid-infrared OP-GaAs optical parametric oscillator

5.1 Introduction

Mid-infrared (mid-IR) ultrashort laser sources with wide tuning capability, narrow spectral linewidth, high average power, high repetition rate, and good beam quality are in demand for many spectroscopic applications [1-3]. Wide tuning allows access to the detection of different molecules, whereas narrow linewidths are important for spectral resolution. High power improves the signal-to-noise ratio and high repetition rate increases the data processing speed. Furthermore, good beam quality is crucial for remote sensing and imaging as it allows a longer measurement distance. Apart from spectroscopic applications, good beam qualities are also of benefit in material processing and surgery, which require strong focusing [4, 5]. High beam quality is also essential for optical fibre integrated systems, such as power delivery and nonlinear optics [6].

Quantum cascade lasers, lead-salt diode lasers and interband cascade lasers can provide mid-IR and even far infrared outputs, but can only produce relatively low peak power and a limited tuning range from single devices. Optical parametric devices (OPDs), specifically based on orientation-patterned gallium arsenide (OP-GaAs), have also received much attention as mid-IR sources. In Chapters 3 and 4, I have demonstrated an OP-GaAs optical parametric generator (OPG), an optical parametric amplifier (OPA) and a cascaded OPG-OPA with useful output features, such as wide tunablity, up to watt-level average power output and kilo-watt-level peak-power. However, their mid-IR output beam qualities were all relatively poor with M^2 parameters larger than 1.7.

Optical parametric oscillators (OPOs), as another type of OPD, can potentially generate high output power, broad tuning range, and good beam quality simultaneously. Signal-resonant OPOs are widely studied because optics and diagnostics are more readily available for shorter wavelengths. Compared with the signal output from signal-resonant OPOs, the generated idler usually has a relatively poor beam quality due to lack of spatial control for the idler. Idler-resonant OPOs have rarely been studied and so far have only been demonstrated at relatively short wavelengths in the mid-IR (< 4.5 μm) [7-10]. In this work, we aim to develop an idler-resonant OPO generating longer wavelengths in the mid-IR up to 6 μm, which could be employed as a potential source tool for power delivery of mid-IR hollow-core fibres, as described in section 2.9.1.

Here in this chapter, I report an idler-resonant, mid-IR, OP-GaAs-based, picosecond OPO with near-diffraction-limited idler beam quality, wide tunablity and watt-level average output power. The OP-GaAs OPO was synchronously pumped by a 2007-nm thulium-doped fibre (TDF) master–oscillator-power-amplifier (Tm:MOPA) system generating ~100 ps duration pulses at 100 MHz repetition rate. A tuning range of 4394-6102 nm (idler) and 2997-3661 nm (signal) was demonstrated by changing the temperature and using different patterning periods of the OP-GaAs crystal. A maximum average power of 1.18 W (idler, 5580 nm) and 0.51 W (signal, 3136 nm) was obtained. The slope efficiency was 19.6% and 8.6% for the idler and signal, respectively. As expected, the idler-resonant OPO provides a high quality mid-IR output beam with measured idler beam quality of $M^2_x = 1.06$ and $M^2_y = 1.03$.

Section 5.2 introduces the pump system for the OP-GaAs OPO, and section 5.3 describes the setup of the OPO. Section 5.4 demonstrates the experimental results and discussion of the OP-GaAs OPO followed by the final summary section (section 5.5). Experimental results described in this chapter have been published, in part, in [11, 12].

5.2 OPO Pump system

5.2.1 Experimental setup

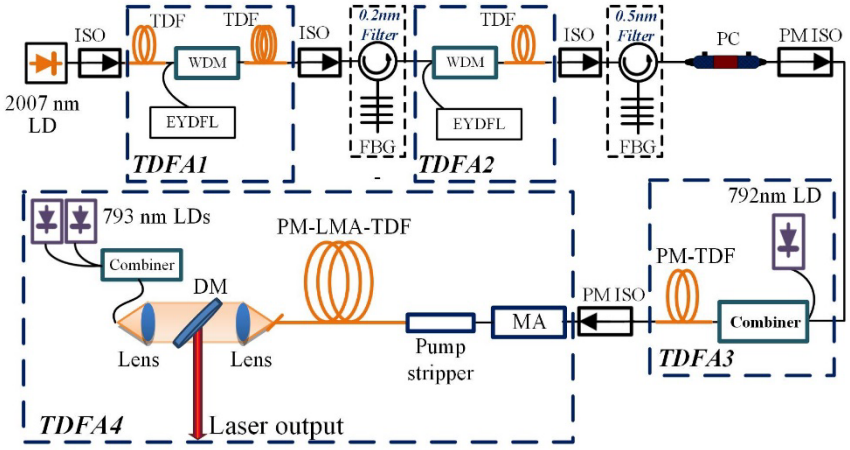

Fig. 5.2.1. Schematic diagram of gain-switched laser diode seeding, Tm:MOPA system. LD: laser diode; ISO: isolator; TDF: thulium-doped fibre; WDM: wavelength-division multiplexer; EYDFL: erbium/ytterbium co-doped fibre laser; FBG: fibre bragg grating. PC: polarisation controller; PM ISO: polarisation maintaining isolator; MA: mode adapter. LMA: large mode-area. DM: dichroic mirror.

Fig. 5.2.1 shows a nearly-all-fiberised picosecond Tm:MOPA system consisting of a gain-switched laser diode as the seed, followed by a four-stage TDF amplifier (TDFA) chain. A discrete mode 2007-nm laser diode (Eblana Photonics, EP2008-0-DM-H17-FM) was biased by a constant current of 11 mA and gain-switched by a pulse generator delivering rectangular pulses of 570 ps duration and maximum amplitude of 5V at repetition rates of 100 MHz. The laser diode generated 80-ps pulses at a repetition rate of 100 MHz and a wavelength of 2008 nm with an average power ~100 µW. TDFA1 consisted of a 12-m-long TDF (OFS TmDF200) core-pumped by a home-made Er/Yb co-doped fiber laser at 1565 nm through a 1565/2000nm wavelength-division multiplexer (WDM) with an additional 4-m-long TDF (OFS TmDF200) placed before the WDM to absorb backward amplified spontaneous emission (ASE), similar to the structure reported in section 3.2.1, but with an overall longer fibre length in turn providing more signal gain at longer wavelengths. The seed signal was amplified to 35 mW by the TDFA1 at a pump power of 0.8 W. Then, a narrow-band spectral filter formed by a fibre bragg grating (FBG) with a bandwidth of 0.2 nm and a circulator (3 dB loss) was used for narrowing the signal linewidth and removing amplified spontaneous emission (ASE) resulted in an output power of 1.5 mW (~13 dB loss). The second core-pumped pre-amplifier (TDFA2, Fig. 5.2.1) composed of a 2-m-long home-made TDF (8.5 µm core, 100 µm cladding, NA=0.2) promoting the signal power to 120 mW at a pump

power of 3 W with a ~19 dB gain. After that, a 0.5-nm FBG spliced to another circulator again improved the output signal noise ratio (OSNR) and removed excess ASE. The two FBGs after TDFA1 and 2 had an identical central wavelength of 2007 nm but with different bandwidths. Starting from the TDFA3, polarisation-maintaining fibres and components were employed, therefore a polarisation controller (PC-1100-15, FibrePro, insertion loss ~1.5 dB) and a polarisation sensitive isolator were used to define a certain linearly polarised direction after the 0.5 nm filter. TDFA3 was cladding pumped a 790 nm laser diode with a maximum output power of 8 W. A 43-mW signal was launched into a pump and signal combiner together with pump light to pump a 4-m-long TDF (PM-TDF-10P/130-HE, Nufern) with a core/cladding diameter of 10 μm/130 μm and NA of 0.15/0.46. TDFA3 provided an output power of 200 mW at an operational pump power of 1.4 W, and its output was spliced to a customised mode adapter (MA) for mode matching between the 10 μm core fibre and a 25 μm core fibre which used for TDFA4. TDFA4 consisted of a 4 m long polarisation-maintaining large-mode-area (LMA) 25 μm core TDF (Nufern, PLMA-TDF-25P/400-HE) counter-pumped by two 793 nm laser diodes with a total pump power of 52 W (pump coupling efficiency ~92%). A pump stripper was placed between the active fibre and the MA for removing the residual pump. A polished coreless 8° endcap (made from in-house-fabricated coreless fibres) was spliced at the output end of the LMA TDF to resist optical feedback and to expand the beam size for avoiding optical damage. Isolators were placed after the seed laser and each amplifier stage in order to avoid back reflections.

The main differences between the setup of the 2007-nm Tm:MOPA system and the previous 1952-nm Tm:MOPA system described in Chapter 3.2 are as follows:

i) Seed diode wavelength. It enabled the generation of idler wavelengths covering 5-6 μm for an unchanged OP-GaAs crystal (see tuning curves in section 2.9.1).

ii) Pulse repetition rate. As mentioned before, an ultrafast OPO requires a high repetition rate (here, 100 MHz) for synchronous pumping, instead of the low repetition rate (1 MHz) generally suitable for OPGs and OPAs.

iii) Management of ASE. Due to the high repetition rate of the 2007-nm seed laser diode (a high average power from the seed), ASE generated in between optical pulses was significantly reduced. Therefore, the 2007-nm MOPA system did not employ an EOM as a time gate in temporal domain but only used the spectral filters to manage ASE.

iv) Polarisation maintaining system. In the 1952-nm MOPA system, no polarisation maintaining components were used apart from the laser diode and the EOM. For

OPDs and other nonlinear optical devices, a well-defined pump polarisation direction is typically required. Therefore, in the 2007-nm MOPA system, polarisation maintaining components were employed for the TDFA3 and TDFA4 giving a linear polarisation at the final output of the Tm:MOPA system.

5.2.2 Experimental results and discussion

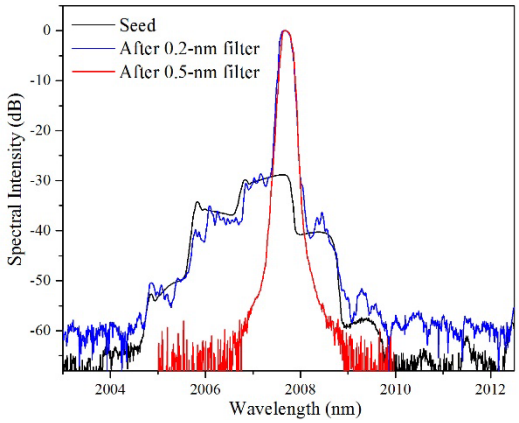

Fig. 5.2.2. The seed laser diode spectra and normalised spectra after the 0.2-nm filter and the 0.5-nm filter.

Fig. 5.2.2 shows the spectral characteristics of the seed, the signal after TDFA1 and the 0.2-nm filter, and the signal after TDFA2 and the 0.5-nm filter. The OSNR of the 2007-nm signal spectra from the seed laser is relatively poor (~6.6 dB), but gradually improved to be ~28 dB and ~60 dB after the 0.2 nm filter and the 0.5 nm filter, respectively. Meanwhile the signal bandwidth was narrowed from a 3-dB bandwidth of ~1 nm, at the seed output, to 0.2 nm at the 0.5 nm filter output.

The four TDFAs offer an overall gain of 51 dB with a maximum output power of 12.6 W. The average output power of TDFA4 is plotted against the launched pump power in Fig. 5.2.3 (a), with a corresponding slope efficiency of 30%. Fig. 5.2.3 (b) shows the spectra from TDFA4 at an output power of 4, 8, and 12.6 W, with its inset showing a broad view of the spectra from TDFA4 at the highest output power of 12.6 W. This figure indicates no spectral broadening was observed in TDFA4 and shows that the 3-dB bandwidth of the Tm:MOPA output was 0.2 nm, which was well within the pump acceptance bandwidth of the OP-GaAs OPO crystal (~1.5 nm, as stated in section 2.9.2).

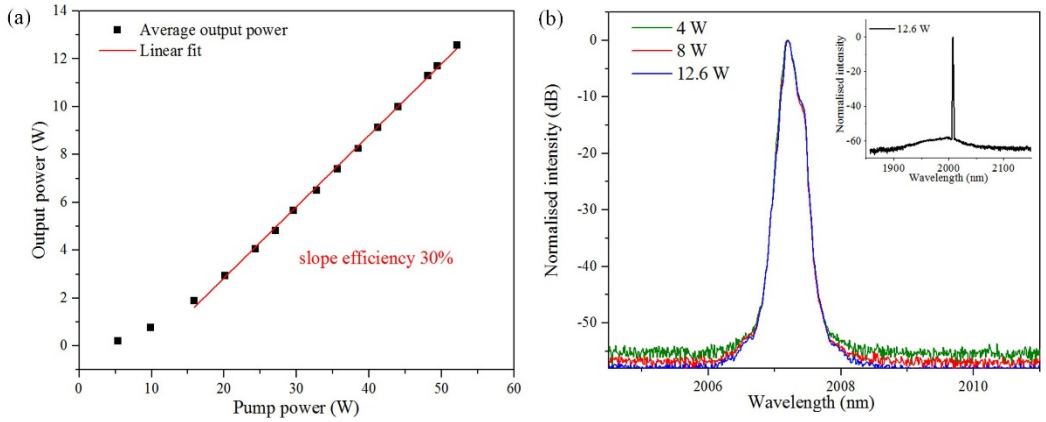

Fig. 5.2.3. (a) Output powers of the Tm-MOPA system. (b) Spectra from TDFA4 at different pump powers. Inset: spectra from TDFA4 at 12.6 W.

The temporal profiles of the seed and the signal after the 0.2-nm FBG-based filter and after TDFA4 at maximum output power were characterised by a >12.5-GHz-bandwidth photodetector (EOT 5000F) and a communication signal analyser (50-GHz bandwidth, Tektronix CSA 803), as sketched in Fig. 5.2.4. The pulse duration of the seed laser was 79 ps (FWHM, black line in Fig. 5.2.4). After TDFA1 and the 0.2-nm filter, the pulse was slightly distorted with a sequence of small following sub-pulses and became broader with a main pulse duration of 100 ps (red line in Fig. 5.2.4), which then remained constant through to the output from the Tm:MOPA system. Given this pulse duration, a maximum peak power of 1.26 kW can be calculated for a maximum average power of 12.6 W and a repetition rate of 100 MHz. The sub-pulses should have no effects on the following nonlinear frequency conversion experiments due to their relatively low peak powers. Beam qualities of the Tm:MOPA system were characterised by a Pyrocam-based beam analyser (NanoScan, Photon). Figure 5.2.5 presents the M^2 values with $M^2_x = 1.3$ and $M^2_y = 1.4$ at an output power of 5 W, while larger values were obtained at the maximum output power of 12.6 W with $M^2_x = 1.5$ and $M^2_y = 1.5$. The elliptical output beam resulted from the 8° endcap on the output fibre end of TDFA4 together with the slightly tilted collimated lens (an uncoated calcium fluoride lens, Fig. 5.2.1) for avoiding back-reflection from the lens into TDFA4. The output from the 2007-nm Tm:MOPA system was linearly polarised with a polarisation extinction ratio of ~14 dB.

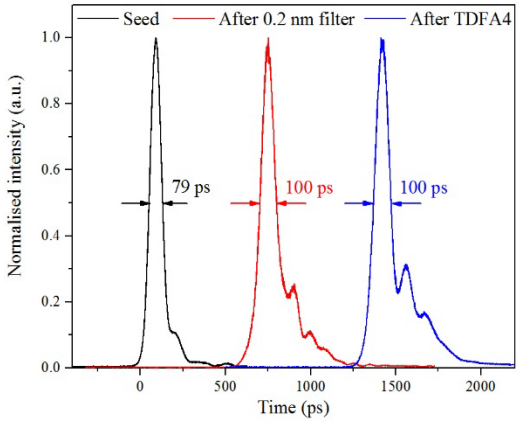

Fig. 5.2.4. Temporal profiles of 2-μm optical pulses from the seed diode, after the 0.2-nm filter, and after TDFA4.

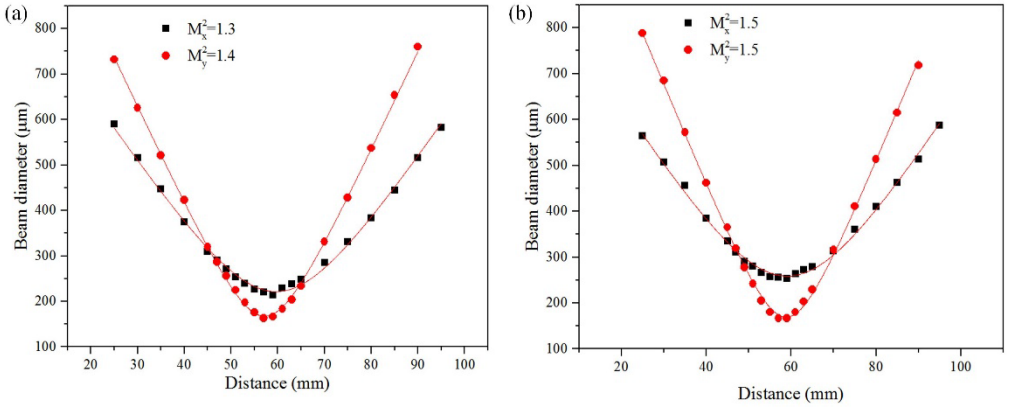

Fig. 5.2.5. Beam qualities at an output power of 5 W (a) and 12.6 W (b).

Overall, the pump system for the OP-GaAs OPO was a 2007-nm Tm:MOPA system operating at a repetition rate of 100 MHz, and at a pulse duration of 100 ps. The final output is linearly polarised, with a spectral bandwidth of 0.2 nm, a beam quality of M^2=1.5, and a maximum output power of 12.6 W (peak power 1.26 kW). During carrying out the OPO experiment, the output power from the Tm:MOPA was fixed at the maximum power of 12.6 W.

5.3 High-beam-quality, idler resonant OP-GaAs OPO setup

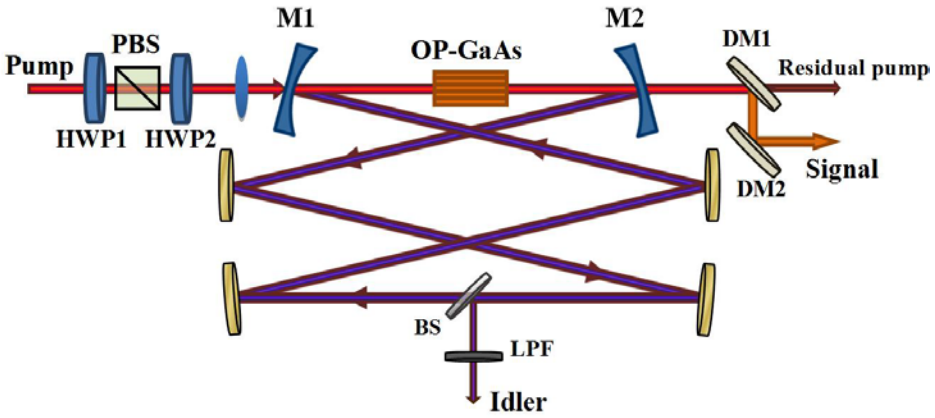

Fig. 5.3.1 OP-GaAs OPO experimental setup. HWP, half-wave plate; PBS, polarising beam splitter; M1,M2, mirror 1,2; DM, dichroic mirror; BS, beam splitter; LPF, long-pass filter.

Fig. 5.3.1 presents the experimental setup for the idler-resonant, high-beam-quality, mid-IR OP-GaAs OPO. Two half-wave plates (HWP1, 2), combined with a polarising beam splitter were used to control both the pump power and the rotation of the linear polarisation incident onto the crystal. The OP-GaAs crystal used in the OPO and the crystal setup (including temperature control and pump polarisation direction) were same as those used for the OPG and OPA (Chapter 3). However, due to the change of operating wavelengths, the anti-reflection (AR) coating of the end facets of the OP-GaAs for idler and signal were different with a lower reflectivity of <1.5% (idler) and <5% (signal), respectively. The OPO cavity consisted of two plane-concave dielectric-coated mirrors (M1, M2, Fig. 5.3.1, radius of curvature =250 mm) and four plane-plane gold-coated mirrors. The plane-concave mirrors were AR coated at the pump wavelength (R<2%) and high-reflection (HR) coated at idler wavelengths (R>99.5%). The plane-concave mirrors coatings were not specifically designed for the signal wavelengths, which led to a variation in reflectivity of 1-70% over the entire signal wavelength range. Note that both the high cavity reflectivity and the low crystal coating reflectivity for idler wavelengths were crucial to enable the idler-resonant cavity to reach an oscillation threshold (as mentioned in section 2.9.4). The total optical cavity length was set to 3 m to match the pump repetition rate of 100 MHz, so as to achieve a synchronously pumped ring resonator. Active stabilization of the cavity length to the pump repetition rate was not required in the course of this work due to the relatively long duration of the pump pulses relative to the small variations in cavity round trip time that might originate from temperature/dispersion changes during the course of the experiments. The OP-GaAs crystal was placed in the middle of two plane-concave mirrors, which were

separated by 276 mm. The cavity mode of the idler beam was calculated to have a beam waist of 90~110 μm inside the crystal, depending on the idler wavelength. In order to match the cavity modes, the pump beam was focused into the OP-GaAs by a coated calcium fluoride lens (f=250 mm) with a beam waist of 100 μm (x direction) and 80 μm (y direction) ($1/e^2$ radius of intensity) due to the slightly elliptical shaped pump beam caused by the angled output facet. The idler output was extracted using a coated calcium fluoride beam splitter (BS, Fig. 5.3.1, BSW511R, Thorlabs) with a reflectivity of ~24-35% over the idler wavelength range. With the pump polarisation set to the [111] crystallographic axis, the output idler is expected to have the same polarisation direction in order to obtain the maximum gain [13]. The idler power was measured after a long-pass filter (LPF, Fig. 5.3.1), which had a short-wavelength cut-off at 4.5 μm. The signal beam was partially extracted from the cavity through M2 and with the aid of two dichroic mirrors (DM1, DM2, Fig. 5.3.1) to separate it from the residual pump light.

5.4 Experimental results and discussion of the high-beam-quality OPO

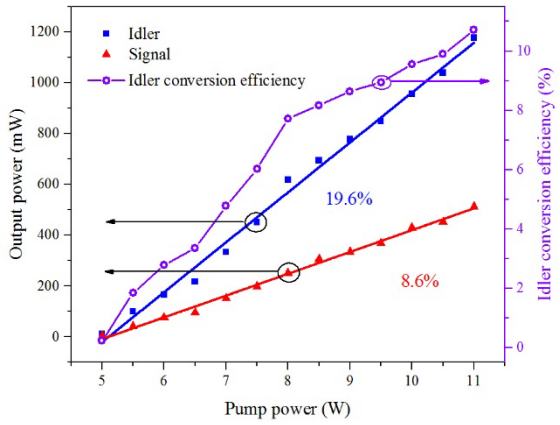

Fig. 5.4.1 (Left) Idler (5580 nm) and signal (3136 nm) output power as a function of pump power from the OPO. Squares and triangles are measured data points and the solid lines are linear fits. (Right) Idler power conversion efficiency versus pump power.

Because of the many optical elements (directing mirrors, an isolator, and a beam expander) between the pump system (Fig. 5.2.1) and the OPO cavity (Fig. 5.3.1), the maximum available pump power immediately before the crystal for the OPO was 11 W. At the pump power of 11 W, a maximum idler average power of 1.18 W was obtained from the 59-μm grating-period OP-GaAs, at an oven temperature of 80°C. Under the same operating conditions, slightly lower maximum idler output powers of 1.1 W and 0.8 W were obtained from the 57-μm and 61-μm grating periods, respectively, which was attributed to the associated changes in cavity mode and/or the lower idler quantum efficiency over the

different wavelengths. Fig. 5.4.1 shows the idler and signal output powers working with 59-μm OP-GaAs period at a temperature of 80°C with the idler and signal wavelengths of 5580 nm and 3136 nm. An oscillation threshold of 5 W was observed, corresponding to a pump intensity of ~2.5 MW/cm^2. According to the theory described in section 2.9.4 and assuming a fractional cavity loss of ~0.4, a theoretical threshold intensity of ~1 MW/cm^2 can be estimated, which is reasonably close to the experimentally observed threshold given the uncertainty in the effective nonlinearity of OP-GaAs, the estimated cavity loss, the non-Gaussian shaped pulse, and imperfect spatial mode matching. As depicted in Fig. 5.4.1, an idler slope efficiency of 19.6% and a maximum optical-to-optical conversion efficiency of 10.7% were observed without any roll-off phenomenon, meaning that the OPO output power was primarily limited by the available pump power. The signal output from DM2 was measured and is plotted in Fig. 5.4.1 (Left) with a maximum output power and slope efficiency of 0.51 W and 8.6%, respectively. Taking into consideration all of the signal outputs from the cavity mirrors, the generated signal power from the crystal was calculated, from the one measured output, to be ~1.96 W. In this experiment, the main emphasis was placed on good-beam-quality idler generation from the OPO, and thus the signal output from the cavity was not optimised (but will be addressed in next chapter).

The pulse duration of the generated signal and idler pulses were not directly measured but are expected to be shorter than the pump pulses, as is common in a nonlinear frequency conversion device due to nonlinear gain narrowing effects [14]. Consequently, it can be inferred that the peak powers of the generated idler and signal pulses were at least 118 W and 51 W, respectively (i.e. the values calculated assuming that the signal and idler pulses had the same pulse duration as the pump (100ps, Fig.5.2.4)). The operation of the Tm:fibre MOPA system and OPO were reasonably stable over time, with a measured <3% drift in the pump power and ~8% in the OPO output power over a period of 30 minutes, as presented in Fig. 5.4.2. The larger drift on the OPO output was due to drift in the OPO cavity alignment and this was readily corrected by mechanical retuning of the cavity mirrors.

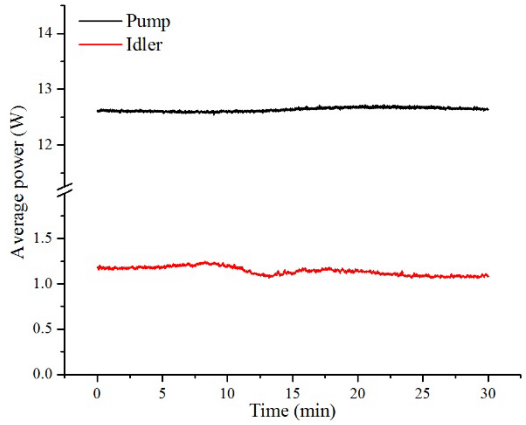

Fig. 5.4.2. Stability of pump power and idler output power measurements over 30 minutes.

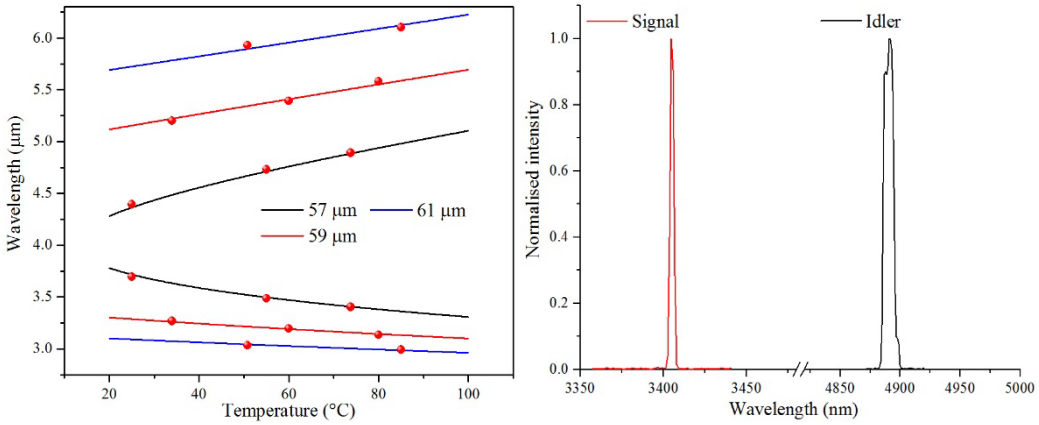

Fig. 5.4.3. (Left) Comparison between theoretical tuning curves with measured OPO spectrum data for signal and idler. (Right) Example spectrum of the OP-GaAs OPO.

The OPO wavelength tunability was studied by using different OP-GaAs grating periods and oven temperatures. The idler and signal wavelength could be tuned over 4394-6102 nm (idler) and 2997-3661 nm (signal). Fig. 5.4.3 (Left) shows a comparison of theoretical curves (as calculated in section 2.9.1) and experimental values for the signal and idler wavelengths. Fig. 5.4.3 (Right) presents an example spectrum at a signal and idler wavelength of 3404 nm and 4892 nm measured with a 57-μm OP-GaAs period and a temperature of 74°C. The idler spectral linewidth of 9 nm (3.8 cm^{-1}) was defined by the BS (Fig. 5.3.1), which also worked as an etalon (a spectral filter) with an estimated bandwidth of ~7 nm and a free spectral range of ~107 GHz. The signal spectral linewidth was measured to be 1 nm (0.9 cm^{-1}), compared to the pump value of 0.2 nm (0.5 cm^{-1}). The OPO was operated with three different OP-GaAs periods of 57 μm, 59 μm and 61 μm, but did not work with periods of 63 μm and 65 μm. With OP-GaAs periods of 63 μm and 65 μm, the OPO idler wavelength should be able to reach ~7 μm, with corresponding signal wavelengths as short as ~2.8 μm. It was believed that the difficulty in reaching a threshold for these wavelengths was due to the higher losses

associated with the crystal AR coatings (10% reflection loss each side at 7 μm), the plane-concave mirrors coatings (12% transmission loss each mirror at 7 μm), and the BS coating (1% absorption at 7 μm). In addition, water vapor absorption inside the OPO cavity induced extra loss at wavelengths beyond 6 μm. For example, a water-vapor-absorption round-trip loss of ~5% loss can be calculated for a wavelength of ~7 μm for the cavity length used here. Without considering intrinsic losses in the OP-GaAs crystal, the total fractional cavity loss at 7 μm was estimated to be ~0.7 in contrast to the value of ~0.3 at 6 μm. Consequently, the theoretical oscillation threshold at 7 μm would be 11.6 W (~2.3 times higher than that at 6 μm), close to the maximum available pump power.

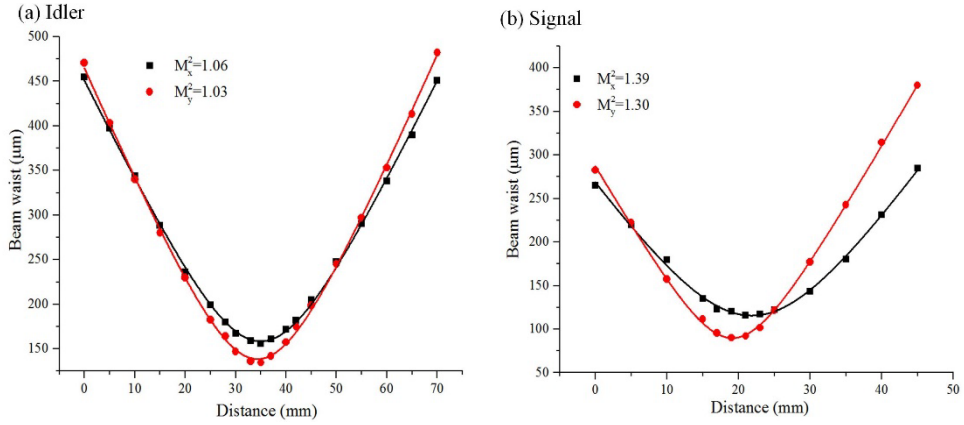

Fig. 5.4.4. OP-GaAs OPO idler (5580 nm, a) and signal (3136 nm, b) beam qualities.

The OPO signal (Fig 5.4.4 (a)) and idler (Fig. 5.4.4 (b)) beam quality were characterised by using a pyroelectric scanning profiler (NanoScan, Photon). At the maximum output power, the idler beam quality was measured to be M_x^2 = 1.06 and M_y^2 = 1.03 due to the spatial control imposed by the idler-resonant OPO cavity. Also at the maximum output, the signal beam quality was characterised to be slightly worse than that of idler, with a value of M_x^2 = 1.39 and M_y^2 = 1.30, which is however marginally better than the pump beam (M^2=1.5). Without any active spatial controls, the slight elliptical beam shape of signal followed that of the pump beam shape, as expected.

The influence of the pump polarisation on the nonlinear frequency conversion in the OP-GaAs was also investigated. As the coated BS (Fig. 5.3.1) was polarisation sensitive, it was replaced with an uncoated calcium fluoride wedge (WW51050, Thorlabs). In order to reduce the influence of different amplitude transmission coefficients for s and p polarisations, the angle of incidence of the light on the uncoated calcium fluoride wedge was limited to ~10°. The generated idler output power against the angle of the input pump polarisation is plotted in Fig. 5.4.5. According to theoretical models demonstrated in section 2.5, the effective

nonlinear coefficient has a maximum value when the pump polarisation is aligned to the [111] direction (35° to the [110]) direction [10]. The results shown in Fig. 5.4.5 are in close agreement with the theoretical prediction, and the discrepancy may due to different thermal- or stress-induced birefringence [15].

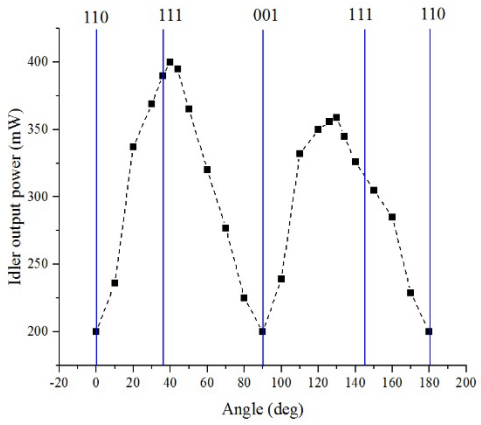

Fig. 5.4.5. Idler average output power versus the angle of pump polarisation. Blue line is the OP-GaAs crystal axis.

5.5 Summary

In summary, an idler-resonant, widely tunable, mid-infrared, picosecond, fibre-laser-pumped OPO based on OP-GaAs has been demonstrated. The OPO tuning range was 4394-6102 nm (idler) and 2997-3661 nm (signal). A maximum average power of 1.18 W (idler, 5580nm) and 0.51 W (signal, 3136 nm) was obtained. The highest peak powers of the idler and signal were calculated to be more than 118 W and 51 W, respectively. The signal beam quality was characterised to be M^2_x = 1.39 and M^2_y = 1.30, whereas the idler beam quality was close to diffraction-limited beam with M^2_x = 1.06 and M^2_y = 1.03. The combination of broadband tunability in the mid-infrared, watt-level average power, and high spatial coherence makes this picosecond OPO a good option for spectroscopic applications. Specifically, its near-diffraction-limited output beam at idler wavelengths is suitable for testing our in-house-made hollow core fibres (chapter 8). In the next chapter, I will focus on investigating the average power scaling of the tunable OP-GaAs OPO.

Reference

[1] F. K. Tittel *et al.*, "Mid-infrared laser applications in spectroscopy," in *Solid-State Mid-Infrared Laser Sources*, Berlin, Germany: Springer Berlin Heidelberg, 2003, pp. 458-529.

[2] Z. Zhang *et al.*, "Active FTIR-based stand-off spectroscopy using a femtosecond optical parametric oscillator," *Optics Letters*, vol. 39, no. 20, pp. 6005-6008, 2014.

[3] M. Kumar *et al.*, "Stand-off detection of solid targets with diffuse reflection spectroscopy using a high-power mid-infrared supercontinuum source," *Applied Optics*, vol. 51, no. 15, pp. 2794-2807, 2012.

[4] A. Godard, "Infrared (2–12 μm) solid-state laser sources: a review," *Comptes Rendus Physique*, vol. 8, no. 10, pp. 1100-1128, 2007.

[5] V. A. Serebryakov *et al.*, "Medical applications of mid-IR lasers. Problems and prospects," *Journal of Optical Technology*, vol. 77, no. 1, pp. 6-17, 2010.

[6] A. Sincore *et al.*, "High power single-mode delivery of mid-infrared sources through chalcogenide fiber," *Optics Express*, vol. 26, no. 6, pp. 7313-7323, 2018.

[7] K. A. Tillman *et al.*, "Idler-resonant femtosecond tandem optical parametric oscillator tuning from 2.1 μm to 4.2 μm," *Journal of the Optical Society of America B*, vol. 21, no. 8, pp. 1551-1558, 2004.

[8] F. Bai *et al.*, "Idler-resonant optical parametric oscillator based on $KTiOAsO_4$," *Applied Physics B*, vol. 112, no. 1, pp. 83-87, 2013.

[9] L. Xu *et al.*, "Yb-fiber amplifier pumped idler-resonant PPLN optical parametric oscillator producing 90 femtosecond pulses with high beam quality," *Applied Physics B*, vol. 117, no. 4, pp. 987-993, 2014.

[10] Y. He *et al.*, "Improved conversion efficiency and beam quality of miniaturized mid-infrared idler-resonant MgO:PPLN optical parametric oscillator pumped by all-fiber laser," *Infrared Physics & Technology*, vol. 95, pp. 12-18, 2018.

[11] Q. Fu *et al.*, "Mid-infrared, idler-resonant, picosecond OP-GaAs OPO with wide tunability and good beam quality," in *Conference on Lasers and Electro-Optics*, 2019, pp. 1-2.

[12] Q. Fu *et al.*, "High-beam-quality, watt-level, widely tunable, mid-infrared OP-GaAs optical parametric oscillator," *Optics Letters*, vol. 44, no. 11, pp. 2744-2747, 2019.

[13] K. L. Vodopyanov *et al.*, "Optical parametric oscillation in quasi-phase-matched GaAs," *Optics Letters*, vol. 29, no. 16, pp. 1912-1914, 2004.

[14] L. Xu *et al.*, "High-energy, near- and mid-IR picosecond pulses generated by a fiber-MOPA-pumped optical parametric generator and amplifier," *Optics Express*, vol. 23, no. 10, pp. 12613-12618, 2015.

[15] J. Wueppen *et al.*, "1.95 μm-pumped OP-GaAs optical parametric oscillator with 10.6 μm idler wavelength," *Optics Letters*, vol. 41, no. 18, pp. 4225-4228, Sep. 2016.

Chapter 6

High-average-power, widely tunable, mid-infrared OP-GaAs optical parametric oscillator

6.1 Introduction

A mid-infrared (mid-IR) optical parametric oscillator (OPO) with high average power and wide tunablity is of importance for spectroscopic applications for detection of different molecules with high signal-to-noise ratio [1, 2]. For a mid-IR OPO based on orientation-patterned gallium arsenide (OP-GaAs), its tunability is delivered via its quasi-phase-matching capability and transparency range, whereas high-average-power operation needs a high-average-power pump source with wavelengths longer than 1.7 μm (avoiding two-photon absorption) [3]. In this wavelengths range, commonly available high-power pump laser solutions include thulium-doped-fiber (TDF) lasers, holmium-doped YAG (Ho:YAG) lasers, near-infrared OPOs, Cr^{2+}-doped II-VI compound (Cr:ZnSe, Cr:ZnS) lasers, and other bulk lasers (as has been summarised in Table. 2.6.1). From these options, 2-μm-wavelength TDF lasers offer outstanding performance in terms of stability, reliability, compactness, beam quality, and, in particular, the production of ultrashort pulses at high average power [4, 5]. Hence, they are ideal sources for pumping power-scaled ultrashort-pulsed OP-GaAs OPOs.

Although a number of OP-GaAs OPOs have already been reported, there are only a few reports on average power scaling. In continuous wave (CW) operation, an OP-GaAs OPO was pumped by a 60-W Ho:YAG bulk laser, which provided a total parametric output power (signal + idler) of 5.3 W [6]. In nanosecond pulsed operation, C. Kieleck et al. demonstrated a 2.85-W OP-GaAs OPO pumped with 65 ns pulses at 20 kHz repetition rate from a Q-switched Ho:YAG laser [7]. In a later report, a higher total output power (signal + idler) of

7.7 W was obtained from a 70-ns pulsed Ho;YAG bulk laser pumped OP-GaAs OPO operating at a higher pulse repetition rate of 100 kHz [8]. In both ns-pulsed works, the OPOs provide limited wavelength tunability with signals and idlers of between 3 and 5 μm and were pumped by solid-state bulk lasers.

In this chapter, I will demonstrate a high-average-power, widely tunable, mid-infrared, picosecond OP-GaAs OPO pumped by a TDF master oscillator power amplifier (Tm:MOPA) system. A maximum total average power of 9.7 W (signal 5.7 W (0.60 kW peak power), idler 4.0 W (0.42 kW peak power)) was obtained at a 100-MHz pulse repetition rate, with signal and idler wavelengths of 3093 and 5598 nm, respectively, and a thermally induced power roll-off was observed. Tuning ranges of 2895 nm-3342 nm (signal) and 4935 nm-6389 nm (idler) were demonstrated. Furthermore, using an optical chopper operating at 25% duty cycle to provide burst mode operation, the power roll-off was eliminated giving maximum signal (3093 nm) and idler (5598 nm) peak powers of 0.79 kW and 0.58 kW, respectively, in this instance. To the best of our knowledge, this work presents the highest average power from an OP-GaAs OPO with wide tunablity.

Section 6.2 introduces the high-average power Tm:MOPA system which is the pump system of the OP-GaAs OPO, and section 6.3 describes the setup of the OPO. Section 6.4 then demonstrates the experimental results and discussion of the OP-GaAs OPO and finally section 6.5 summarise this chapter. The work described in this chapter has been previously published, in part, in the following references [9, 10].

6.2 High-average-power Tm:MOPA - OPO pump system

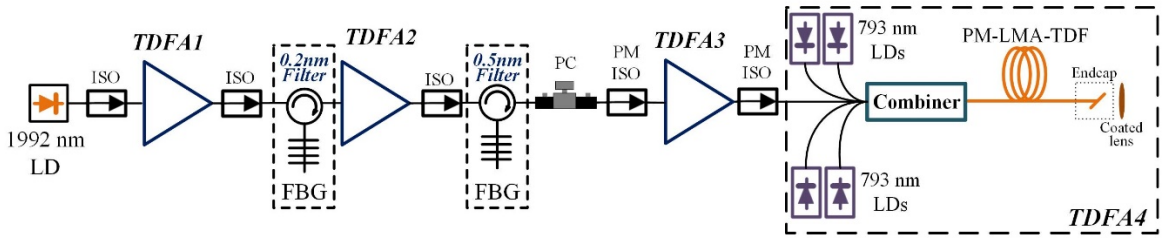

Fig. 6.2.1. Schematic diagram of gain-switched laser diode seeding, Tm:MOPA system. LD: laser diode. ISO: isolator. FBG: fiber bragg grating. PC: polarisation controller. PM: polarisation maintaining. TDF: thulium-doped fiber. LMA: large mode-area.

Figure 6.2.1 illustrates the experimental setup of the Tm:MOPA system which was a modified version of the setup presented in Fig. 5.2.1. The Tm:MOPA system similarly

consisted of four amplifier stages seeded by a gain-switched laser diode, and the main differences between the setup in Fig. 6.2.1 and Fig. 5.2.1 are as follows:

i) Seed diode wavelength. The 2007-nm seed diode used in section 5.2 had suffered from electrical-surge-induced damage, and a laser diode with a reasonably close wavelength of 1992 nm was available for substitution. It was a PM fibre-pigtailed 1992-nm laser diode (Eblana Photonics, EP1993-DM-D-PM) operating at the same 100-MHz repetition rate and delivered a similar ~100 μW average power. The following TDFA1, 2, and 3 remained the same and provide a similar gain compared with those seeded by the 2007-nm laser diode. However, the two FBG-based spectral filters (each after TDFA1 and 2) were replaced by two new ones with a central wavelength of 1992 nm and with same bandwidths of 0.2 nm and 0.5 nm, respectively.

ii) Polarisation controller (PC). The previous PC placed between TDFA2 and 3 (PC-1100-15, FibrePro, Fig. 5.2.1) had an insertion loss of 1.5 dB due to its original wavelength design of 1550 nm. Here, it was replaced by another in-line fibre optic PC (CPC250, Thorlabs, Fig. 6.2.1) combined with single mode fibres (SM2000, Thorlabs), which was more endurable and lower loss (<0.5 dB) for 2-μm operation.

iii) TDFA4. The TDF used in this stage was the same as before (a 4-m-long 25-μm-core PM TDF (PLMA-TDF-25P/400-HE, Nufern)), but here was pumped in a forward configuration with four 30-W 793 nm laser diodes combined via a (4+1) × 1 fibre-based pump combiner, which resulted in an all-fiberized system providing a higher average power output. Additionally, the output fibre endcap suffered frequent damage during this work, possibly due to parasitic absorption of the endcap glass and/or fibre end surface contamination from the environment. This problem was solved by re-fabricating the endcap from low OH^{-1} fibres (FP400ERT, Thorlabs) and operating it under a partially sealed cover. Following the endcap, a coated calcium fluoride lens (LA5315-E, Thorlabs) was employed, which enabled a better collimation than the previous slightly tilted uncoated collimating lens described in section 5.2.1 (Fig. 5.2.1).

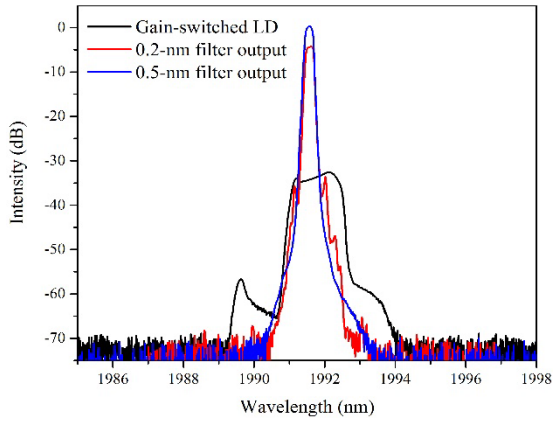

Fig. 6.2.2. Spectra of the gain-switched seed diode, and spectra at the outputs of the 0.2-nm and 0.5-nm spectral filter.

Since the seed diode was changed to the 1992-nm laser diode, its output spectral characteristic was studied, as depicted by the black line in Fig. 6.2.2. The spectra of the seed laser had a 3-dB bandwidth of 1.3 nm, and was narrowed by the two FBG-based spectral filters (Fig. 6.2.1). The spectra at the input to TDFA3 was narrowed to 0.2 nm (3-dB bandwidth) with an improved signal-to-noise ratio (OSNR) of 70 dB (Fig. 6.2.1 blue line). The output power of the seed laser was ~100 μW, and was boosted by the first three amplifiers to 600 mW before being launched into TDFA4. Fig. 6.2.3 depicts the output characteristics of TDFA4. An output power of 40 W was obtained, at a pump power of 107 W, and with a slope efficiency of 41%.

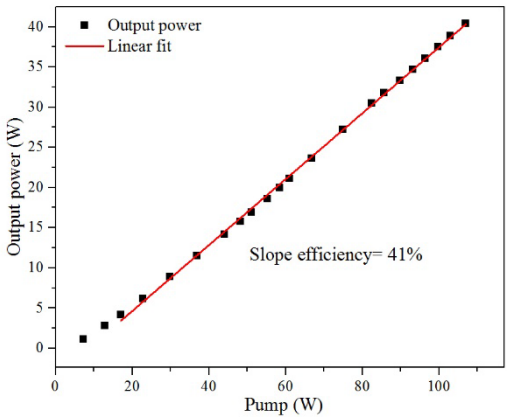

Fig. 6.2.3. Output powers from TDFA4 and an associated linear fit.

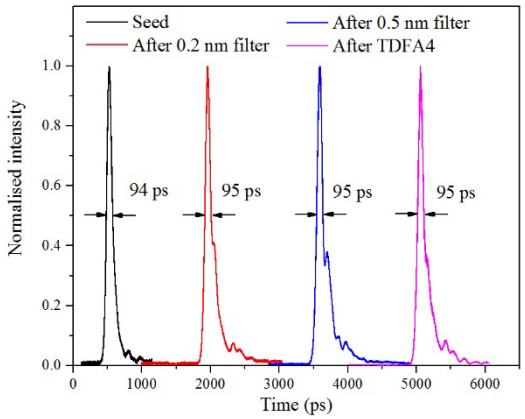

Fig. 6.2.4. Temporal profile of the pulses from the seed laser, after 0.2 nm filter, after 0.5 nm filter, after TDFA4 at maximum output power;

The temporal profiles of the 1992-nm pulses from the seed laser, after 0.2 nm filter, after 0.5 nm filter, and after TDFA4 were shown in Fig. 6.2.4, which were characterised by a fast photodetector (EOT, ET-5000F, Bandwidth>12.5 GHz) and an oscilloscope (Tektronix, CSA 803A, with 50 GHz bandwidth). The seed pulse duration (94 ps) did not change significantly through the TDFAs and filters, with a final pulse duration of 95 ps from TDFA4. Fig. 6.2.5 depicts the TDFA4 spectra at different power levels. The spectral bandwidth gradually broadened with increasing power due to self-phase modulation, while no other nonlinear effects were observed providing an excellent OSNR of >60 dB (inset of Fig. 6.2.5). Its effective 10-dB linewidth at the maximum output power of 40 W was 0.4 nm, which was considered to be a suitable bandwidth for pumping an OP-GaAs OPO.

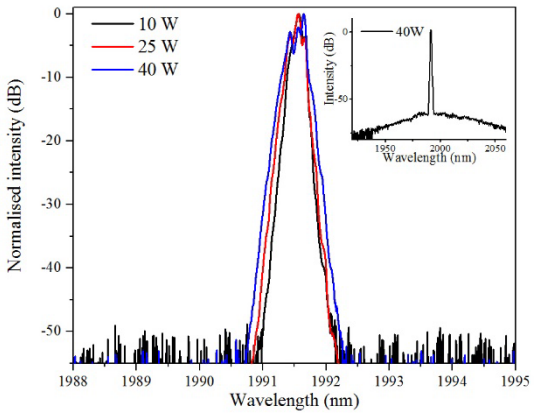

Fig. 6.2.5 TDFA4 spectra at different output power levels. Inset: TDFA4 spectra at maximum output power shown for a wider wavelength range.

The beam quality of the Tm:MOPA was characterised with a Pyrocam-based beam profiler (NanoScan, Photon Inc.) performed by measuring beam diameter as a function of propagation position through a beam focus. The beam quality from the Tm:MOPA at the

maximum output power of 40 W was measured to be M_x^2=1.1 and M_y^2=1.2, as sketched in Fig. 6.2.6.

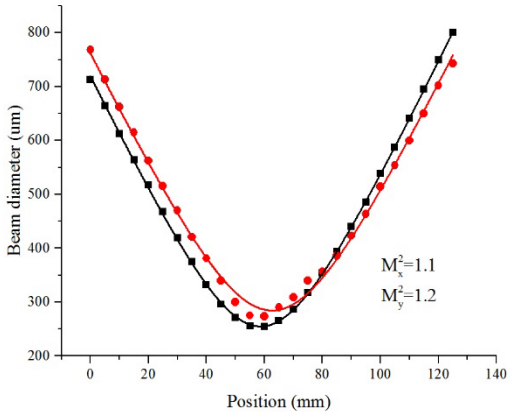

Fig. 6.2.6. Beam quality measurement of the Tm:MOPA system at maximum output power of 40 W.

Overall, the 1992-nm Tm:MOPA system had a maximum output power of 40 W operating at a repetition rate of 100 MHz with a pulse duration of 95 ps. The effective 10-dB bandwidth and beam quality of OPO pump at maximum output power of 40 W were 0.4 nm and M^2=1.2, respectively. The polarisation extinction ratio at 40 W was measured to be ~14 dB. This source can therefore serve as a pump source for a high-average-power OP-GaAs OPO.

6.3 High-average-power, widely-tunable OPO setup

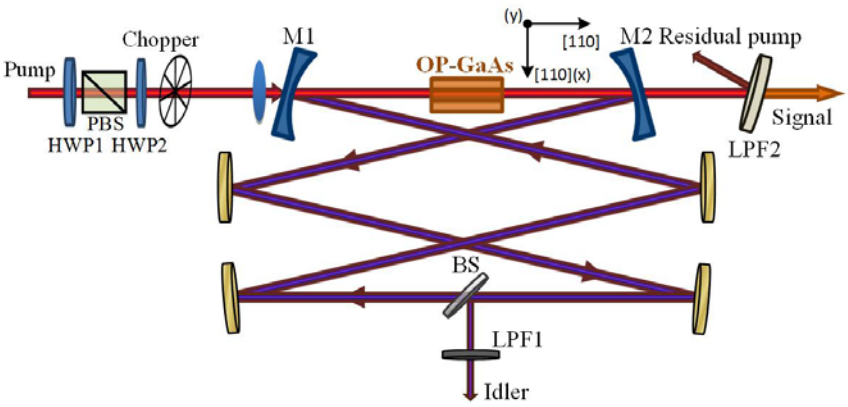

Fig. 6.3.1 Schematic of the OP-GaAs OPO. HWP: half-wave plate; PBS: polarising beam splitter; M1, M2: mirror 1,2; LPF1,2: long-pass filter 1,2.

Fig. 6.3.1 presents the setup of the high-average-power, widely tunable, picosecond mid-IR OPO, similar to the setup shown in Fig. 5.3.1. The major differences are:

i) Optical chopper. An optical chopper (25% duty cycle) was placed prior to the OPO cavity to enable the OPO operating at two modes - continuous mode

(without chopper or chopper turned off) and burst mode (chopper in place and turned on). It provided a control of thermal effects during the investigation of the OPO output power characteristics (details explained in next section).

ii) Coating reflectivity of OP-GaAs and cavity mirrors (M1, M2) at new operational wavelengths. The OP-GaAs crystal and OPO cavity mirrors were the same as described in the last chapter. However, due to the change of the pump wavelength, the OPO was operating at slightly different wavelengths for the signal and idler, where the anti-reflection (AR) coating of the end facets of the OP-GaAs had a reflectivity of <4% (signal) and <1% (idler). M1 and M2 provided AR>98% for the pump and high-reflection (HR) >99.5% for the idler, while the reflectivity for the signal varied between ~10% and ~75% over the full signal wavelength range.

iii) Pump beam. The pump beam was focused by an AR coated calcium fluoride lens (f=200 mm) into the OP-GaAs crystal with a beam waist of 96/90 μm ($1/e^2$ radius of intensity) in the x/y direction, which was similar in size but less elliptical (due to better collimation from the fibre output) compared to that used in last chapter (100/80 μm). To match the pump beam, the distance between M1 and M2 was then changed to 268 mm giving a calculated idler beam waist of 86~98 μm at the centre of the crystal, depending on the idler wavelength.

Due to various optics between the OPO pump and the OPO cavity, the maximum available pump power launched onto the OP-GaAs crystal was 35.3 W. Two long pass filters, LPF1/2, were used to separate the residual pump and idler/signal, respectively. The quoted output powers of signal and idler were calculated from the direct measurements and by considering the losses of the LPFs.

6.4 Results and discussion of high-average-power, widely-tunable OPO

The OPO output power characteristics and conversion efficiency were first investigated in continuous mode (without the chopper), giving the data shown in Fig. 6.4.1. At 40°C oven temperature, a pump threshold of 4.3 W was observed from the 59-μm grating OP-GaAs with signal and idler wavelengths of 3093 and 5598 nm, respectively. At such operating wavelengths M2 had a transmission of 90% for the generated signal, whereas 27.5% of generated idler was coupled out via BS. The signal and idler output powers increased linearly for pump power up to 25.5 W at slope efficiencies of 22.8% and 16.4%, respectively, reaching 4.8 W and 3.5 W, and the corresponding overall power conversion efficiency reached 32.6%. However, the conversion efficiency started to drop (the shaded roll-off region in Fig. 6.4.1) when the pump power was increased further with a total maximal output

power of 9.7 W (signal 5.7 W, idler 4.0 W) obtained with 27.6% conversion efficiency at the maximum available pump power of 35.3 W incident on the OP-GaAs crystal. Note that the output power ratio between signal and idler (~1.4) is not equal to their photon frequency ratio (1.8) due to different losses for the generated signal and idler, including parasitic crystal losses and cavity mirror losses.

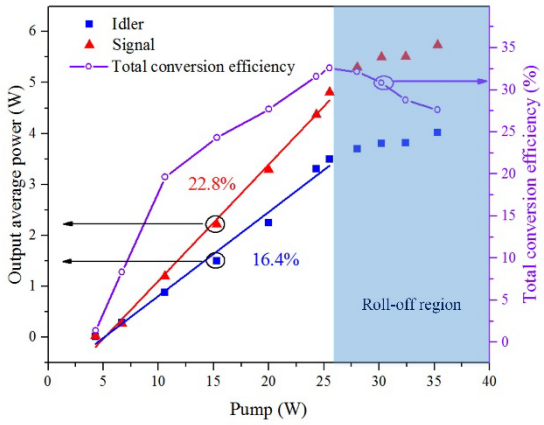

Fig. 6.4.1. Output powers and conversion efficiencies (signal 3093 nm, idler 5598 nm).

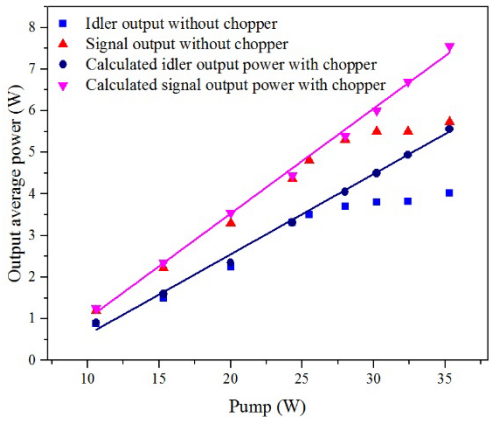

Fig. 6.4.2. OPO output powers comparison with chopper and without chopper.

In order to investigate the roll-off effect, an optical chopper was placed in front of the OPO cavity, and the output-versus-input powers were compared with and without the chopper, as shown in Fig. 6.4.2. The OPO operates in a burst mode with the chopper in place, and the associated OPO output powers presented are calculated quasi-continuous-wave average powers (i.e. average powers when the chopper was open) by taking the duty cycle of the chopper (25%) into consideration. Such calculated output powers of the signal and idler were identical to the output powers without the chopper when the pump power was less than 25.5 W, but increased consistently and linearly with pump powers higher than 25.5 W. Thus, the power roll-off was attributed to average-power-induced thermal effects in the OP-GaAs crystal. A similar roll-off phenomenon has also been seen in a high-power CW OPO based

on OP-GaAs [6]. The intensity of the pump pulses (maximum ~15 MW/cm^2) is not considered to be a factor in the roll-off, because OP-GaAs has previously been pumped by a higher intensity beam of >100 MW/cm^2 in the picosecond OP-GaAs OPG/A (Chapter 3 and 4) without any roll-off effects. Possible explanations for the roll-off were thermal lensing effects induced by parasitic-absorption-related local heating, and/or the degradation of the beam qualities (as will be investigated at the end of this section). By mitigating the thermal effects with the aid of a chopper (25% transmission duty cycle), a maximum average output power of 3.25 W (signal 1.88 W, and idler 1.37 W) was achieved corresponding to a calculated quasi-continuous-wave average power of 13 W (signal 7.52 W, and idler 5.48 W). An overall conversion efficiency of 36.8% was achieved at a pump power of 35.3 W in the burst mode OPO operation. The durations of the signal and idler pulses were not measured due to the lack of suitable instruments, but they are expected to be equal to, or slightly shorter than, the pump pulses (95 ps, Fig. 6.2.4 pink line) due to the parametric conversion process [11]. Therefore, the corresponding maximum peak powers of the signal and idler were estimated to be equal to or greater than 0.79 kW and 0.58 kW, respectively.

The wavelength tunability of the OPO using different OP-GaAs grating periods and range of oven temperatures was also investigated. The idler and signal wavelength could be continuously tuned from 2895-3342 nm (signal) and 4935-6389 nm (idler), and example spectra are shown in Fig. 6.4.3(a). The signal and idler spectra were characterised using an optical spectrum analyser (Bristol instruments 721 series, ~0.1-GHz resolution) and a monochromator (Bentham TMc300, 1-nm resolution at <5.5 μm and 3-nm resolution at >5.5 μm), respectively. Typical spectral linewidths of 1 nm (1 cm^{-1}) and 5 nm (1.6 cm^{-1}) were observed for the generated signal (3107 nm) and idler (5552 nm), respectively, as shown in Fig. 6.4.3(b).

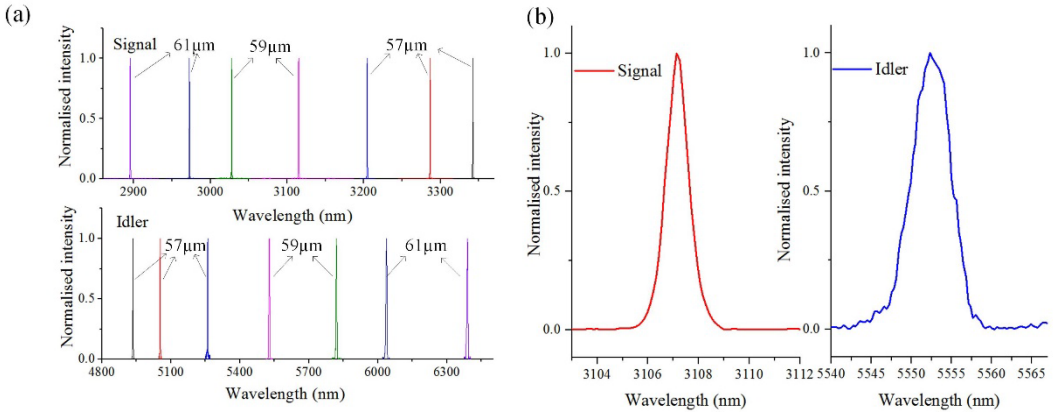

Fig. 6.4.3. (a) Tunability of the signal and idler from the OP-GaAs OPO; (b) Typical spectra of generated signal and idler.

The OPO signal and idler beam qualities were characterised at both low pump power (15.3 W) and high pump power (25.5 W), without the chopper in place, by using a pyroelectric scanning profiler (NanoScan, Photon), as presented in Fig. 6.4.4. At low pump power, the beam quality of the signal and idler was measured to be M_x^2 = 1.18 / M_y^2 = 1.18 and M_x^2 = 1.03 / M_y^2 = 1.01, respectively. The better beam quality displayed by the idler was expected as it was controlled by the idler-resonant OPO cavity. At high pump power, the beam qualities of idler and signal were measured to be M_x^2 = 1.12/ M_y^2 = 1.02 and M_x^2 = 1.45 / M_y^2 = 1.21, respectively. The beam qualities at or within the thermal roll-off region were not measured due to the risk of crystal damage from long-term operation in this regime.

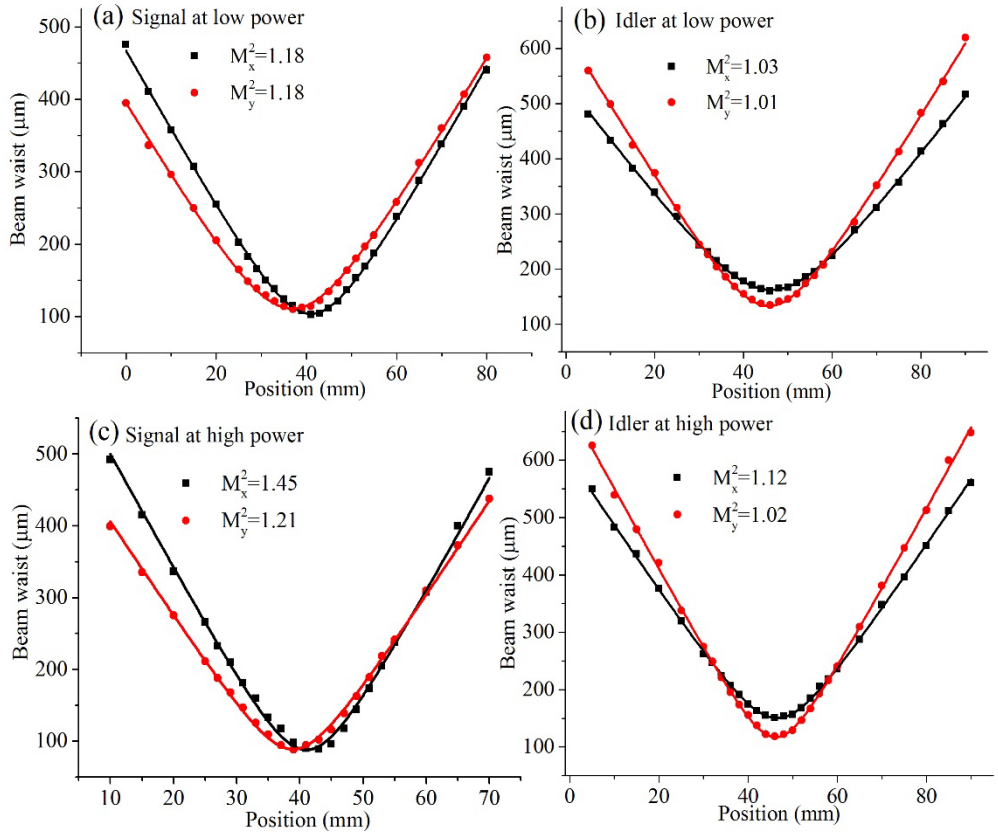

Fig. 6.4.4. Beam qualities of generated signal and idler at low and high pump power.

6.5 Summary

In conclusion, I demonstrate a high-average-power, widely-tunable, mid-infrared picosecond OP-GaAs OPO in this chapter. A tuning range of 2895 – 3342 nm for signal and 4935 – 6389 nm for idler was demonstrated. A thermally induced roll-off in the output power of the OPO was observed and a maximum power of 9.7 W (signal 5.7 W (0.60 kW peak power), idler 4.0 W (0.42 kW peak power)) was achieved at a pump power of 35.3 W and a repetition rate of 100 MHz. The OPO was also operated in a burst mode with a 25% duty cycle optical chopper placed in front of the OPO cavity to mitigate the thermal effects. In

this regime, maximum peak powers of the signal and idler of 0.79 kW and 0.58 kW were obtained, respectively. In next chapter, further power scaling and mitigation of thermal effects in the OPO are investigated by employing a water cooling system, and a versatile OP-GaAs OPO with variable repetition rates and pulse durations will be demonstrated.

Reference

[1] I. T. Sorokina, and K. L. Vodopyanov, *Solid-State Mid-Infrared Laser Sources*: Springer Science & Business Media, 2003.

[2] B. J. Orr *et al.*, "Tunable laser applications," in: CRC press, 2016,

[3] P. G. Schunemann, "New nonlinear optical crystals for the mid-infrared," in *Advanced Solid State Lasers Conference*, Berlin, 2015, pp. AM2A.2.

[4] W. Yao *et al.*, "Gain-switched laser diode seeded TDFA with 409 W picosecond pulses and 142 W spectrally flat supercontinuum output," *Optics Express*, vol. 27, no. 2, pp. 1276-1282, 2019.

[5] S. Liang *et al.*, "295-kW peak power picosecond pulses from a thulium-doped-fiber MOPA and the generation of watt-level >2.5-octave supercontinuum extending up to 5 μm," *Optics Express*, vol. 26, no. 6, pp. 6490-6498, 2018.

[6] P. G. Schunemann *et al.*, "CW mid-IR OPO based on OP-GaAs," in *2013 Conference on Lasers and Electro-Optics - International Quantum Electronics Conference*, Munich, 2013, pp. JSII_2_3.

[7] C. Kieleck *et al.*, "High-efficiency 20–50 kHz mid-infrared orientation-patterned GaAs optical parametric oscillator pumped by a 2 μm holmium laser," *Optics Letters*, vol. 34, no. 3, pp. 262-264, 2009.

[8] A. Hildenbrand *et al.*, "Compact efficient mid-infrared laser source: OP-GaAs OPO pumped by Ho^{3+}: YAG laser," in *Proc. SPIE 8187*, 2011, pp. 81870H.

[9] Q. Fu, "High-average-power, mid-infrared, widely tunable, picosecond optical parametric oscillator based on OP-GaAs (Conference Presentation)," in *Photonics West*, 2020, pp.

[10] Q. Fu *et al.*, "High-average-power picosecond mid-infrared OP-GaAs OPO," *Optics Express*, vol. 28, no. 4, pp. 5741-5748, 2020.

[11] L. Xu *et al.*, "High-energy, near- and mid-IR picosecond pulses generated by a fiber-MOPA-pumped optical parametric generator and amplifier," *Optics Express*, vol. 23, no. 10, pp. 12613-12618, 2015.

Chapter 7

Controllable repetition-rate and pulse-duration, high-power OP-GaAs optical parametric oscillator

7.1 Introduction

Output power, pulse repetition rate and pulse duration are key parameters for mid-infrared (mid-IR) pulsed optical parametric oscillators (OPOs), and matching these to particular application requirements is vitally important. For example, in remote chemical sensing applications, high output power improves the signal-to-noise ratio associated with long-range measurement and high pulse repetition rate reduces the signal processing time for fast-speed chemical detection [1]. For biological applications, adjustable pulse durations could allow the investigation of pulse-duration-dependent laser ablation [2], such as skin ablation using mid-IR lasers [3] and hard dental tissue treatments by mid-IR lasers [4]. In addition, flexible temporal properties could be useful for dynamic studies [5] and performance optimization of material processing [6, 7] and microscopy [8].

In the ultrafast pulsed regime, OPOs need to be synchronously pumped by ultrafast laser sources, such as mode-locked lasers [9-11]. However, mode-locked laser sources typically operate at a fixed repetition rate and pulse duration to deliver OPO outputs at the same repetition rate and at a similar pulse duration. In contrast, amplified gain-switched laser diodes offer flexible output temporal characteristics and have previously been used to pump a high power variable repetition rate (115 – 918 MHz) periodically-poled-lithium-niobate (PPLN) -based picosecond OPO by allowing one or more pulses to circulate within the OPO cavity while still achieving synchronous pumping. However, this demonstration was operated at a fixed pump pulse duration (~17 ps) and at relatively short wavelengths (no longer than 4.4 μm) [12].

In this chapter, I demonstrate a high-power mid-IR orientation-patterned gallium arsenide (OP-GaAs) OPO with flexible repetition rates and user-defined pulse durations. The OPO was first investigated at a repetition rate of 100 MHz, corresponding to one pulse circulating within the cavity, and a 95-ps pump pulse. This fundamental operation delivered a maximum total average output power of 13.7 W, which contained 9.2 W signal and 4.5 W idler at wavelengths of 3.3 μm and 4.9 μm, respectively. By controlling the electrical driving signal to the gain-switched laser diode, and without the need to alter the following fibre amplifier chain, a variable repetition-rate and pulse-duration OPO was realised with a repetition rate from 100 MHz to 1 GHz, by increasing the number of circulating pulses within the cavity from 1 to 10, and pulse durations from ~95 ps – ~1.1 ns, respectively. The OPO offered >3 W total average output power for all the demonstrated repetition rates and pulse durations. To the best of our knowledge, this is the first demonstration of mid-IR high-power, variable repetition rate and controllable pulse duration ultrafast pulses from an optical parametric device.

The following contents of this chapter introduce the experimental setup (section 7.2) and then describe the experimental results and analysis of the fundamental operation of the high-power OPO (section 7.3), the variable repetition-rate OPO (section 7.4) and the controllable pulse-duration OPO (section 7.5). Finally, section 7.6 summarises this chapter and gives a concluding summary. The experimental results described in this chapter have been, in part, published [13, 14].

7.2 Experimental setup

A block diagram of the pump system for the OP-GaAs OPO is shown in Fig. 7.2.1 (a). The pump laser is the same 1992-nm laser diode seeding thulium-doped fibre amplifier (Tm:MOPA) system described in section 6.2. However, in this chapter, the Tm:MOPA was operated at three different modes – fundamental mode, variable repetition rate mode, and controllable pulse duration mode. The previous repetition rate of 100 MHz and the final output pulse duration of 95 ps was considered as the fundamental mode (section 6.2). By manipulating the electrical pulses imposed on the 1992-nm seed diode, the repetition rate and the pulse duration of the pump laser can be varied from 100 MHz to 1 GHz and 95 ps to 1.1 ns, respectively, whilst maintaining the same maximal average power at the final output. It should be noted that the Tm:MOPA spectral bandwidths at the three operation modes were slightly different (but were still well within the acceptance bandwidth for the OP-GaAs crystal), while other output characteristics, such as average output power (39 W), beam

quality (M^2=1.2), and polarisation extinction ratio (14 dB) remained the same in the different operation modes.

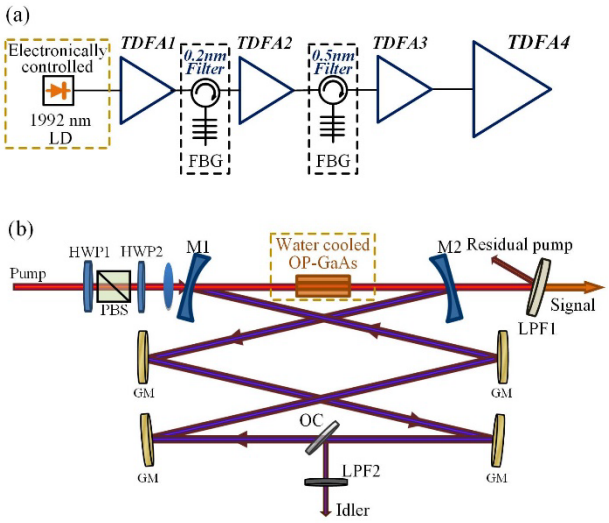

Fig. 7.2.1. (a) Block diagram for setup of OPO pump – Tm:MOPA system, LD: laser diode; TDFA: thulium-doped fibre amplifier; FBG: fibre bragg grating. (b) Setup of OP-GaAs OPO HWP: half-wave plate, PBS: polarisation beam splitter; M1,2: mirror 1,2; GM: gold mirror; LPF: long-pass filter; OC: output coupler.

Fig. 7.2.1 (b) depicts the schematics of the OP-GaAs OPO, which was a modified version of that demonstrated in section 6.3. The main differences are

i) Water cooling on OP-GaAs. The OP-GaAs was previously mounted in a temperature-control oven, which was now replaced by a water-cooling plate with a fixed temperature of 17.5°C in order to mitigate the previously observed thermal effects. The optical chopper used in last chapter (Fig. 6.3.1) was also removed.

ii) OP-GaAs period. In last chapter, three different grating periods were utilised in the experiments, whereas in this chapter only the 57-μm period was used for the experiment (the 59-μm-period OP-GaAs had suffered from thermally induced damage during previous investigation). The distance between the two concave mirrors (M1,M2) was slightly modified to 270 mm, resulting in a calculated idler beam waist of 92 μm to match the pump spot size (~93 μm), and the total optical cavity length was maintained at 3 m to match the fundamental pump repetition rate of 100 MHz.

iii) Idler output couplers. Apart from the previous coated calcium fluoride output coupler used in section 6.3 (OC1, Thorlabs, BSW511R, coating reflectivity ~31% for idler), an additional pellicle beam splitter (OC2, Thorlabs, BP108, reflectivity

~3% for idler), was employed for the investigation of the variable repetition-rate OPO.

The signal beam was predominantly extracted (~82%) from the cavity through M2. The OPO signal and idler output powers were measured after two long-pass filters (LPF1, 2) respectively, and the quoted signal and idler output powers correspond to those available immediately after exiting the cavity, taking into account the losses of the LPFs.

7.3 Fundamental operation of the high-power OP-GaAs OPO

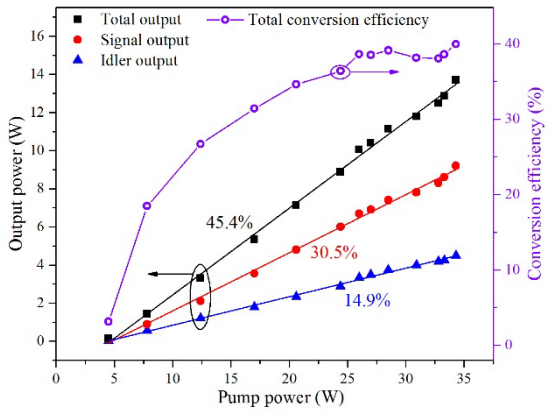

Fig. 7.3.1. Output powers at a pump repetition rate of 100 MHz and a pump pulse duration of 95 ps.

The OPO fundamental regime was operated at a repetition rate of 100 MHz and a pump pulse duration of 95 ps (pulse profile shown in Fig. 6.2.4). In last chapter (section 6.4), a thermally induced power roll-off phenomenon had been observed at a pump power of more than 25 W. However, in this chapter, with a water-cooling system in place, the power roll-off has been significantly mitigated achieving a linear output power growth in the full range of pump power, as plotted in Fig. 7.3.1. With a water-cooling temperature of 17.5°C and an OP-GaAs grating-period of 57 μm, an OPO oscillation threshold of 4.5 W was observed at signal and idler wavelengths of ~3.3 μm and ~4.9 μm, respectively. A slope efficiency of 45.4% and a maximum total OPO average power of 13.7 W were achieved at a maximum pump power of 34.3 W. The corresponding signal and idler maximum output powers were 9.2 W and 4.5 W, respectively. Assuming the pulse duration of the signal and idler pulses were equal to or slightly shorter than that of pump pulses (95 ps), the peak powers of the generated signal and idler pulses were more than 0.97 kW and 0.47 kW, respectively. A total OPO maximum optical-to-optical conversion efficiency of ~40% was obtained without any obvious roll-off, which indicates that the OPO output power was only limited by the currently available pump power. This should be compared to results in last chapter at the same pump power level but without water cooling, where a thermally induced roll-off was

observed. Note that without the water cooling, a thermally induced crystal damage has been observed at a pump power of ~32 W (~1.3 mJ/cm^2) under long-term operation.

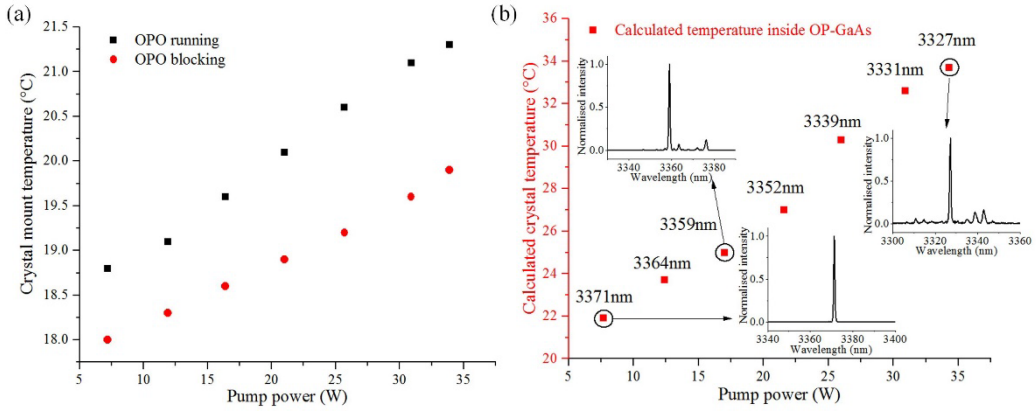

Fig. 7.3.2. (a) Direct temperature measurements of OP-GaAs crystal mount with the OPO operated and blocked. (b) Measured signal central wavelength shift at different pump powers and their corresponding calculated temperatures inside OP-GaAs. Insets: example spectra at signal central wavelengths of 3371, 3359, and 3327 nm.

In order to further investigate the thermal effects of the high-power OP-GaAs OPO, a digital thermometer (Fluke 51 II) was utilised for monitoring the temperature of the water-cooled OP-GaAs mechanical mount, which had 2-mm thickness and was directly attached to the top surface of the OP-GaAs crystal (Fig. 2.5.1 (b)). With the water cooling in place, the mount temperatures with OPO in operation were measured at different pump powers, as shown by the black squares of Fig. 7.3.2 (a), rising from 18.8°C to 21.3°C with increasing pump powers from 7.2 W to 34.3 W. When using a beam-block placed next to OC (Fig. 7.2.1) (ie. the OPO was not operating and the pump beam simply passed through the OP-GaAs crystal), lower temperatures were measured, as shown by the red circles of Fig 7.3.2 (a). This proved that the frequency conversion process made its own thermal contribution to the OP-GaAs OPO, resulting from possible crystal parasitic absorptions of the generated signal and/or idler. Further investigation found that the signal peak wavelength shifted for different pump powers, as shown in Fig. 7.3.2 (b). The signal wavelength gradually shifted to shorter wavelengths at increasing pump powers, corresponding to the temperature changing inside the OP-GaAs crystal. The temperatures for the different signal wavelengths were then calculated based on the Sellmeier equations of the OP-GaAs crystal, while assuming no thermal expansion of the grating periods [15], as shown in Fig. 7.3.2 (b). A maximum theoretical temperature of 33.7°C was then estimated at the maximum pump power of 34.3 W with a signal wavelength of 3327 nm. The side peaks observed in the signal spectra at high pump powers correspond to those observed in the idler spectra and originate from the etalon effect of OC1 as discussed below.

OC1 acted as both an etalon (spectra filter) and an output coupler, and a central idler wavelength of 4960 nm was measured at the maximum output power with a central spectra bandwidth of 3 nm (1.2 cm^{-1}), as shown in Fig. 7.3.3 (a). The corresponding signal wavelength was 3327 nm (Fig. 7.3.2 (b) inset) with a peak spectral bandwidth of 0.8 nm (0.7 cm^{-1}), which was obtained at a pump bandwidth of 0.4 nm (1 cm^{-1}). The measured spacing of spectral peaks of 111 GHz for the idler spectra (marked in Fig. 7.3.3 (a)) corresponded to the similar calculated free spectral range of OC1 (107 GHz), as shown in Fig. 7.3.3 (b). The small discrepancy was probably from the inaccuracy in the thickness of OC1 and the angle of beam incidence.

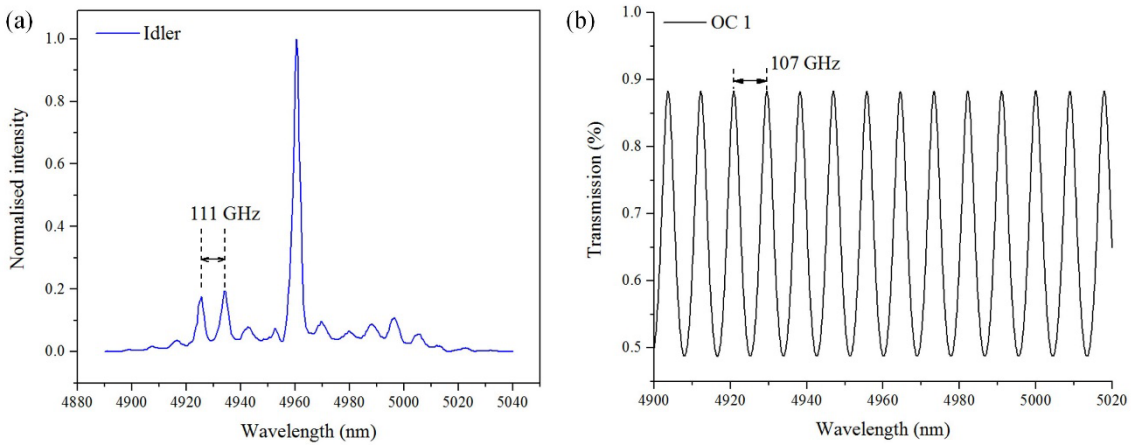

Fig. 7.3.3. (a) Idler spectra at maximum output power; (b) Calculated spectra response of OC1.

The beam qualities of both the generated idler (3327 nm) and signal (4960 nm) at maximum output power were characterised, as presented in Fig. 7.3.4. The idler beam had a near-diffraction limited performance with M_x^2=1.09 and M_y^2=1.12, constrained by the idler resonant cavity, whereas the unconstrained signal beam shows a departure from diffraction-limited performance with M_x^2=1.37 and M_y^2=1.55.

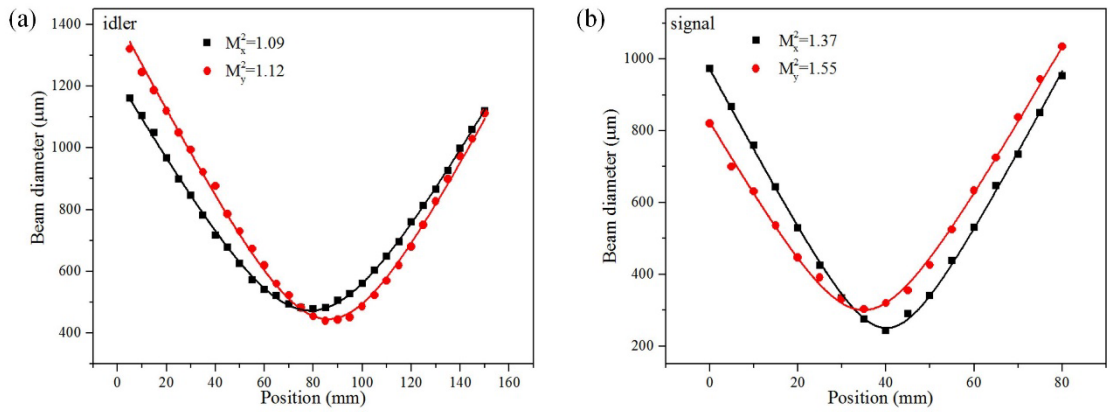

Fig. 7.3.4. Beam qualities of 4960-nm idler (a) and 3327-nm signal (b) at maximum output power.

7.4 Variable repetition-rate OPO – 100 MHz to 1 GHz

A variable repetition-rate OPO, and in particular a high repetition rate, can benefit many applications such as materials processing and remote sensing [16, 17]. The repetition rate of a synchronously pumped OPO is determined by that of its pump while the OPO cavity length should match the round-trip time of resonant signal/idler. At a fixed cavity length, it can theoretically support a repetition rate corresponding to one round trip time (fundamental repetition rate) or its harmonic repetition rates. By harmonically changing the repetition rates of the pump, a variable repetition rate OPO can be achieved with a corresponding variable number of pulses circulating within the cavity. Here with a fundamental repetition rate of 100 MHz, an idler resonant OP-GaAs OPO operating at ten different repetition rates from 100 MHz to 1 GHz (1 to 10 idler pulses in the cavity, respectively) was experimentally achieved by changing the corresponding repetition rates of the pump system.

Benefiting from gain-switched laser diode seeding, the repetition rate of the Tm:MOPA OPO pump can be easily changed, by modifying the repetition rates of its driving electrical pulses from 100 MHz to 1 GHz. Regardless of the variations of the pulse repetition rate, the final output from the Tm:MOPA system remained at a constant output average power. Consequently, different peak powers of output pulses at different repetition rates were achieved resulting in different nonlinear effects in TDFA4. Fig. 7.4.1 shows the different spectra from the Tm:MOPA system at maximum output power at different repetition rates. The spectra at 100 MHz, with an effective 10-dB bandwidth of 0.4 nm and a modulated peak feature induced by SPM, has already been discussed in section 6.2. The SPM effect was progressively relieved with increasing repetition rates and was eliminated at repetition rates of 600 MHz and higher, with a 3-dB bandwidth of 0.2 nm.

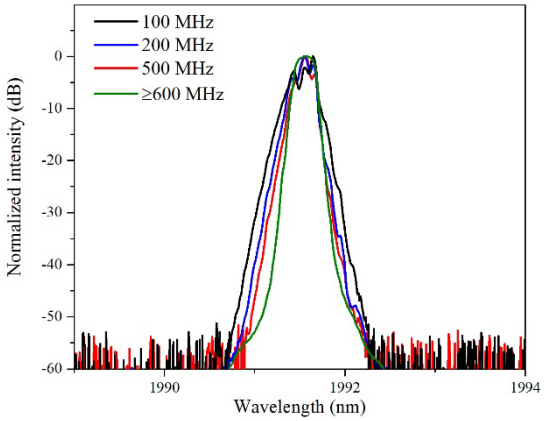

Fig. 7.4.1. Spectra of Tm:MOPA at maximum output power but different repetition rates.

With OC1 placed in the cavity, a variable repetition-rate OPO was realised from 100 to 800 MHz, and the signal and idler powers are presented in Fig. 7.4.2. The thresholds increased at higher repetition rates due to the lower pump peak powers compared with that at the fundamental operation. At 800 MHz repetition rate, 2.2 W and 1.1 W of signal and idler output power were obtained at a maximum pump power of 34.3 W, respectively. Repetition rates higher than 800 MHz were difficult to achieve with OC1 in the cavity because their corresponding thresholds exceeded the maximum pump power.

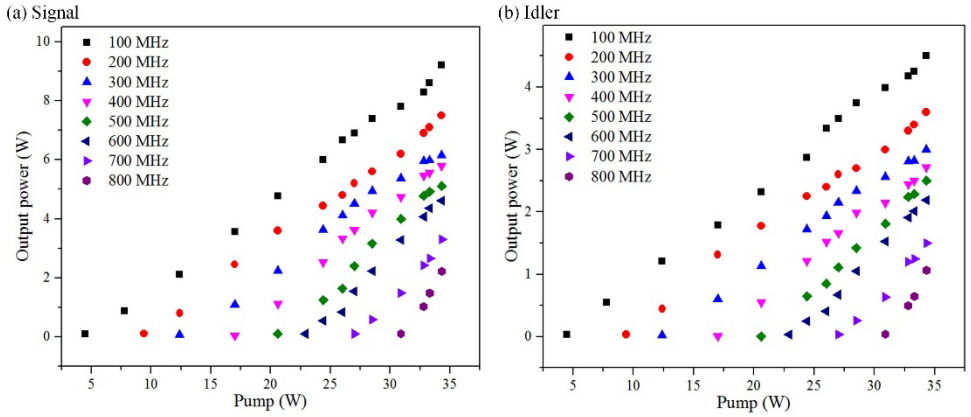

Fig. 7.4.2. Signal (a) and idler (b) output powers at 100 – 800 MHz repetition rates OPO.

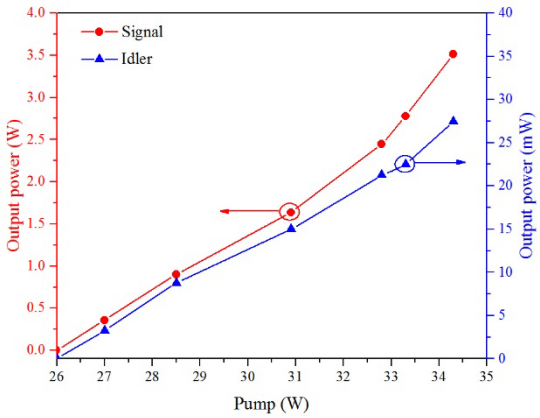

Fig. 7.4.3. Signal and idler output powers at a repetition rate of 1 GHz.

In order to make the OPO work at even higher repetition rate (>800 MHz), OC2 was utilised giving a lower cavity loss meanwhile extracting ~3% of idler out of the cavity. With an oscillation threshold of 27 W, a 1 GHz OP-GaAs OPO was successfully realised. The signal and idler output powers are plotted in Fig. 7.4.3. Although only 27 mW of idler was extracted from the cavity, 3.5 W of signal output power was obtained at a maximum pump power of 34.3 W. Spectra of the signal and idler at maximum output power at 1 GHz were characterised, as presented in Fig. 7.4.4. The central signal and idler wavelengths of 3356

nm and 4897 nm were observed with a FWHM bandwidth of 1.3 nm (1.1 cm^{-1}), and 4 nm (1.7 cm^{-1}).

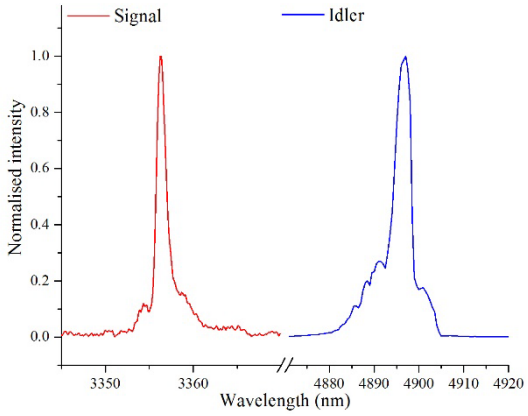

Fig. 7.4.4. Signal and idler spectra at a repetition rate of 1 GHz.

The total output powers (signal and idler) for the variable repetition rate OPO are summarised in Fig. 7.4.5. More than 3 W total OPO output power was obtained at all repetition rates (100 MHz – 1 GHz).

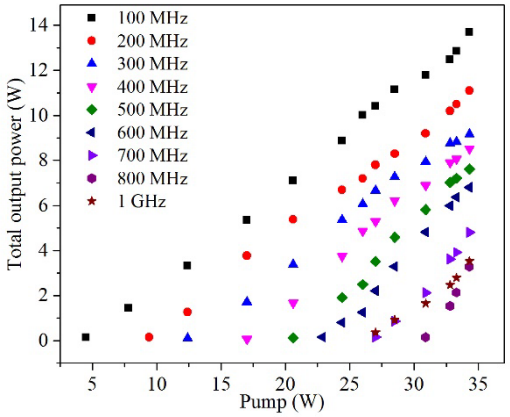

Fig. 7.4.5. Total output powers of variable repetition rate OPO.

7.5 Controllable pulse-duration OPO – 95 ps to 1.1 ns

A controllable pulse-duration OPO was realised with a pump pulse duration from 95 ps to 1.1 ns, profiting again from the ease of tailoring temporal properties of the gain-switched laser diode seeding Tm:MOPA pump system. At a fundamental repetition rate of 100 MHz, the duration of the rectangular electronic drive-pulses was increased leading to longer laser output pulses, as shown in Fig. 7.5.1 (a). The tails of the optical pulses grew when long electronic pulses were imposed on the seed laser diode, as expected from Fig. 2.7.1 (section 2.7). Fig. 7.5.1 (b) shows the corresponding spectra changing with the drive-pulse duration. As the pulse duration became longer, a narrow spectral spike at wavelength of ~1991.4 nm started to emerge (the shaded area in Fig. 7.5.1 (b)). The first peak in the temporal domain

remained constant, corresponding to the unchanging base spectra with a spanning bandwidth of 4.3 nm, whereas the tail part of the gain-switched pulses can have a controlled duration, corresponding to the spectral spike. The two FBG-based filters (Fig. 7.2.1 (a)) were used to narrow the spectral bandwidth, which also has the effect of removing the leading spike of the pulse in the temporal domain. Fig. 7.5.2 shows the spectra after the FBG-based filters, compared to the gain-switched spectra driven by 880-ps electronic pulses. The selected spectra has an excellent OSNR of ~60 dB at a 3-dB linewidth of <0.05 nm. The wavelength of the seed diode was tuned to 1991.0 nm by lowering its temperature in order to match the wavelength of the FBGs.

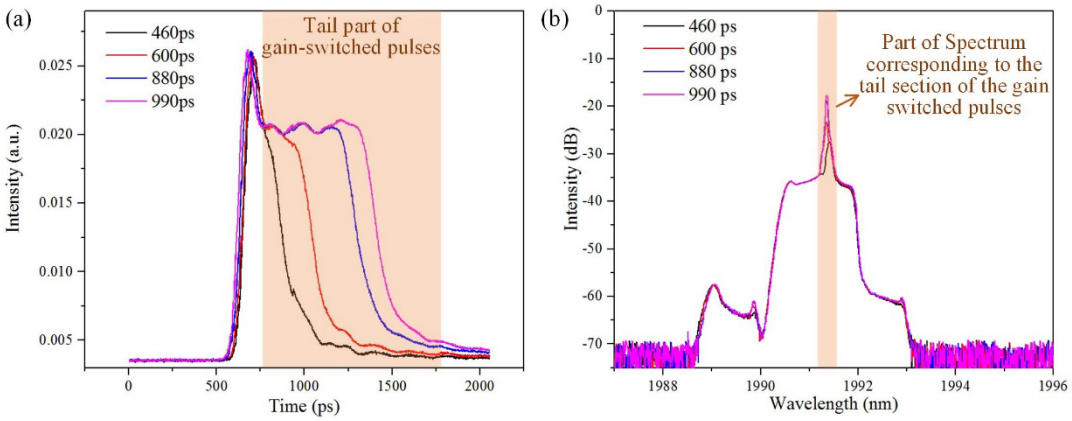

Fig. 7.5.1. Optical pulses (a) and spectra (b) from the seed laser diode gain-switched by electronic pulses with different pulse durations.

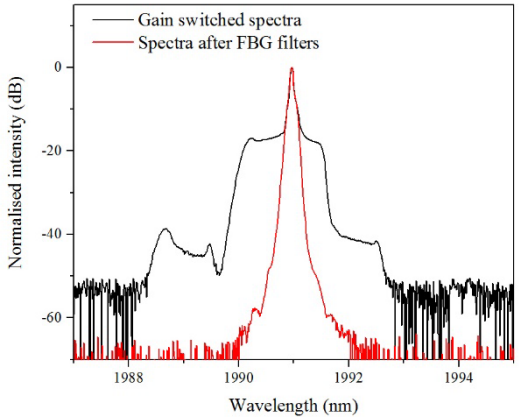

Fig. 7.5.2. Spectra after FBG filters and gain switched spectra.

The pulse duration of the Tm:MOPA system was continuously tunable, from 95 ps to 1.1 ns, with the same average output power. Example pump pulses, 300, 600, 800 ps, and 1.1 ns, are presented in Fig. 7.5.3 with the seed diode driven by 680, 990 ps, 1.2 ns and 1.5 ns electronics pulses, respectively.

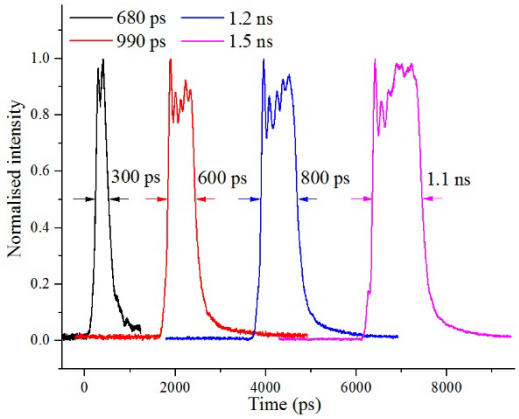

Fig. 7.5.3. Example variable duration pulses from the final stage of the Tm:MOPA system.

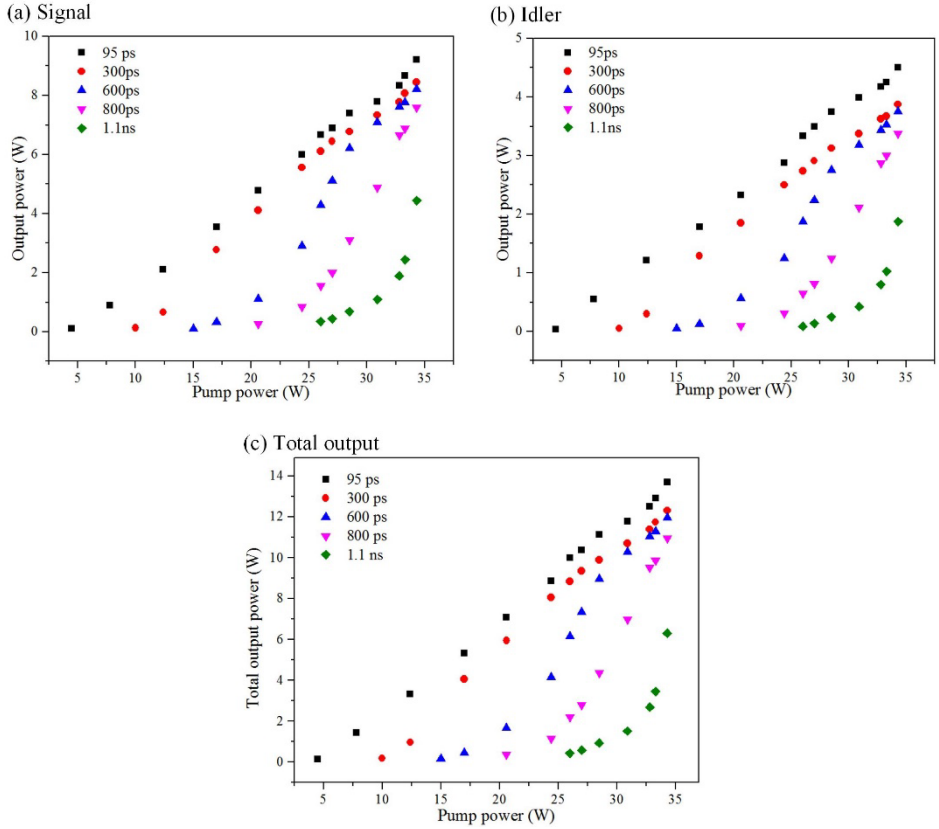

Fig. 7.5.4. Signal, idler and total output powers from the variable pulse-duration OPO.

Fig. 7.5.4 plots the generated signal (a), idler (b) and total output (c) powers of the controllable pulse-duration OPO at a repetition rate of 100 MHz with OC1 in the cavity. At the longest pulse duration of 1.1 ns, a total OPO output power of 6.3 W was obtained with generated signal and idler powers of 4.4 W and 1.9 W, respectively. The OPO did not oscillate for pulses longer than 1.1ns due to the increased threshold power requirement. The pulse shapes of the pump were measured for both the input (undepleted pump) and output (depleted pump) of the OPO. Fig. 7.5.5 depicts two example depleted pump pulses at an original undepleted pump pulse duration of 190 ps (a) and 800 ps (b). Both traces

demonstrate a relatively constant depletion across the pump pulse with strong depletion occurred for higher peak power part in the pump pulse, as expected.

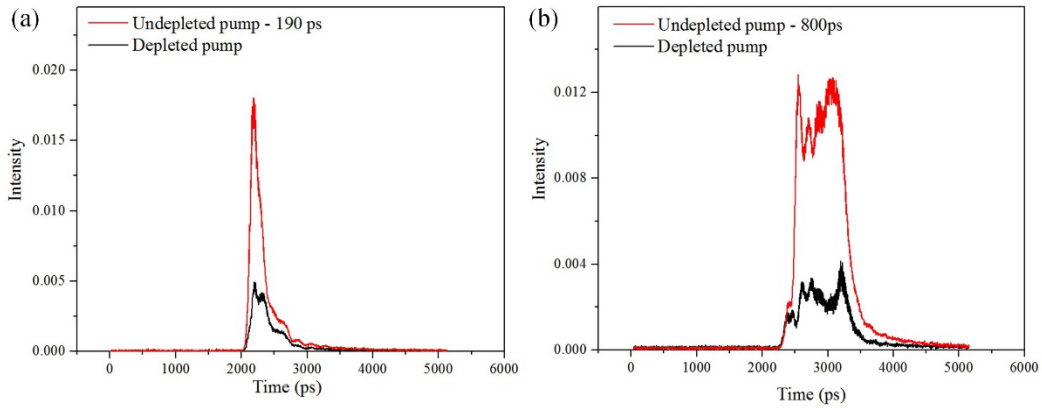

Fig. 7.5.5. Residual pump shapes compared with their corresponding pump pulse shapes at a pulse duration of 190 ps (a) and 800 ps (b).

7.6 Summary

In conclusion, a high-power, mid-infrared variable repetition rate and pulse duration OP-GaAs OPO has been demonstrated. At a fundamental operation with a pump duration of 95 ps at 100 MHz repetition rate, the maximum OPO output powers of signal (3.3 μm) and idler (4.9 μm) were 9.2 W and 4.5 W, respectively, achieved at a total slope efficiency of 45.4% and pumped at 34.3 W. Taking advantage of the versatility of the pump system, the pulse repetition rate of the OPO can be changed from 100 MHz to 1 GHz, while the pulse durations of the OPO can be varied from ~95 ps to ~1.1 ns. This OPO should be suitable for mid-IR pulse applications that require variable and/or particular repetition rates and pulse durations. In the next chapter, I will summarise the thesis and give future prospects.

References

[1] C. Gu *et al.*, "High-repetition-rate femtosecond mid-infrared pulses generated by nonlinear optical modulation of continuous-wave QCLs and ICLs," *Optics Letters*, vol. 44, no. 23, pp. 5848-5851, 2019.

[2] M. A. Mackanos *et al.*, "Pulse-duration-dependent mid-infrared laser ablation for biological applications," *IEEE Journal of Selected Topics in Quantum Electronics*, vol. 18, no. 4, pp. 1514-1522, 2012.

[3] H. El-Khalil *et al.*, "Investigation of laser pulsing parameters' importance in Er:YAG laser skin ablation: a theoretical study conducted via newly developed thermo-mechanical ablation model," *International Journal of Hyperthermia*, vol. 36, no. 1, pp. 612-623, 2019.

[4] L. T. Trevelin *et al.*, "Impact of Er:YAG laser pulse duration on ultra-structure of dentin collagen fibrils," *Lasers in Dental Science*, vol. 2, no. 2, pp. 73-79, 2018.

[5] C. B. Schaffer *et al.*, "Dynamics of femtosecond laser-induced breakdown in water from femtoseconds to microseconds," *Optics Express*, vol. 10, no. 3, pp. 196-203, 2002.

[6] P. E. Schrader *et al.*, "High-power fiber amplifier with widely tunable repetition rate, fixed pulse duration, and multiple output wavelengths," *Optics Express*, vol. 14, no. 24, pp. 11528-11538, 2006.

[7] J. Cheng *et al.*, "A review of ultrafast laser materials micromachining," *Optics & Laser Technology*, vol. 46, pp. 88-102, 2013.

[8] K. Charan *et al.*, "Fiber-based tunable repetition rate source for deep tissue two-photon fluorescence microscopy," *Biomedical optics express*, vol. 9, no. 5, pp. 2304-2311, 2018.

[9] S. Lecomte *et al.*, "Synchronously pumped optical parametric oscillator with a repetition rate of 81.8 GHz," *IEEE Photonics Technology Letters*, vol. 17, no. 2, pp. 483-485, 2005.

[10] M. V. O'Connor *et al.*, "Synchronously pumped optical parametric oscillator driven by a femtosecond mode-locked fiber laser," *Optics Letters*, vol. 27, no. 12, pp. 1052-1054, 2002.

[11] S. Lecomte *et al.*, "Optical parametric oscillator with a pulse repetition rate of 39 GHz and 2.1-W signal average output power in the spectral region near 1.5 μm," *Optics Letters*, vol. 30, no. 3, pp. 290-292, 2005.

[12] F. Kienle *et al.*, "High-power, variable repetition rate, picosecond optical parametric oscillator pumped by an amplified gain-switched diode," *Optics Express*, vol. 18, no. 8, pp. 7602-7610, 2010.

[13] Q. Fu *et al.*, "High-power mid-infrared OP-GaAs OPO with controllable pulse repetition-rates and durations," in *High-Brightness Sources and Light-driven Interactions*, Prague, Czech Republic, 2020, pp. MM2C.2.

[14] Q. Fu *et al.*, "Controllable duration and repetition-rate picosecond pulses from a high-average-power OP-GaAs OPO," *Optics Express*, vol. 28, no. 22, pp. 32540-32548, 2020.

[15] T. Skauli *et al.*, "Improved dispersion relations for GaAs and applications to nonlinear optics," *Journal of Applied Physics*, vol. 94, no. 10, pp. 6447-6455, 2003.

[16] P. J. Phillips *et al.*, "High-repetition-rate, all-solid-state, Ti:sapphire-pumped optical parametric oscillator for the mid-infrared," *Applied Physics Letters*, vol. 77, no. 4, pp. 469-471, 2000.

[17] D. M. Kane, and J. P. Toomey, "Variable pulse repetition frequency output from an optically injected solid state laser," *Optics Express*, vol. 19, no. 5, pp. 4692-4702, 2011.

Chapter 8

Conclusion and future work

8.1 Introduction

This thesis concerned the study and development of various types of mid-infrared (mid-IR) optical parametric devices (OPDs) based on orientation-patterned gallium arsenide (OP-GaAs) pumped by 2-μm gain-switched-laser-diode-seeded thulium-doped fibre master oscillator power amplifiers (Tm:MOPA). In this chapter, I will summarise the main results and conclusions of this thesis in section 8.2 and then give the future prospects in section 8.3.

8.2 Summary of results

The experimental work in this thesis includes the systematic investigation of three basic mid-IR OP-GaAs OPDs – optical parametric generators (OPGs), amplifiers (OPAs), oscillators (OPOs) and their variants. They offer a range of useful output characteristics that are summarised in Table 8.2.1. The OP-GaAs OPG (Chapter 3) had the simplest configuration and offered a wide tuning range of 2550-2940 nm (signal) and 5800-8300 nm (idler), but had high pump threshold and provided a maximum output average (peak) power of 0.26 W and 0.16 W (3 kW and 2 kW) for the signal and idler respectively. As is the nature of OPGs, it generated broad spectra with bandwidths of 29 cm^{-1} and 33 cm^{-1} for signal and idler, respectively. This work represents the highest average power OP-GaAs OPG being reported to date, and its output characteristics together with its simple structure could enable the OP-GaAs OPG to be used in many fields, such as spectroscopy [1] and biomedicine [2].

For some remote spectroscopic applications where high resolution and long distance are required, mid-IR sources with narrower spectral linewidth and higher output power are preferred [3]. In order to narrow the linewidth and boost the power on the basis of the mid-IR OPG, a 0.6-cm^{-1}-bandwidth seed laser was employed to convert the system into an OPA (Chapter 3). In the OPA operation, both the output signal and idler spectral linewidth were significantly narrowed to 0.7 cm^{-1} (signal) and 1.4 cm^{-1} (idler), meanwhile, the average (peak)

powers were increased to 1.07 W and 0.26 W (11.3 kW and 2.7 kW) for signal and idler, respectively. This is the first report of an ultrashort-pulsed OPA based on OP-GaAs. Due to the limited tunability of the seed laser, the tuning range of the OPA was narrower than the OPG, but this was explored and overcome by realising a cascaded OPG-OPA (Chapter 4). The combination of wide-tunability, narrow-linewidth, and high-peak-power of the cascaded OPG-OPA (Table 8.2.1) makes it attractive for spectroscopic applications.

The OP-GaAs OPG and OPA have limited or no control of the spatial coherence of the generated beam and consequently offer mid-IR waves with relatively poor beam qualities. However, a high beam quality OP-GaAs OPO (OPO1) was demonstrated in Chapter 5 with idler M^2 values of 1.06 (x-direction) by 1.03 (y-direction) in a wavelength tuning range of 4394 - 6102 nm. Compared to the OPGs and OPAs, the picosecond-pulsed OPO was pumped and operated at a higher repetition rate (100 MHz) and associated higher pump powers. Power scaling of the OP-GaAs OPO has been studied in Chapter 6 where another OPO (OPO2) was developed and investigated. OPO2 was operated in two modes – continuous mode and burst mode. In continuous mode operation, maximum average powers of 5.7 W (signal) and 4.0 W (idler) were obtained and a thermal roll-off was observed. In contrast, the bust mode was operated with an optical chopper and thus the thermal effect was mitigated. The maximum peak power was achieved in burst mode operation with a value of 0.79 kW and 0.58 kW for signal and idler, respectively. To date, OPO2 presents the highest average power OP-GaAs OPD with wide tunability. OPO3 (Chapter 7) performed a high degree of flexible control on the OPO pulse repetition rates and durations. By simply manipulating the electrical signals of the gain-switched seed laser of the Tm:MOPA system (OPO pump) and without disturbing its optical components, the pulse repetition rate of the mid-IR OP-GaAs OPO can be varied from 100 MHz to 1 GHz, while the pulse durations of the OPO can be changed from ~95 ps to ~1.1 ns. This mid-IR device could benefit in many practical applications, such as material processing.

Overall, in this thesis I have presented a systematic study of mid-IR OP-GaAs OPDs pumped by gain-switched-diode-seeded Tm:MOPA systems. It is believed that these mid-IR laser sources can find a wide range of applications in industrial, scientific, medical, and environmental fields.

Table. 8.2.1. A summary for key experimental results related to OP-GaAs OPDs.

		OPG	**OPA**	**Cascaded OPG-OPA**	**OPO1**	**OPO2**	**OPO3**
Wavelength (μm)	S[a]	2.6-2.9	2.6-2.7	2.6-3.0	3.0-3.7	2.9-3.3	3.3
	I[b]	5.8-8.3	7.2-8.3	5.7-8.3	4.4-6.1	4.9-6.4	4.9
Maximum average power (W)	S	0.26	1.07	0.40	0.51	5.7	9.2
	I	0.16	0.26	0.16	1.18	4.0	4.5
Maximum peak power (kW)	S	3	11.3	11.1	0.12	0.79[c]	0.97
	I	2	2.7	4.5	0.05	0.58	0.47
Pulse duration		94 ps	94 ps	36 ps	100 ps	95 ps	95 ps – 1.1 ns
Repetition rate		1 MHz	1 MHz	1 MHz	100 MHz	100 MHz	100 MHz – 1 GHz
Linewidth (cm^{-1})	S	29	0.71	1.4	0.9	1	0.7
	I	33	1.4	9	3.8	1.6	1.2
Beam quality ($M^2_{x/y}$[d])	S	1.7/1.8	2.8/2.7	2.4/2.2	1.39/1.30	1.45/1.21	1.37/1.55
	I	2.3/2.4	1.9/1.8	3.4/3.4	1.06/1.03	1.03/1.01	1.09/1.12
Pump wavelength (μm)		1.952	1.952	1.952	2.007	1.992	1.992
Pump linewidth (cm^{-1})		0.63	0.63	2.1	0.5	1	< 1
Pump power (W)		3.5 W	3.7 W	5.2 W	11 W	35.3 W	34.3 W

[a] S for signal.
[b] I for idler.
[c] Maximum peak powers of signal and idler for OPO2 were obtained in burst mode operation.
[d] Beam qualities measured in x (horizontal) and y (vertical) direction, respectively.

8.3 Future work

8.3.1 Power delivery by mid-IR fibres

Laser power delivery based on optical fibres is of importance for applications in optical communication, sensing, surgery, and material processing [4-6]. Solid-core silica fibres are the most common and well-fabricated fibres for near-infrared beam delivery. In the mid-IR region, solid-core silica fibres find difficulties for beam delivery due to relatively high material absorption. As an alternative, soft-glass-based solid-core fibres and hollow-core fibres (HCFs) have been developed for operation in this regime [7, 8]. Another requirement for efficient mid-IR beam delivery based on optical fibres is to have a high-beam-quality mid-IR laser source. The mid-IR idler-resonant OP-GaAs OPOs demonstrated in Chapter 5

and 6 are well-suited to this application, offering near-diffraction-limited ($M^2 < 1.1$ for idler), wavelength-tunable (4.4 - 6.4 μm for idler), high-average-power (watt level) mid-IR output.

As a first demonstration, the OPO (described in Chapter 6) was utilised for guiding tests, loss measurements and beam monitoring in in-house-fabricated tellurite HCFs. The following experimental results were performed in collaboration with my colleagues Andrea Venura and Dr. Juliano Hayashi, and have been published, in part, here [9]. Fig. 8.3.1 shows scanning electron microscope (SEM) photos of two in-house fabricated tellurite HCFs, fibre A (left) and fibre B (right). Fibre A had a core diameter of 187 μm and a capillary thickness of 5.7 μm and was designed for transmission at ~5 μm, while fibre B had a 139-μm core surrounding by six capillaries with a thickness of 4.96 μm and was designed for transmission at ~5.6 μm. Both fibre structures were not perfectly centrosymmetric, leaving room for future optimisation. Moreover, the OPO was operated at a relatively low average power (<500 mW) as fibre damage was observed at ~300 mW.

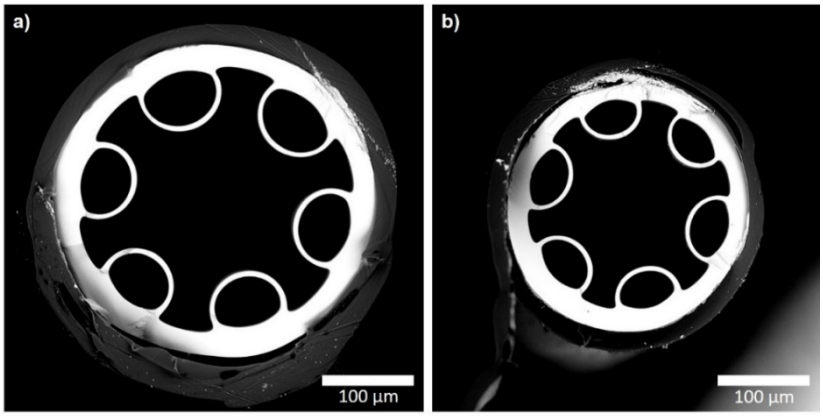

Fig. 8.3.1. Scanning electron microscope photo of tellurite-based HCFs with different parameters: fibre A (left) and B (right).

For fibre A, the OPO beam was focused with a beam waist of ~70 μm at the fibre input, matching a calculated fundamental fibre mode waist of ~65 μm. With the OPO tuned to a wavelength of 4.9 μm, the output power from the HCF was measured for a fibre length of 1.10 m and 0.91 m (1 cut), leading to a calculated fibre loss of 14.7 dB/m. Whereas for the OPO wavelength of 5 μm, the output powers from the HCF were measured for four times cutting from 91 cm to 69.1 cm (3 cuts) with an average loss of 8.2 dB/m. Fig. 8.3.2 shows the loss results comparison between OPO measurements and Fourier-transform infrared spectroscopy (FTIR) measurements, which are in a good agreement. The FTIR measurement

instrument, with a working wavelength range of 2-5.5 μm, contained an FTIR spectrometer (ARoptix, FT-IR Rocket) combined with a lamp source (Thorlabs SLS202).

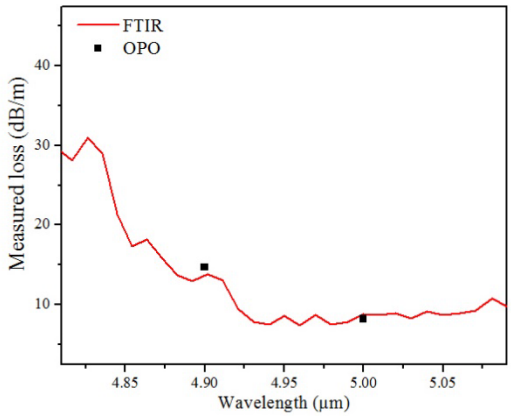

Fig. 8.3.2. Loss measurement comparison between using FTIR and OPO.

For fibre B, the mid-IR OPO beam was launched into the fibre with a beam waist of ~40 μm, similar to the calculated fundamental fibre mode waist (~49 μm). With the OPO tuned to a wavelength of 5.6 μm, three cuts were performed reducing the fibre length from 116 cm to 90.3 cm. The corresponding measured transmitted powers led to a calculated average loss of 5.0 dB/m, whereas with the OPO tuned to a wavelength of 5.8 μm two cuts were made reducing the fibre length from 99.4 cm to 70.4 cm and leading to a calculated loss of 6.4 dB/m. The OPO loss measurements are compared with simulation results calculated from a Comsol Multiphysics software, as shown in Fig. 8.3.3. The measured losses were higher than the simulation results, and when the OPO wavelength was tuned to longer than 5.8 μm, no output was observed from fibre B. This can be attributed to a slight non-uniformity, scattering and microbend in the fiber which were not included in the simulation.

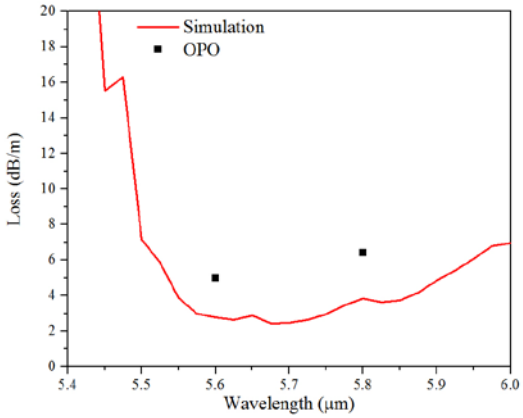

Fig. 8.3.3. A loss comparison between simulation results and OPO measurements.

The measured coupling efficiency for the mid-IR beam launched into HCF fibre B was ~65%, measured with a short-length (13-cm-long). The relatively low coupling efficiency was

attributed to the slight fundamental mode mismatch and possible consequent excitation of high-loss high-order modes. The transmitted beam profile from the 13-cm-long fibre B, with the OPO tuned to a wavelength of 5.6 μm, was monitored by a Pyrocam-based profiler and the M^2 factor was measured to be 1.2, as shown in Fig. 8.3.4.

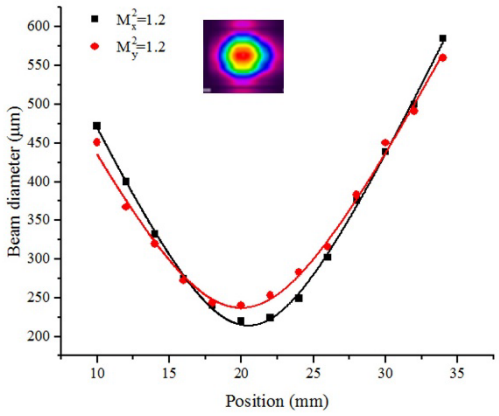

Fig. 8.3.4. Beam quality measurement for telluride HCFs (fibre B).

Future work on mid-IR power delivery will be carried out in further optimised in-house-fabricated HCFs using the mid-IR OP-GaAs OPO. Moreover, the OPO will stay as an available laser source once other types of mid-IR delivery fibres become available.

8.3.2 Further power scaling of the mid-IR picosecond OP-GaAs OPO

Power scaling of mid-IR laser sources is beneficial to their spectroscopic and material processing applications [3]. In Chapter 6 and 7, I have investigated a high-average-power picosecond OP-GaAs OPO with an observed thermally induced power roll-off, which could be mitigated by thermal management using optical chopper or water cooling. Current maximum OPO output average powers of the signal (3.3 μm) and idler (4.9 μm) were 9.2 W and 4.5 W, respectively with corresponding peak powers of 0.97 kW and 0.47 kW, respectively and without any power roll-off. Therefore, the output power of the OPO was limited by the maximum pump power. In future work, the power of the Tm:MOPA system (OPO pump) will be enhanced via further power scaling of the fourth fibre amplifier stage and/or adding extra fibre amplifier stages.

Regardless of any potential thermal-effect-limited average power scaling, the peak power of the mid-IR picosecond OP-GaAs OPO can also be further scaled in the future. High-peak-power OPOs can be achieved by lowering the repetition rate of the pump at a constant average power. However, the synchronously pumping would normally lead to an impractically long OPO cavity length in this case. In order to solve this problem, a high-

harmonic cavity can be considered for the mid-IR OPO, in which the cavity length is configured to be a fraction of that for synchronous pumping (i.e. the resonant signal/idler needs to multi-pass the nonlinear crystal to overlap with the pump pulse) [10]. Such cavity needs low cavity loss in order to reach an oscillation threshold and thus only the non-resonant parametric light is considered to couple out from the cavity. Another low-repetition-rate OPO solution is utilisation of a fibre feedback cavity [11]. Such design requires low loss optical fibres at resonant signal/idler wavelengths. Thus, for mid-IR wavelength-tunable OPOs, mid-IR broad-band low-loss optical fibres are in demand and we are targeting such fibres by optimising the fibre fabrication process, as stated in last section. Apart from the OPO structure modification, the low-repetition-rate OPO also require low-repetition-rate pump. For our OPO, the repetition rate of the pump can be easily changed by manipulating the seed laser diode, as demonstrated in Chapter 7, and for low repetition rates, nonlinear effects in the fibre amplifier chain need to be carefully considered. The flexibility of the pump source would also allow burst mode operation by direct manipulation of the driving electrical pulses, which could then provide pulses at high intra-pulse repetition rates and high peak powers. Such burst-mode-pumped OPOs can be considered as another solution for high-peak-power OPOs while maintaining compact OPO structures [12, 13].

8.3.3 Chalcogenide supercontinuum generation pumped by OP-GaAs OPOs

Spectrally broadband mid-IR laser sources are valuable for many practical applications [14-16], and supercontinuum (SC) generation in optical fibres offers a simple route to mid-IR sources with broad bandwidth, and high-brightness. Chalcogenide (ChG) nonlinear fibres have high nonlinearity and broad transmission windows in the mid-IR region (sulphides up to ~8.5 μm, selenides up to ~14 μm, and tellurides up to ~20 μm). For the development of the ChG SC source, there is a need to select an appropriate pump source with a wavelength that can reach just into the anomalous dispersion region, as required for broadband SC generation. However, zero dispersion wavelengths of standard ChG fibres are around 5 μm or longer, which are difficult to find suitable pump sources. Special ChG fibre geometries, such as tapered fibres and microstructure fibres, are therefore typically required for shifting the zero dispersion wavelength to enable a pumping wavelength down to ~3 μm [17].

The OP-GaAs OPOs demonstrated in this thesis had a wide tunablity that can match the zero dispersion wavelengths of standard ChG fibres and, combined with the high beam quality and high power of the OP-GaAs OPOs, it can be considered as an excellent potential pump source for ChG SC generation. According to reported ChG experimental works [18, 19], the

peak power requirement for reaching a threshold for SC generation using standard step-index fibres is at least 3 kW, which is ~6.4 times higher than the current maximum OPO idler output (0.47 kW). The possible solutions for peak power scaling of the OPO have been discussed in the previous section. In future work, the OP-GaAs-OPO-pumped ChG SC will be investigated, with the aim of producing a watt-level SC output power.

8.3.4 Other possibilities

The works presented in previous three sections are significant and practical works that can be considered in the near future. Other possible future prospects can also be considered but not are not given in such detail here, for example:

i) Idler-seeded cascaded OPG-OPAs. In Chapter 4, a signal-seeded cascaded OPG-OPA was realised by narrowing the linewidth of the generated signal from the OPG, which in turn seeded the OPA. The amplified signals maintained the seed signal narrow-linewidth (1.4 cm^{-1}), whilst the linewidth of the generated idler from the OPA was relatively broad (9 cm^{-1}). If narrow-linewidth idlers are in demand, an idler-seeded cascaded OPG-OPA can be developed by seeding the OPA with a spectrally filtered OPG idler.

ii) Narrow-linewidth OPOs by injection seeding. To realise narrow-linewidth singly-resonant OPOs, complex internal components for their cavities are typically needed [20, 21]. An alternative solution is to inject the OPO with narrow-linewidth lasers at signal or idler wavelengths [22]. Such techniques can simplify OPO cavity structures but require extra seed lasers.

iii) OP-GaAs-based waveguide OPDs. Waveguide OPDs with tight optical confinement can efficiently operate at low powers, and are useful for many applications, such telecommunication [23]. However, only a limited number of demonstrations towards OP-GaAs waveguide frequency convertors were reported so far, including second harmonic generators [24] and OPOs [25]. Other OP-GaAs waveguide OPDs could be developed and investigated in the future, such as waveguide OPAs.

Reference

[1] K. L. Vodopyanov, "Mid-infrared optical parametric generator with extra-wide (3–19-μm) tunability: applications for spectroscopy of two-dimensional electrons in quantum wells," *Journal of the Optical Society of America B,* vol. 16, no. 9, pp. 1579-1586, 1999.

[2] G. Edwards *et al.*, "Tissue ablation by a free-electron laser tuned to the amide II band," *Nature,* vol. 371, no. 6496, pp. 416-419, 1994.

[3] B. J. Orr *et al.*, "Tunable laser applications," in: CRC press, 2016,

[4] T. Miya *et al.*, "Ultimate low-loss single-mode fibre at 1.55 μm," *Electronics Letters,* vol. 15, no. 4, pp. 106-108, 1979.

[5] S. Allison *et al.*, "Fiber optic pulsed laser delivery for remote measurements," *Optical Engineering,* vol. 26, no. 6, pp. 266538, 1987.

[6] J. D. Shephard *et al.*, "Silica hollow core microstructured fibers for beam delivery in industrial and medical applications," *Frontiers in Physics,* vol. 3, no. 24, 2015.

[7] W. Ding *et al.*, "Recent progress in low-loss hollow-core anti-resonant fibers and their applications," *IEEE Journal of Selected Topics in Quantum Electronics,* vol. 26, no. 4, pp. 1-12, 2020.

[8] G. Tao *et al.*, "Infrared fibers," *Advances in Optics and Photonics,* vol. 7, no. 2, pp. 379-458, 2015.

[9] A. Ventura *et al.*, "Extruded tellurite antiresonant hollow core fiber for Mid-IR operation," *Optics Express,* vol. 28, no. 11, pp. 16542, 2020.

[10] L. Xu *et al.*, "Fiber-laser-pumped, high-energy, mid-IR, picosecond optical parametric oscillator with a high-harmonic cavity," *Optics Letters,* vol. 40, no. 14, pp. 3288-3291, 2015.

[11] F. Kienle *et al.*, "High pulse energy, picosecond MgO:PPLN optical parametric oscillator using a single-mode fiber for signal feedback," in *Advances in Optical Materials,* Istanbul, 2011, pp. AMB3.

[12] K.-H. Wei *et al.*, "Fiber laser pumped burst-mode operated picosecond mid-infrared laser," *Chinese Physics B,* vol. 24, no. 2, pp. 024217, 2015.

[13] Y. Wu *et al.*, "Compact picosecond mid-IR PPLN OPO with controllable peak powers," *OSA Continuum,* vol. 3, pp. 2741-2748, 2020.

[14] S. Dupont *et al.*, "IR microscopy utilizing intense supercontinuum light source," *Optics Express,* vol. 20, no. 5, pp. 4887-4892, 2012.

[15] A. Labruyère *et al.*, "Compact supercontinuum sources and their biomedical applications," *Optical Fiber Technology,* vol. 18, no. 5, pp. 375-378, 2012.

[16] M. N. Islam *et al.*, "Field tests for round-trip imaging at a 1.4 km distance with change detection and ranging using a short-wave infrared super-continuum laser," *Applied Optics,* vol. 55, no. 7, pp. 1584-1602, 2016.

[17] S. Shabahang *et al.*, "Dispersion characterization of chalcogenide bulk glass, composite fibers, and robust nanotapers," *Journal of the Optical Society of America B,* vol. 30, no. 9, pp. 2498-2506, 2013.

[18] Y. Yu *et al.*, "1.8-10 μm mid-infrared supercontinuum generated in a step-index chalcogenide fiber using low peak pump power," *Optics Letters,* vol. 40, no. 6, pp. 1081-1084, 2015.

[19] S. Dai *et al.*, "A Review of Mid-Infrared Supercontinuum Generation in Chalcogenide Glass Fibers," *Applied Sciences,* vol. 8, no. 5, pp. 707, 2018.

[20] F. Ganikhanov *et al.*, "Narrow-linewidth middle-infrared $ZnGeP_2$ optical parametric oscillator," *Journal of the Optical Society of America B,* vol. 18, no. 6, pp. 818-822, 2001.

[21] M. Vainio *et al.*, "Singly resonant cw OPO with simple wavelength tuning," *Optics Express,* vol. 16, no. 15, pp. 11141-11146, 2008.

[22] M. Milton *et al.*, "Injection seeding of an infrared optical parametric oscillator with a tunable diode laser," *Optics Letters*, vol. 19, no. 4, pp. 281-283, 1994.
[23] C. Wang *et al.*, "Ultrahigh-efficiency wavelength conversion in nanophotonic periodically poled lithium niobate waveguides," *Optica*, vol. 5, no. 11, pp. 1438-1441, 2018.
[24] K. Fedorova *et al.*, "Second harmonic generation in a low-loss orientation-patterned GaAs waveguide," *Optics Express*, vol. 21, no. 14, pp. 16424-16430, 2013.
[25] M. Oron *et al.*, "Optical parametric oscillation in orientation patterned GaAs waveguides," in *Nonlinear Frequency Generation and Conversion: Materials, Devices, and Applications XI*, 2012, pp. 82400C.

List of Publications

Journals

- **Q. Fu**, Y. Wu, S. Liang, P. C. Shardlow, D. P. Shepherd, S.-u. Alam, L. Xu, and D. J. Richardson, "Controllable duration and repetition-rate picosecond pulses from a high-average-power OP-GaAs OPO," ***Optics Express***, vol. 28, no. 22, pp. 32540-32548, 2020.
- **Q. Fu**, L. Xu, S. Liang, P. C. Shardlow, D. P. Shepherd, S.-u. Alam, and D. J. Richardson, "High-average-power picosecond mid-infrared OP-GaAs OPO," ***Optics Express***, vol. 28, no. 4, pp. 5741-5748, 2020.
- Y. Wu, S. Liang, **Q. Fu**, L. Xu, and D. J. Richardson, "Compact picosecond mid-IR PPLN OPO with controllable peak powers," ***OSA Continuum***, vol. 3, pp. 2741-2748, 2020.
- A. Ventura, J. G. Hayashi, J. Cimek, G. Jasion, P. Janicek, F. B. Slimen, N. White, **Q. Fu**, L. Xu, H. Sakr, N. V. Wheeler, D. J. Richardson, and F. Poletti, "Extruded tellurite antiresonant hollow core fiber for Mid-IR operation," ***Opt. Express***, vol. 28, no. 11, pp. 16542, 2020.
- Z. Ren, **Q. Fu**, L. Xu, J. H. V. Price, S. -u. Alam, and D. J. Richardson, "Compact, high repetition rate, 4.2 MW peak power, 1925 nm, thulium-doped fiber chirped-pulse amplification system with dissipative soliton seed laser," ***Opt. Express***, vol. 27, no. 25, pp. 36741-36749, 2019.
- **Q. Fu**, L. Xu, S. Liang, P. C. Shardlow, D. P. Shepherd, S.-u. Alam, and D. J. Richardson, "A high beam quality, watt-level, widely tunable, mid-infrared OP-GaAs optical parametric oscillator," ***Optics Letters***, vol. 44, pp. 2744-2747, 2019.
- **Q. Fu**, L. Xu, S. Liang, D. P. Shepherd, D. J. Richardson, and S.-u. Alam, "Widely tunable, narrow-linewidth, high-peak-power, picosecond midinfrared optical parametric amplifier," ***IEEE Journal of Selected Topics in Quantum Electronics***, vol. 24, no. 5, pp. 1-6, 2018.
- S. Liang, L. Xu, **Q. Fu**, Y. Jung, D. P. Shepherd, D. J. Richardson, and S.-u. Alam, "295-kW peak power picosecond pulses from a thulium-doped-fiber MOPA and the generation of watt-level >2.5-octave supercontinuum extending up to 5 μm," ***Optics Express***, vol. 26, no. 6, pp. 6490-6498, 2018.
- L. Xu, S. Liang, **Q. Fu**, D. P. Shepherd, D. J. Richardson, and S.-u. Alam, "Highly efficient frequency doubling and quadrupling of a short-pulsed thulium fiber laser," ***Applied Physics B***, vol. 124, no. 4, pp. 59, 2018.
- L. Xu, **Q. Fu**, S. Liang, D. P. Shepherd, D. J. Richardson, and S.-u. Alam, "Thulium-fiber-laser-pumped, high-peak-power, picosecond, mid-infrared orientation-patterned GaAs optical parametric generator and amplifier," ***Optics Letters***, vol. 42, no. 19, pp. 4036-4039, 2017.

Conferences

- **Q. Fu**, L. Xu, S. Liang, P. C. Shardlow, D. P. Shepherd, S.-u. Alam, and D. J. Richardson, “High-power mid-infrared OP-GaAs OPO with controllable pulse repetition-rates and durations,” in ***High-Brightness Sources and Light-driven Interactions***, Prague, Czech Republic, 2020, pp. MM2C.2.
- **Q. Fu**, “High-average-power, mid-infrared, widely tunable, picosecond optical parametric oscillator based on OP-GaAs (*Conference Presentation*)”, in ***Photonics West***, 2020.
- **Q. Fu**, L. Xu, S. Liang, P. C. Shardlow, D. P. Shepherd, S.-u. Alam, and D. J. Richardson. "Mid-infrared, idler-resonant, picosecond OP-GaAs OPO with wide tunability and good beam quality," in ***Conference on Lasers and Electro-Optics***, San Jose, 2019, pp. JW2A.44
- **Q. Fu**, L. Xu, S. Liang, D. P. Shepherd, D. J. Richardson, and S.-u. Alam, "Picosecond fiber-laser-pumped widely tunable, narrow-linewidth, high-peak-power, mid-infrared OP-GaAs OPA," in ***Conference on Lasers and Electro-Optics***, San Jose, 2018, California, pp. STh3F.2.
- L. Xu, **Q. Fu**, S. Liang, D. P. Shepherd, D. J. Richardson, and S.-u. Alam. "High-peak-power, picosecond, mid-infrared optical parametric generator and amplifier pumped by Tm:fiber laser," in ***High-Brightness Sources and Light-driven Interactions***, Strasbourg, 2018, pp. MW1C.3.
- L. Xu, S. Liang, **Q. Fu**, D. P. Shepherd, D. J. Richardson, and S.-u. Alam, "High-peak-power, high-efficiency, frequency doubled and quadrupled thulium fiber laser," in ***Conference on Lasers and Electro-Optics***, San Jose, 2018, California, pp. SM4K.5.
- S. Liang, L. Xu, **Q. Fu**, D. P. Shepherd, D. J. Richardson, and S.-u. Alam. "A watt-level supercontinuum source from a fiber-laser-pumped fluoroindate fiber spanning 750 nm to 5 μm," in ***Conference on Lasers and Electro-Optics***, San Jose, California, 2018, pp. 1-2.
- S. Liang, L. Xu, **Q. Fu**, Y. Jung, D. P. Shepherd, D. J. Richardson, and S.-u. Alam. "High peak power picosecond pulses from an all-fiber master oscillator power amplifier seeded by a 1.95 μm gain-switched diode," in ***Advanced Solid State Lasers***, Nagoya, Aichi, 2017, pp. ATh3A.4.